1987

An Experimental and Theoretical Analysis of a Laser Beam Propagating Through Multiple Phase Screens

Arthur R. Weeks
University of Central Florida

AN EXPERIMENTAL AND THEORETICAL ANALYSIS OF A LASER BEAM PROPAGATING THROUGH MULTIPLE PHASE SCREENS

by

Arthur R. Weeks, Jr.

A dissertation submitted in partial fulfillment of the requirements for the degree of Doctor of Philosophy in the Department of Electrical Engineering at the University of Central Florida Orlando, Florida

August 1987

Major Professor: Dr. Ronald L. Phillips

ABSTRACT

An experimental and a theoretical analysis for a laser beam propagating through multiple phase screens was performed. The theoretical analysis showed that the statistics for the intensity fluctuations, which can be predicted by the HK and the I-K distributions, could be derived from a multiplicative process using statistical distributions derived from Gaussian statistics. For the single phase screen experiment, the experimental normalized moments were compared with the normalized moments of both the HK and I-K distributions. In addition, the intensity data was lowpass filtered to yield moments that are predicted by the gamma distribution. The single phase screen data was segmented into small time intervals, and all time segments with approximately the same variance were grouped together into bins to yield normalized moments for each bin that are predicted by the Rician distribution. Also, the normalized moments for two and three phase screen experiments were measured. Finally, a computer program was written to simulate K distributed noise from two independent Gaussian noise sources.

ACKNOWLEDGEMENTS

I would like to acknowledge and thank the many people who have contributed to the completion of this dissertation. I would like to thank both the Center for Research in Electro-Optics and Lasers (CREOL) and the Electrical Engineering Department at the University of Central Florida for their help and patience.

I would like to thank my advisor, Dr. Ronald L. Phillips, for the many hours of help and the extensive discussions that we had during the past year.

I would also like to thank Dr. Larry Andrews for guiding me in the right direction and for the countless number of hours that he spent proof reading this document.

Finally, but not least, I would like to thank my wife, Dian, for her patience, love, and help during the long hours that it took to complete this dissertation.

TABLE OF CONTENTS

LIST OF FIGURES v

INTRODUCTION 1

INTENSITY STATISTICS 12

SINGLE PHASE SCREEN INTENSITY EXPERIMENTS 21

EXPERIMENTAL MEASUREMENTS OF THE CONDITIONAL STATISTISTICS 36
Gamma Statistics 37
Rician Statistics 55

MULTIPLE PHASE SCREEN INTENSITY EXPERIMENTS 67

COMPUTER SIMULATION OF THE K DISTRIBUTION 82

CONCLUSION 96

APPENDICES 103
A. Summary of Probability Density Functions . . . 104
B. Stationary Statistics Derived From Gaussian Processes 107
Rayleigh Distribution 108
Negative Exponential Distribution 111
Gamma Distribution 111
Rician Distribution 113
Gamma Moments 117
Rician Moments 119
C. Nonstationary Statistics Derived From Compound Gaussian Processes 123
K Distribution 125
HK Distribution 132
I-K Distribution 141
K Moments 148
HK Moments 150
I-K Moments 152
D. High Speed Movie Experiment 155
E. IBM PC Data Acquisition System 160

LIST OF REFERENCES 165

LIST OF FIGURES

1. A Typical Detector Output 6

2. Block Diagram for Single Phase Screen Intensity Experiments 23

3. Maximum Normalized Second Moment Experiment . . . 27

4. Normalized Moments for a Single Phase Screen as a Function of Distance 29

5. Time Series Plot for a Single Phase Screen for a Distance of 5 Feet 31

6. Time Series Plot for a Single Phase Screen for a Distance of 100 Feet 32

7. Spectrum Data for a Single Phase Screen for a Distance of 5 Feet 33

8. Spectrum Data for a Single Phase Screen for a Distance of 100 Feet 34

9. Proposed Spectrum for N(t) and W(t) 38

10. Proposed Spectrum for $|N(t)|^2$ and $|W(t)|^2$ 41

11. Proposed Spectrum for $|N(t) \cdot W(t)|^2$ 42

12. Normalized Moments for the Lowpass Filter Experiment 47

13. Normalized Second Moment vs. Distance for the Lowpass Filter Experiment 48

14. ρ vs. Distance for the Lowpass Filter Experiment 49

15. α vs. Distance for the Lowpass Filter Experiment 50

16. HK and I-K Normalized Moments vs. Distance Using the Lowpass Filter Parameters in Figures 14 and 15 53

17. Normalized Moments for the Lowpass Filter Experiment by Segmenting the Data 54

18. Normalized Moments for a Segment Size of 150 Milliseconds and a Distance of 10 Feet . . . 57

19. Normalized Moments for a Segment Size of 50 Milliseconds and a Distance of 10 Feet 58

20. Normalized Moments for a Segment Size of 15 Milliseconds and a Distance of 10 Feet 59

21. Normalized Moments for a Segment Size of 8 Milliseconds and a Distance of 5 Feet 61

22. Normalized Moments for a Segment Size of 60 Milliseconds and a Distance of 35 Feet 62

23. Normalized Moments for a Segment Size of 150 Milliseconds and a Distance of 100 Feet . . . 63

24. Segment Size vs. Distance 65

25. Block Diagram for the Multiple Phase Screen Intensity Experiments 69

26. Normalized Moments for a Double Phase Screen as a Function of Distance 71

27. Spectrum Data for a Double Phase Screen for a Distance of 25 Feet 74

28. Spectrum Data for a Double Phase Screen for a Distance of 100 Feet 75

29. Normalized Moments for a Triple Phase Screen as a Function of Distance 77

30. Spectrum Data for a Triple Phase Screen for a Distance of 45 Feet 79

31. Spectrum Data for a Triple Phase Screen for a Distance of 100 feet 80

32. Comparison of the Normalized Moments for the Single, Double, and Triple Phase Screens 81

33. Block Diagram for the Computer Simulation of the K Distribution for $\alpha = 1$ 86

34. Time Series Plot for $N_1(t)$ and $W_1(t)$ 88

35. Time Series Plot for I(t) 89

36. Spectrum for $N_1(t)$ 91

37. Spectrum for $W_1(t)$ 92

38. Spectrum for I(t) 93

39. Hurter-Driffield Curve for KODAK 7240 16 Millimeter Film 159

INTRODUCTION

As an electromagnetic (EM) wave propagates through the atmosphere, it encounters fluctuations in temperature, wind velocity, pressure, and humidity. Variations in these atmospheric conditions cause the index of refraction of the air to fluctuate. Since the wave number of the EM wave is proportional to the index of refraction, any fluctuations in the refractive index cause fluctuations in the EM wave's amplitude and phase. With the atmospheric conditions being random in nature, predicting the fluctuations in the amplitude and phase requires the use of probability theory [1].

For a propagating optical (laser) beam, fluctuations in the index of refraction cause several different problems. If the size of the largest turbulent eddies (outer scale) are on the order of the optical beam size, the whole beam will tend to wander about its optical axis. On the other hand, if the smallest eddy size (inner scale) is much smaller than the optical beam, the intensity across the beam will appear to have random intensity patches. This is similar to what is observed in laser speckle. In the case of a laser beam propagating through

the atmosphere, the observed speckle pattern is moving with time. If an interferometer is used to measure the phase front of the laser beam, the observed phase would be random and distorted from its original shape. For a coherent optical beam, the phase distortion will manifest itself as intensity fluctuations appearing as an interference term [2; 3]. For long propagation distances, the fluctuations in the EM wave result in the beam expanding in size beyond the diameter predicted by Gaussian laser beam theory. The beam diverges beyond the expected divergence angle. This effect is known as blooming due to its similarity to the electron blooming effect in cathode ray tubes.

If the optical beam is used as a communication link, the random intensity and phase fluctuations result in noise in the received signal. For the case of fluctuations due to a large outer scale, the beam incident on the detector could wander off the detector's surface. This will then result in the loss of information while the beam is displaced from the detector's aperture. As the fluctuations in the atmosphere cause the intensity patches to move over the detector, there will be periods of time when the beam completely fades to zero. During this time, all information contained in the beam is lost.

In every optical communication link there is a need to know the statistical nature of the medium through which the information must pass. Understanding the underlying statistics enables the system engineer to properly predict the required detector threshold level, the probability of detection, the average fade time, and the signal to noise ratio (SNR) of the system. For the case of an optical beam propagating through the atmosphere, the predominant noise source is due to the intensity and phase fluctuations in the optical beam.

For optical communication systems that are using coherent detection to increase performance, the phase noise that is introduced by the atmosphere seriously limits the SNR of the system. If the phase noise becomes large enough so that the received signal phase is in quadrature with the heterodyne receiver oscillator, the total demodulated signal will go to zero, resulting in the loss of the desired signal [4].

Tatarski showed that for short distances, the intensity statistics followed the log-normal distribution [1]. For years this distribution became the standard model for the intensity probability density function (PDF). Unfortunately, this distribution yields incorrect results for long propagation distances. Attempts have been made to fit the experimental intensity PDF with the

statistical theory for radio waves traveling through the atmosphere that was developed during the forties [5; 6; 7]. Nakagami assumed that the fluctuations in the EM wave were Gaussian in nature. This assumption led to the development of the m distribution. Rice went one step further by separating the problem into two parts. He assumed the process contained a random part added to a deterministic part and that the underlying process for the random part was Gaussian. This led to the development of the Rician distribution for the amplitude of the wave.

Attempts were made to fit the m and the Rician distributions to the experimentally measured amplitude (and thereby the intensity) PDF, but with no success. Researchers noticed that the variance of the field was changing slowly with time and that the fundamental assumption that the random part of the field was stationary was possibly incorrect [8; 9; 10; 11; 12; 13; 14]. Jakeman and Pusey developed a class of K distributions by using the model of a random walk in the complex plane in which the total number of steps was also a random variable. By assuming that the number of steps was governed by the negative-binomial distribution, and taking the limit as the number of steps became large, they were led to the K distribution for the resulting amplitude or intensity of the field. Jakeman's approach in

developing the K distribution was equivalent to assuming that the random process was doubly stochastic.

In the case of the propagation problem, the term doubly stochastic means that the random process is the modulation of a noise source with a noise source. If one noise source is slowly varying compared with the other noise source, the resulting output will appear as if it is nonstationary [15]. This is a natural conclusion, since the resulting output will look as if its variance is slowly varying with time.

Referring to Figure 1, a typical output from a detector is plotted as a function of time. The plot of the intensity data shown in Figure 1 illustrates how the mean value varies with time due to the slowly varying noise source. One definition of nonstationarity might be that the PDF, the auto-correlation function, or the spectrum of the random process varies with time.

To handle the nonstationary (modulation) model, the approach taken was to hold one of the noise variables fixed and find the conditional PDF due to the other noise variable [16; 17]. Once this conditional PDF was found, the total PDF due to both noise variables was computed by averaging the conditional PDF with the PDF from the noise variable that was originally held fixed [18].

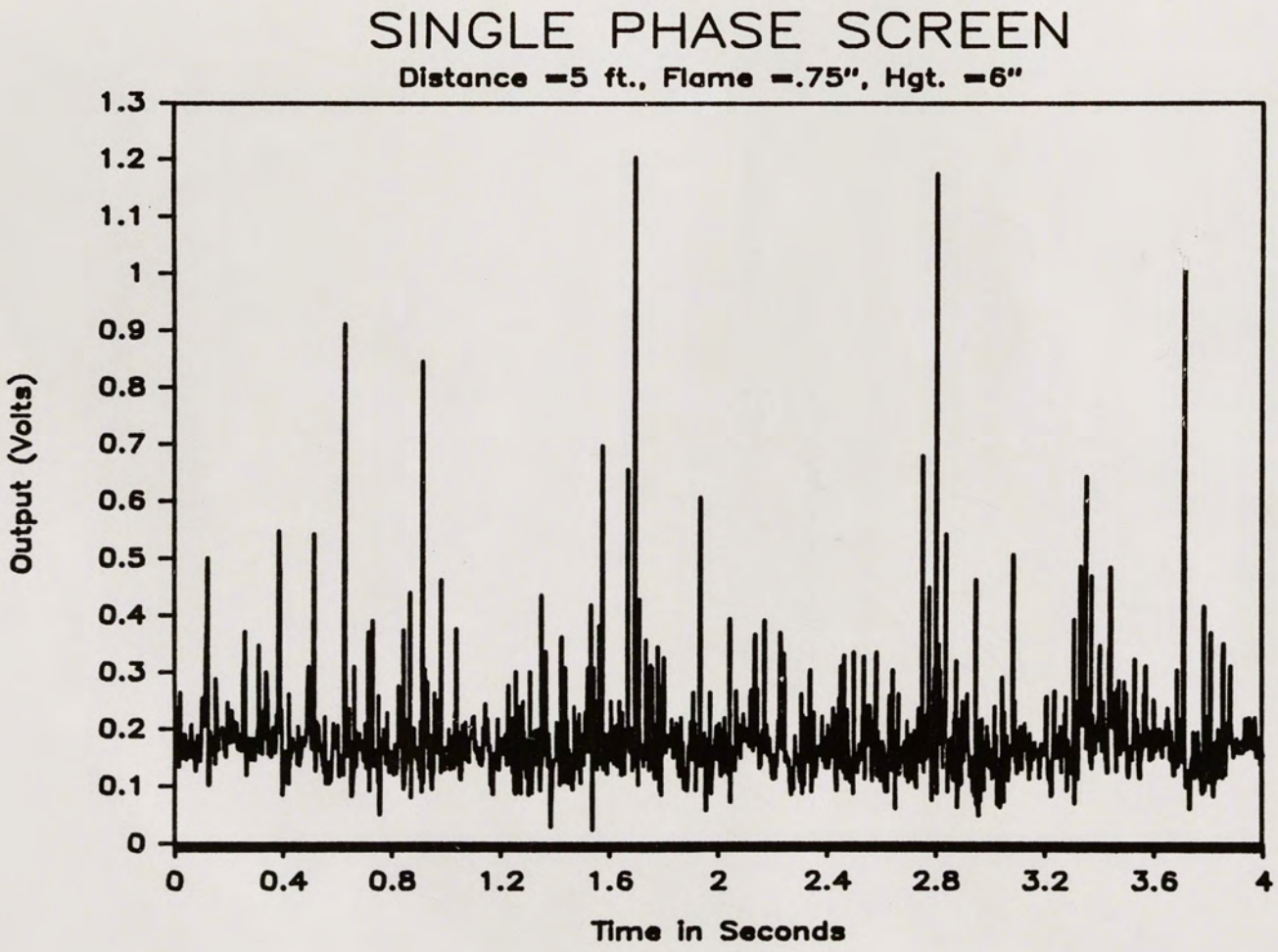

Figure 1. A Typical Detector Output.

The first step in finding the intensity PDF was to fix the slowly varying noise term. The next step was to find the conditional PDF as if the remaining random process (the fast-varying noise term) was statistically stationary and then average this conditional PDF with the PDF of the slowly varying noise term. Andrews and Phillips assumed that the stationary part of the field contained both a deterministic part plus a random part. They also assumed that the random part was (conditional) Gaussian distributed with zero mean [12; 13]. This approach is similar to the approach that was originally proposed by Rice, except Rice did not average his results for a nonstationary process. From previous work, Andrews and Phillips chose the PDF for the slowly varying variance to be a gamma distribution [8; 9; 10; 11; 12; 13].

Assuming a first order Rician distribution for the stationary part of the field and a gamma distribution for the slowly varying variance, the unconditionalized intensity PDF was then computed as an infinite series of K and I Bessel functions. This PDF was derived by Link and is called the Homodyned K (HK) distribution [19]. However, the HK PDF was originally suggested by Jakeman, but he only computed the moments rather than the PDF. It is interesting to note that as the deterministic part of the field goes to zero, the HK distribution reduces to

the K distribution that was developed by Jakeman and Pusey for non-Rayleigh random processes [8; 9; 10; 11].

In an effort to reduce the complexity of the HK distribution, an approximation was made to the characteristic function of the intensity PDF. The HK distribution then reduces to simply a single product of I and K Bessel functions. Andrews and Phillips appropriately named this PDF the I-K distribution.

For the PDF of the phase, Link followed the same procedures that were used to derive the HK distribution for the intensity distribution. Instead of integrating over the phase PDF, however, he integrated over the intensity PDF. His work resulted in an infinite series of K Bessel functions [19]. This series can be evaluated for special cases where the two free parameters of the HK distribution, the number of scatterers (modes) and the signal to noise ratio (SNR), are known. For low turbulence, the number of modes is about one and the SNR is large. In the saturation region (i.e., strong turbulence) the number of modes is large and the SNR is nearly zero.

Since long propagation distances, on the order of 1 to 10 kilometers, are needed to make experimental measurements, difficulties arise in finding locations where measurements can be taken. To solve this problem, and to

enable the experiments to be performed in the laboratory, a burner was used to introduce random phase fluctuations in the optical beam. The turbulence caused by the burner introduces only random fluctuations in the index of refraction of the air, thereby creating a phase screen. By using a phase screen to introduce random fluctuations into the optical beam, the distance required for the experiments was scaled to 100 feet. In addition to smaller distances, the laboratory can be environmentally controlled so that experiments can be repeated.

In this dissertation, the experimental measurements of a collimated laser beam propagating through phase screens will be discussed. Several experiments were performed using one, two, and three phase screens. For the experiments using multiple phase screens, the distance between the screens was set at 20 feet. The distance of 20 feet was chosen so that the turbulence induced phase fluctuations, due to each phase screen, could be assumed to be independent of the previous screen.

For a single phase screen, several different experiments were performed. In the first experiment, the normalized moments were measured as a function of distance behind the phase screen. This data was compared with the I-K distribution for the extended range model. In

addition to the normalized moments, the spectrum was measured at various distances behind the screen.

The next two experiments were conducted to verify the conditional statistical approach in solving the nonstationary problem. In the first experiment, the detected signal was lowpass filtered to verify that the slowly varying noise term did indeed follow the gamma statistics. The experimental moments were measured and compared with the theoretical moments for the gamma distribution. From the data, the number of modes and the SNR as a function of distance were also computed. The computed number of modes and the SNR were then used to compute the normalized moments for the HK and the I-K distributions. The computed normalized moments for both the HK and the I-K distributions were compared with the actual experimental data.

The second experiment to verify the conditional statistics approach was to segment the experimental data into small intervals over which the variance of the field was, for the most part, constant. All segments with the same variance or within 1 percent deviation were combined together into one bin. The normalized moments for each bin were then computed and compared with the normalized moments for the Rician distribution. Once the correct segment size was chosen, the computed normalized moments

were found to match the normalized moments of the Rician distribution. An additional result of this experiment was a plot of segment size as a function of distance behind the phase screen.

The next experiments involved the use of two and three phase screens. Both the normalized moments and the spectrum were measured as a function of distance. Attempts were made to fit the extended turbulence model with the data from the multiple phase screen experiments.

Since the underlying statistical phenomenon was not a function of the physics of the problem, a simulation was performed with two band limited Gaussian noise generators. One noise generator output was lowpass filtered to 20 Hz, while the other noise generator output was bandpass filtered at 325 Hz with a bandwidth of 125 Hz. The filtered generator outputs were then sampled by an IBM PC computer with a data acquisition board. The two noise sources were sampled twice so that two complex Gaussian random variables were generated. These two random variables were then multiplied to yield the time series, the spectrum, and the normalized moments. The normalized moments of the computer simulated output were then compared with the normalized moments of the K distribution.

INTENSITY STATISTICS

When a laser beam propagates through the atmosphere, the variations in the index of refraction of the atmosphere along the propagation path produce fluctuations in the phase and magnitude of the electric field, producing fluctuations in the intensity of the laser beam. These intensity fluctuations result in degradation of the laser beam as it propagates through the atmosphere.

Since the variation in the index of refraction of the atmosphere is mainly the result of temperature differences caused by shear layers, convection, and air motion, turbulence plays an important role in determining the random nature of the intensity variations of a laser beam propagating through the atmosphere. Throughout the atmosphere there exist localized volumes (eddies) in which the temperature is approximately constant. The smallest eddies are known as inner scale, while the largest eddies are known as outer scale. For the case in which the laser beam is propagating parallel to the ground, the size of the largest eddies is approximately equal to the distance between the laser and the ground.

Since each eddy is at a different average temperature, the index of refraction for each of the eddies will be different. Each of these small eddies acts like a small lenses that refracts the laser beam in different directions. If the laser beam contains many of these small eddies, there will be many rays (scatterers or modes) within the beam that will be propagating in many different directions. If two of the rays arrive at a detector in phase, constructive interference occurs. On the other hand, if two of the rays arrive out of phase, destructive interference occurs. The net effect is a random speckle pattern across the laser beam's surface. Unlike speckle patterns that are the result of fixed rough surfaces, this speckle pattern is changing with time, since the eddies are moving across the laser beam in the direction of the wind velocity. In addition, new eddies are constantly being created.

If a small aperture detector is placed in the path of the laser beam, fluctuations in the detector output with time will be observed [12; 13]. These fluctuations are the result of the atmospheric induced speckle pattern moving across the detector's surface. Previous attempts by researchers to predict these random fluctuations with stationary statistics have failed [5; 6; 7]. Researchers believed that the detected field should contain both a

random part and a deterministic part. It also was assumed that the random part was the sum of many rays as a consequence of the Central Limit Theorem. The random part was, thereby, assumed to be complex Gaussian distributed with a zero mean. Immediately, the derivation of the PDF for the intensity fluctuations for a laser beam propagating through the atmosphere yields the Rician distribution. Yet, the Rician distribution does not fit the experimental data.

Researchers noticed that the intensity fluctuations were intermittant. In other words, the experimental data showed periods of time in which the detected laser beam was very erratic, and other periods of time in which the fluctuations in the laser beam intensity were very small. From this, researchers concluded that the variance of the process was changing with time and that the underlying process for the electric field was nonstationary [8; 9; 10; 11; 12; 13].

A typical output from a detector is shown in Figure 1 and illustrates the two time scale effect of the fluctuations in the laser beam intensity. The small turbulent eddies produce very fast random spikes in the intensity, while the larger turbulent eddies tend to modulate the amplitude of the fast random spikes. One way of modeling the electric field for a nonstationary

scattering process in which the variance is changing with time is to write the scattering process as the modulation of a fast varying noise process with a slowly varying noise process. For the laser beam propagation problem, the electric field can be written as

$$U(t) = Ae^{i\theta} + N(t)\cdot W(t) \ , \tag{1}$$

where $Ae^{i\theta}$ is the deterministic part and $N(t)\cdot W(t)$ is the random part of the electric field [15; 17]. $N(t)$ is assumed to be slowly varying compared to $W(t)$ and is used to model the slowly fluctuating variance of the electric field. $N(t)$ is assumed to be due mainly to the larger turbulent eddies, while $W(t)$ is the result of the small turbulent eddies.

One of the ways to handle the modulation of a noise variable with a noise variable is to fix one of the random variables and then find the conditional statistics [16]. Once the conditional statistics are found, the total unconditional statistical process for the intensity is found by using

$$p(I) = \int_0^\infty p(I|n)\ p(n)\ dn \ , \tag{2}$$

where n is the random variable describing the process for the slowly fluctuating variance of the electric field,

$|N(t)|^2$. Since W(t) is the result of a large number of small turbulent eddies acting like little lenses, the process for W is assumed to be complex Gaussian distributed with a mean of zero and a variance of w_o as a consequence of the Central Limit Theorem. For the case where the deterministic part of the electric field is zero, and fixing $|N(t)|^2$ at n, the conditional PDF for the intensity fluctuations is given by the negative exponential distribution.

Assuming that the total number of modes is the result of the larger turbulent eddies and that the total number of modes is negative binomial distributed, Jakeman derived the K distribution for the intensity fluctuations for a laser beam propagating through the atmosphere when the deterministic part is zero. Andrews and Phillips proposed that the total number of modes be replaced by the effective number of modes α, enabling α to be a continuous variable. In the limit, the negative binomial PDF which is used to describe discrete processes reduces to the gamma PDF for continuous processes. Using the definitions for the negative exponential distribution and the gamma distribution as defined in Appendix A along with eq. 2, the unconditional PDF for the intensity fluctuations can be found and it is given by the family of K distributions

$$p(I) = \frac{2I^{(\alpha-1)/2}}{\Gamma(\alpha)} \left[\frac{\alpha}{b_o}\right]^{(\alpha+1)/2} K_{\alpha-1}(2\sqrt{\alpha I/b_o}) \ , \qquad (3)$$

where $0 \leq I < \infty$, α is the average number of modes, and $b_o = n_o w_o$. The mean of the intensity is simply the product of the variance of the slowly varying process, n_o, and the fast varying process, w_o.

The K distribution has been able to predict the random fluctuations in the intensity of a laser beam propagating through the atmosphere once the random fluctuations were in the saturation region [12; 13]. Also, the K distribution has been able to predict the random fluctuations that occur in both the radar sea echo and the star twinkle problems [11].

Taking the same approach that was used to derive the K distribution for the case when the deterministic part of the signal is not zero yields a conditional PDF for the intensity fluctuations that is Rician distributed. Using eq. 2 and assuming that the slowly changing random variance is again gamma distributed yields the unconditional PDF for the intensity fluctuations,

$$p(I) = \left[\frac{\alpha}{n_o w_o}\right]^{\alpha} \frac{2(A\sqrt{I})^{\alpha-1}}{\Gamma(\alpha)} \sum_{n=0}^{\infty} \frac{(2n+1-\alpha)\Gamma(1-\alpha+n)^2}{n!n! \quad \Gamma(1-\alpha)} E_{2n} \qquad (4)$$

where

$$E_{2n} = \begin{cases} I_{2n+1-\alpha}(2A\sqrt{\alpha/n_o w_o})\, K_{2n+1-\alpha}(2\sqrt{\alpha I/n_o w_o}) & I > A^2 \\ I_{2n+1-\alpha}(2\sqrt{\alpha I/n_o w_o})\, K_{2n+1-\alpha}(2A\sqrt{\alpha/n_o w_o}) & I \leq A^2 \end{cases} . \quad (5)$$

Eq. 4 is known as the HK distribution and was originally proposed by Jakeman but was derived by Link [19].

Previously, only the moments had been computed for the HK distribution. Because of the complexity of the HK distribution, Andrews and Phillips sought a closed form approximation to the HK distribution [13]. In deriving the characteristic function for the HK distribution, it was noticed that the characteristic function contained the confluent hypergeometric function. It was also noticed that the confluent hypergeometric function was approximately unity for both weak and strong turbulent conditions. Andrews and Phillips approximated the confluent hypergeometric function as unity for all turbulent conditions. Then by taking the inverse Fourier transform of the characteristic function, a closed form approximation for the HK distribution was found and was named the I-K distribution, i.e.,

$$p(I) = \frac{2\alpha}{n_o w_o}\left[\frac{\sqrt{I}}{A}\right]^{\alpha-1}$$

$$\cdot \begin{cases} I_{\alpha-1}(2A\sqrt{\alpha/n_o w_o})\, K_{\alpha-1}(2\sqrt{\alpha I/n_o w_o}) & I > A^2 \\ I_{\alpha-1}(2\sqrt{\alpha I/n_o w_o})\, K_{\alpha-1}(2A\sqrt{\alpha/n_o w_o}) & I \leq A^2 \end{cases} . \quad (6)$$

For the case when A equals zero, the I-K distribution also reduces to the K distribution. For the special case when α equals unity, the I-K PDF and the HK PDF are identical.

Preliminary work has lead to an extended turbulence model that predicts the parameter α and the SNR, $A^2/n_o w_o$, as a function of propagation distance [20]. The extended turbulence model uses an initial normalized second moment at a short distance from the laser to compute the index of refraction structure parameter, C_n^2. Once the index of refraction structure parameter, inner scale, and the wavelength of the laser are known, the normalized moments of the I-K distribution as a function of distance can then be predicted. The normalized moments for the I-K distribution with the parameters chosen in this way seems to fit the experimental data remarkably well.

Detailed derivations of stationary statistical models derived from Gaussian processes is given in Appendix B. In Appendix B, the gamma, the negative exponential and the Rician distributions are derived. In Appendix C, a

detailed development of nonstationary statistical models is provided, all of which are derived from stationary Gaussian statistics. These include the K, HK, and I-K distributions. Also in Appendix C, the normalized moments for the K, HK, and I-K distributions are derived.

SINGLE PHASE SCREEN INTENSITY EXPERIMENTS

To scale within several hundred feet the several kilometer path lengths required for the intensity experiments of a laser beam propagating through the open atmosphere, a thin propane burner was used to introduce a thin layer of hot air to impress random spatial phase fluctuations across the laser beam surface. The burner produced a flame that was 0.375 inches wide, 12 inches long and 0.75 inches high. These random phase fluctuations introduce a random interference term in the equation defining the intensity fluctuations. The random phase fluctuations are the result of small turbulent eddies acting like small random lenses. The distances required to reach the focusing region (maximum statistical normalized moments) for the statistics can be scaled from several hundred meters to approximately 50 feet. The burner induced phase fluctuations scale the propagation distance because the temperature gradients of the turbulent eddies produced by the burner are much larger than the temperature gradients of the turbulent eddies existing in the open atmosphere. Hence, the random lenses produced by the burner have focal lengths that are much

smaller than the random lenses produced in the open atmosphere. Since the burner introduces random phase fluctuations, it has been appropriately referred to in the literature as a random phase screen [8; 9].

In Figure 2, the block diagram for single phase screen experiments is given. A 10 mw linearly polarized helium-neon laser from Hughes Corporation was used as the laser source. The laser beam was collimated at two inches in diameter so that the laser beam's size was much larger than most of the turbulent eddies introduced by the phase screen. At the focal plane of the collimator, a 10 μm pinhole was used to spatially filter the spatial modes from the laser so that the number of modes emerging from the collimator was about unity. The collimator was aligned by adjusting the laser beam size to two inches at a distance of 300 feet. Under these conditions, the two inch laser beam emerging from the collimator was considered to be a plane wave.

The phase screen was placed in front of the collimator of 6 inches below the optical axis of the collimator. A flame height of 0.75 inches was found to be the most optimal, since at this flame height the burner's flame produced a laminar flow immediately above the flame's tip. Mirrors were used to fold the laser beam

SINGLE PHASE SCREEN BLOCK DIAGRAM

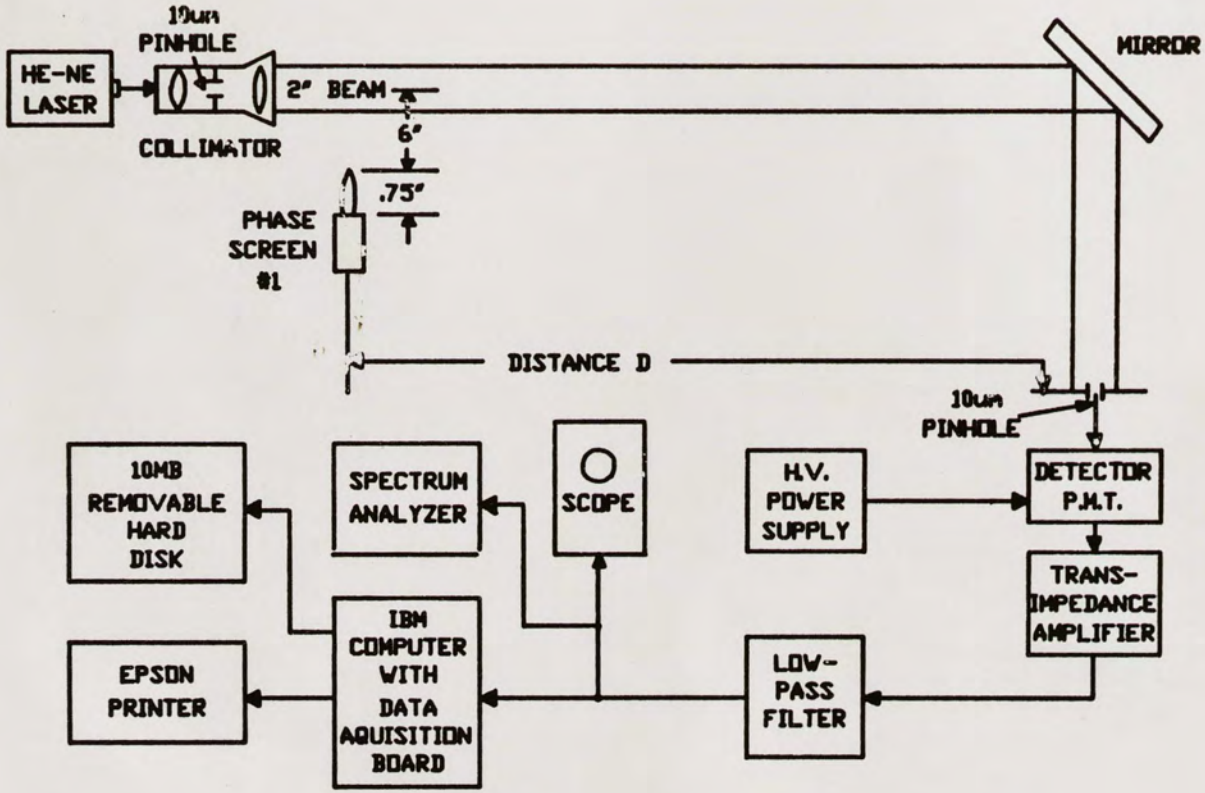

Figure 2. Block Diagram for Single Phase Screen Intensity Experiments.

path so that a propagation distance of 100 feet could be achieved in a 30 foot long laboratory.

For set distances, a 10 μm pinhole and a photo-multiplier tube (PMT) were used to detect the random fluctuations introduced into the laser beam by the phase screen. The pinhole was used to limit the aperture size of the detector in order to minimize aperture averaging of the spatial fluctuations. During a preliminary setup of the experiment, it was noticed that a 50 μm pinhole averaged some of the spatial fluctuations. Averaging the spatial fluctuations by the detector reduced the experimentally measured statistical moments.

The output of the PMT was tied directly into the input of a transimpedance amplifier where the high impedance output of the PMT was converted to a low impedance output. The transimpedance amplifier's output was then fed to the input of a single pole lowpass filter to reduce the bandwidth of the system. If the lowpass filter was not used, the shot noise from the PMT would dominate the low level variations in the intensity fluctuations and modify the computed statistical moments. The lowpass filter setting was set to a cutoff frequency of 1 kHz, which was about the same frequency where the spectrum of the intensity fluctuations was approximately zero.

The output of the lowpass filter was then fed into an oscilloscope for viewing, a Hewlett Packard HP-3551A spectrum analyzer, and an IBM Personal Computer (PC) with a data acquisition board. The spectrum analyzer was used to measure the spectrum of the intensity fluctuations, whereas the IBM PC sampled the intensity fluctuations. The computer sampled the intensity fluctuations at a rate of 1 kHz for 100 seconds. This resulted in a total of 100,000 sampled data points. For a detailed discussion of the data acquisition system, refer to Appendix E.

To maintain a somewhat controlled laboratory environment, the thermostat for the laboratory was set to 60 degrees Farenheit, and the phase screen was left on only during the short sampling time of the experiment. When an experiment was started, the phase screen was turned on and allowed to reach a steady state condition before any data was taken. After the data was collected by the computer, the phase screen was turned off and the laboratory was allowed to cool back down to its steady state temperature of 60 degrees Farenheit.

The first experiment performed was to vary the height of the burner with respect to the optical axis of the collimator, and compute the normalized moments of the intensity fluctuations induced by the phase screen. The normalized moments were computed by the expression

$$\frac{\langle I^n \rangle}{\langle I \rangle^n} = \frac{\frac{1}{m} \sum_{k=1}^{m} I_k^n}{\left[\frac{1}{m} \sum_{k=1}^{m} I_k\right]^n} , \qquad (7)$$

where m is the total number of sampled data points, I_k is the kth sample of the intensity data, and $\langle I^n \rangle$ is the nth moment of the intensity data.

In Figure 3, the normalized second moment versus the distance between the collimator's optical axis and the burner is shown. With the detector placed at a distance of 30 feet behind the phase screen, a height of 6 inches produced the highest normalized second moment indicating that at this distance the phase screen introduced the maximum random phase fluctuations across the laser beam surface. Since the phase screen produced a laminar flow immediately above the flame, it is not unreasonable to expect the normalized second moment to drop as the distance between the flame and the optical axis of the collimator decreased. As the distance between the phase screen and the optical axis of the collimator became increasingly larger, the temperature differential induced by the burner became smaller, resulting in the phase screen introducing weaker random phase fluctuations across the laser beam surface. Again, the normalized second

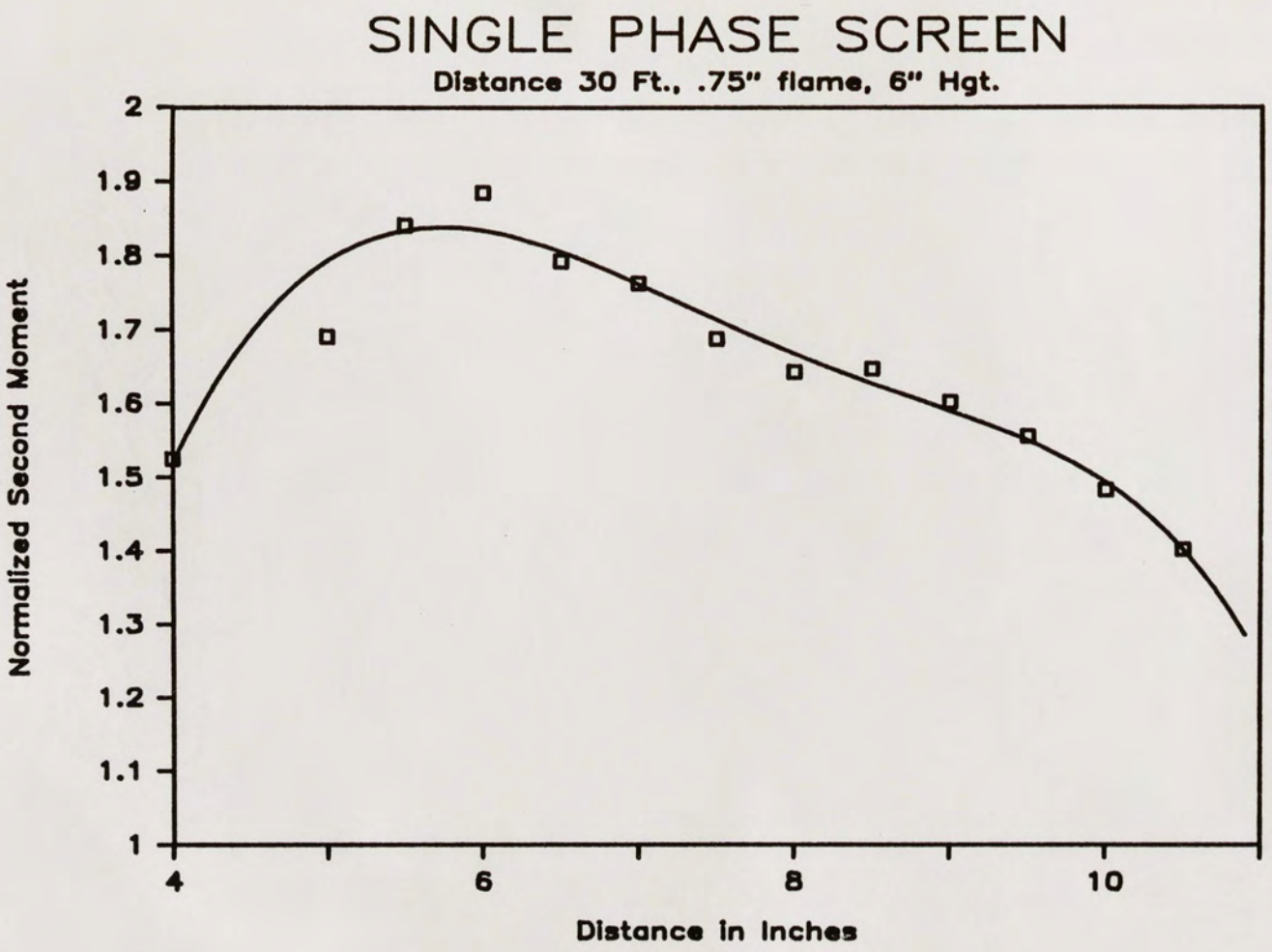

Figure 3. Maximum Normalized Second Moment Experiment.

moment for the intensity fluctuations decreased at the greater heights.

Setting the distance between the phase screen and the center of the laser beam at 6 inches so that the highest normalized moments could be achieved, the next experiment performed measured the normalized moments as a function of propagation distance behind the phase screen. In Figure 4, the normalized second, third, fourth and fifth moments are plotted as a function of distance. The normalized moments are approximately unity for a short distance behind the phase screen, indicating that there were very small fluctuations in the intensity of the laser beam. The normalized moments continued to increase in value until the saturation region was reached around 47 feet. At a distance of 47 feet, the maximum value for the normalized second moment was obtained and was 2.73. For distances beyond 47 feet, the moments tend to decrease with distance. It previously has been shown theoretically that for long propagation distances, the intensity statistics eventually converge to the negative exponential distribution [13]. From Figure 1, at a distance of 100 feet, the normalized moments for the experimental data are approaching the normalized moments of the negative exponential distribution.

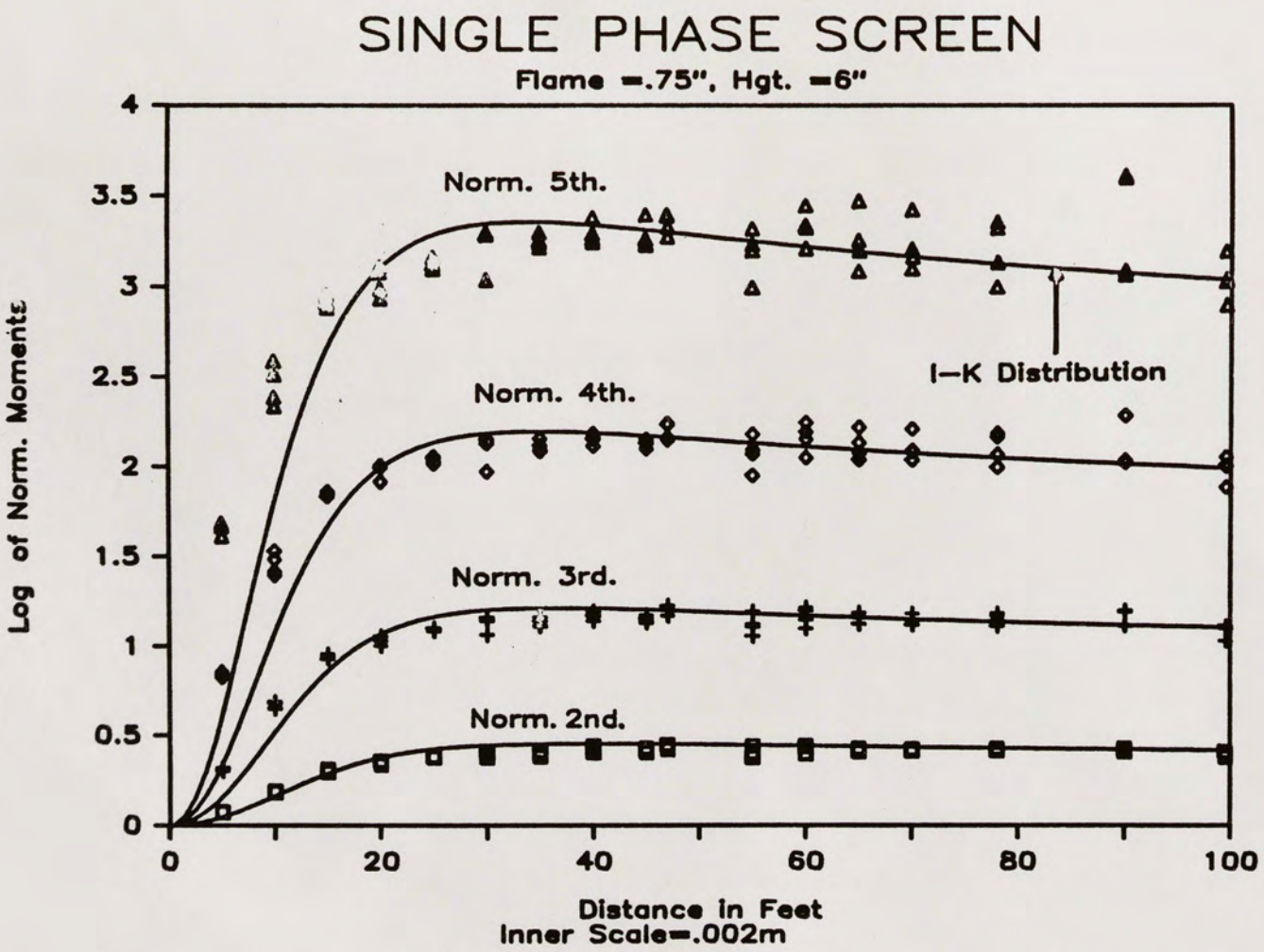

Figure 4. Normalized Moments for a Single Phase Screen as a Function of Distance.

The solid curve in Figure 4 is the prediction of the moments using the extended turbulence model to select the parameters of the I-K distribution with an inner scale of .002 meters. To compute the effective index of refraction structure parameter C_n^2, the normalized second moment for 10 feet was used, yielding an effective C_n^2 of 3.9E-10 $m^{-2/3}$. Except for short distances up to 30 feet, the extended turbulence model predicts the normalized moments extremely well. Currently, there is no extended turbulence model using the HK distribution.

Figures 5 and 6 display the time series plots for the intensity fluctuations for 5 feet and 100 feet, respectively, behind the phase screen. The time series plot for a distance of 5 feet behind the phase screen shows that the random nature of the intensity fluctuations is very intermittant. In other words, the time in which the variance of the electric field is constant is very short. For a distance of 100 feet, the time series plot shows that the variance is more uniform and appears to be constant for longer periods of time.

The spectrum for the intensity fluctuations is given in figures 7 and 8 for distances of 5 feet and 100 feet, respectively. Both spectrum plots show a dual slope power law spectrum relation. The lower frequency slope is calculated to be -0.6 log(volts)/log(hz), at both

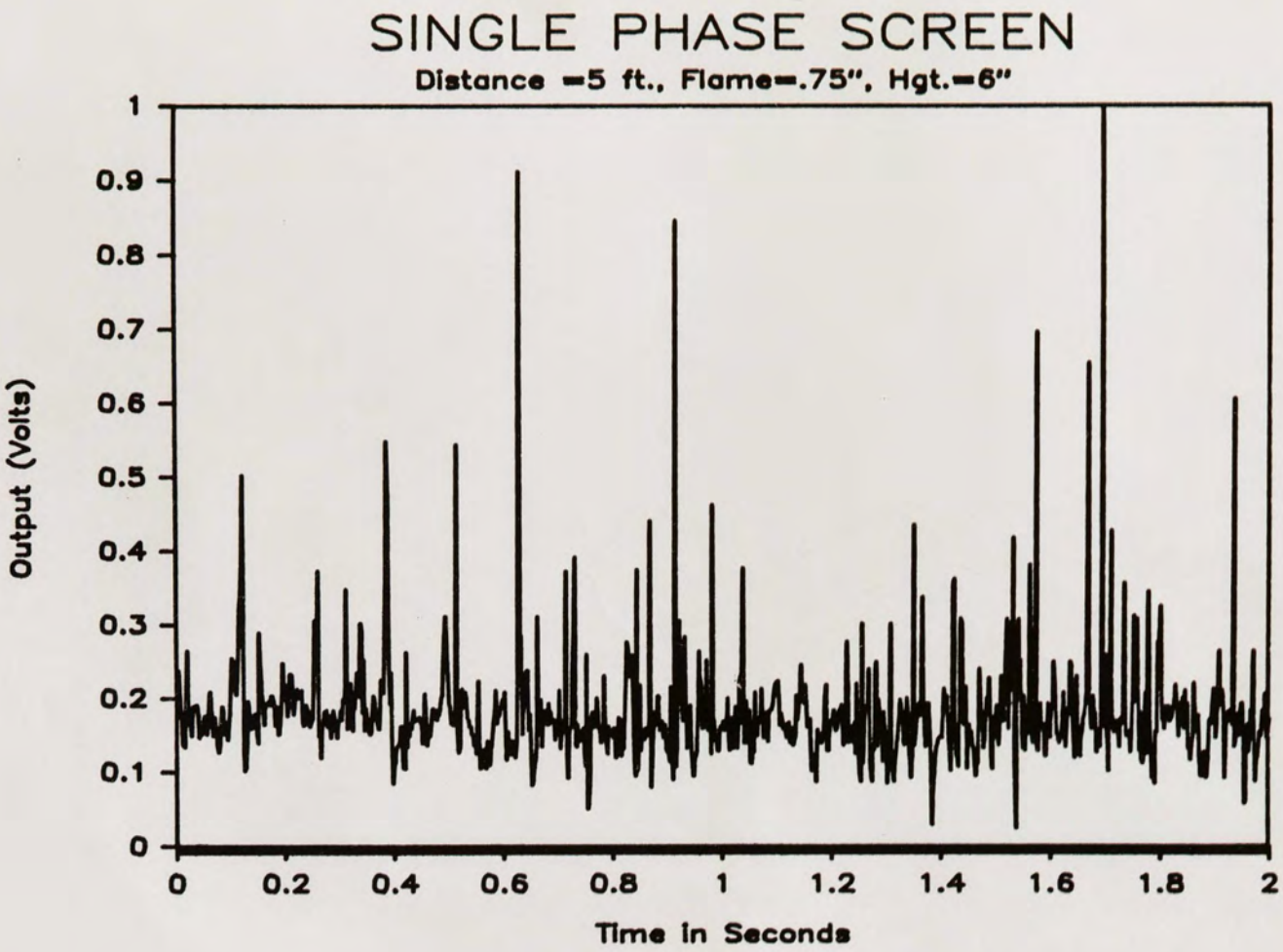

Figure 5. Time Series Plot for a Single Phase Screen for a Distance of 5 Feet.

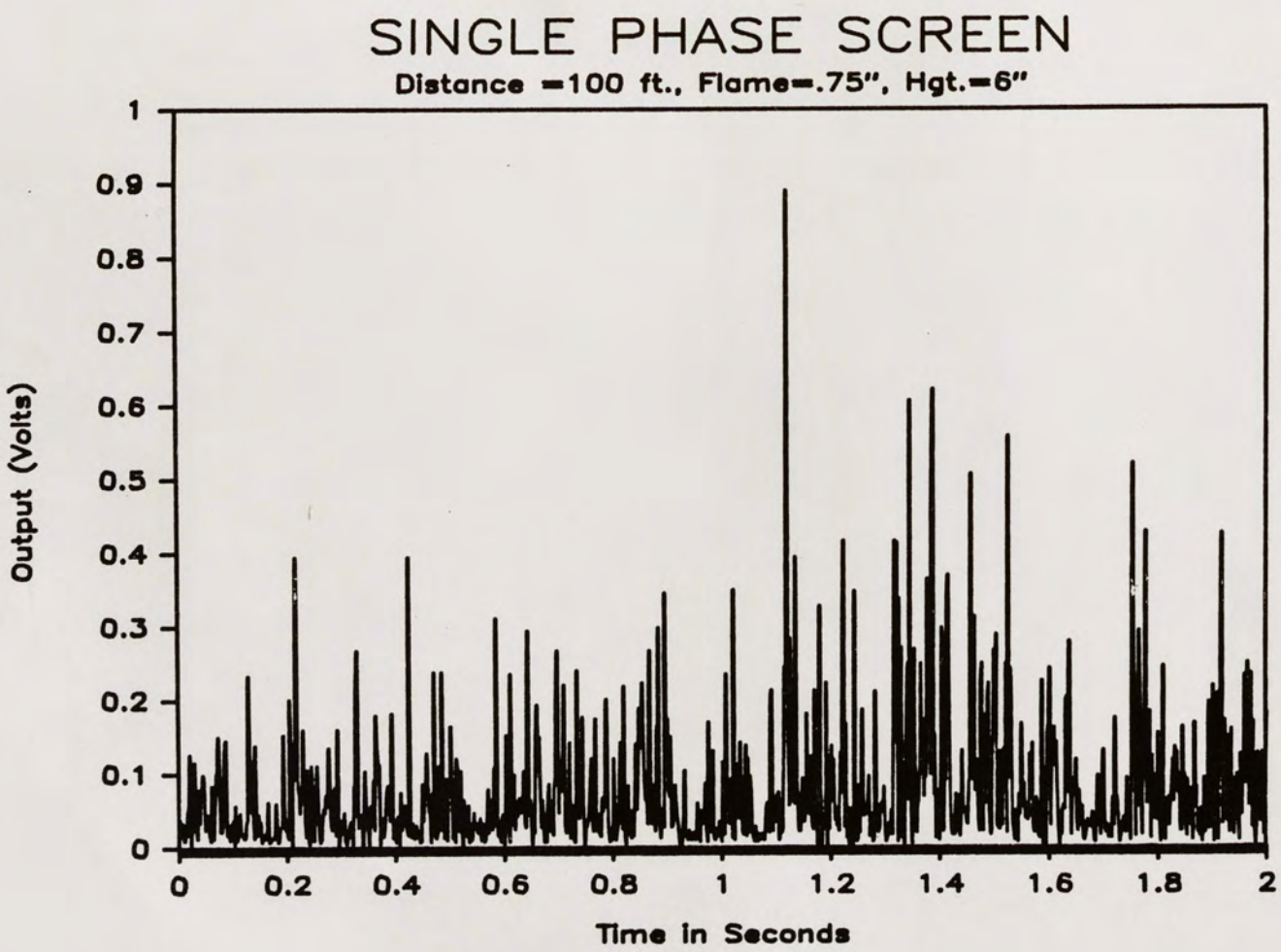

Figure 6. Time Series Plot for a Single Phase Screen for a Distance of 100 Feet.

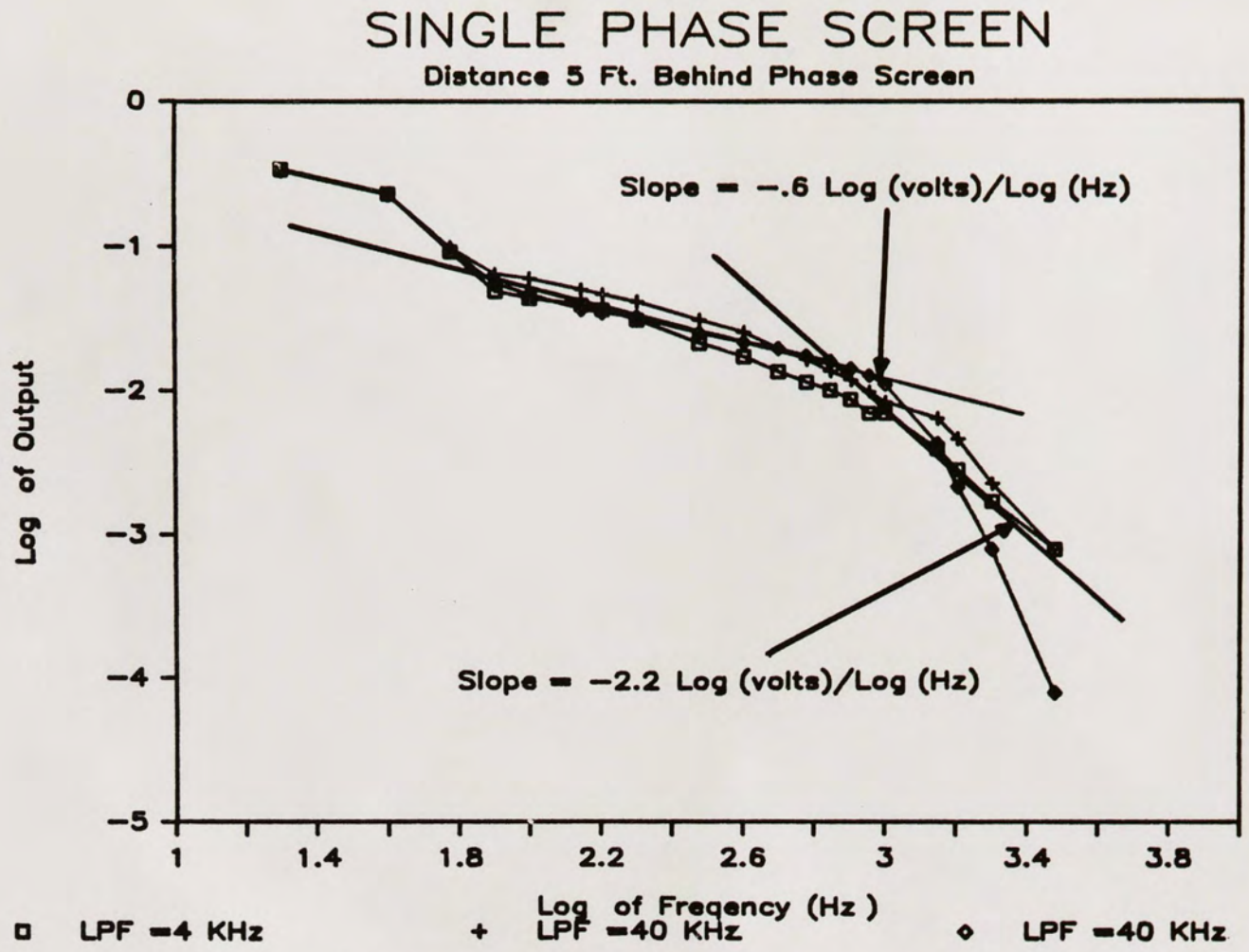

Figure 7. Spectrum Data for a Single Phase Screen for a Distance of 5 Feet.

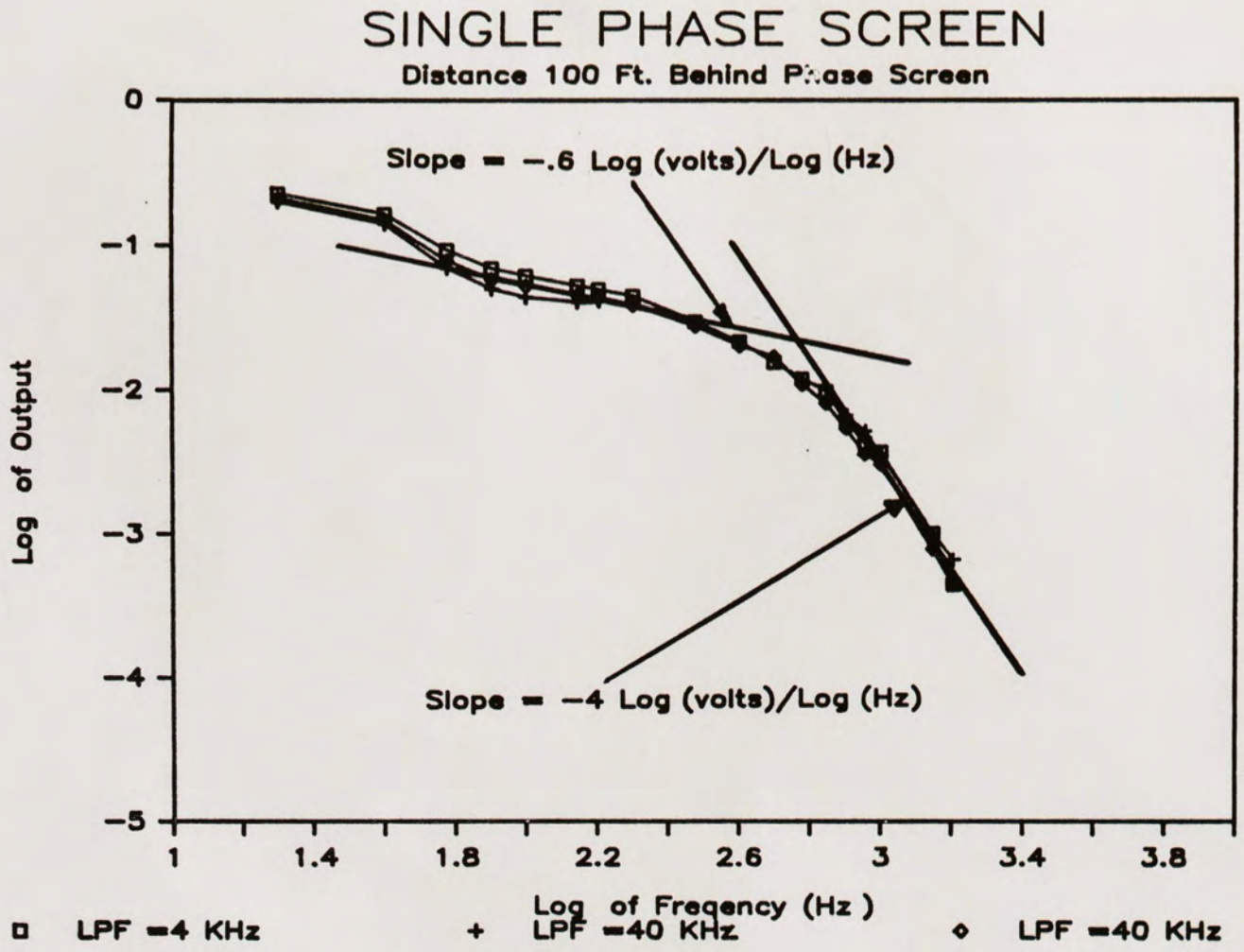

Figure 8. Spectrum Data for a Single Phase Screen for a Distance of 100 Feet.

distances of 5 and 100 feet from the phase screen. The higher frequency slopes were calculated to be -2.2 log(volts)/log(hz) at a distance of 5 feet and -4 log(volts)/log(Hz) at a distance of 100 feet behind the phase screen. The only difference in the two spectrums is the data taken at a distance of 5 feet from the phase screen has more energy contained in the higher frequencies.

EXPERIMENTAL MEASUREMENTS OF THE CONDITIONAL STATISTICS

In the development of the HK distribution, the conditional statistics for the fluctuations in the intensity of the laser beam were derived as a Rician distribution. In addition, the fluctuations in the variance of the electric field were assummed to be gamma distributed. Then by using eq. 2, the unconditional PDF was found to be the HK PDF. In this derivation, both the Rician and the gamma distributions were used because of the assumption that the underlying physical processes were Gaussian distributed.

Recall that the electric field can be written in the form

$$U(t) = A + N(t) \cdot W(t) \ , \tag{8}$$

where the deterministic phase term has been assumed to be zero for ease of notation. N(t) represents the slow fluctuating variance and W(t) describes the fast fluctuations in the electric field. By proper filtering of the experimental data, such as lowpass filtering or segmenting the data into small segments in which the

variance is constant, the two random processes describing the field can be approximately separated from each other.

Gamma Statistics

Since the slowly fluctuating variance is assumed to be gamma distributed, the most obvious method of removing the fast varying fluctuations in the intensity would be to lowpass filter the intensity data. Using eq. 8 for the electric field, the intensity is then given by

$$I(t) = A^2 + A \cdot W(t) \cdot N(t)^* + A \cdot W(t)^* \cdot N(t) + |N(t)|^2 \cdot |W(t)|^2 \ , \qquad (9)$$

where N(t) and W(t) are assumed to be complex valued functions of time and * denotes the complex conjugate. Since multiplication in the time domain yields convolution in the frequency domain, the product of N(t) with W(t) results in their spectrums being smeared together. Hence, the last three terms in eq. 9 involve the convolution of the spectrum of N(t) with the spectrum for W(t).

In Figure 9, the proposed spectrums for N(t) and W(t) are given. The N(t) spectrum is assumed to be centered around DC and to have a much wider bandwidth than W(t). On the other hand, W(t) is assumed to be shifted up in spectrum with a narrow bandwidth relative to its center frequency. The assumption that the spectrum for W(t) is very narrow physically implies that the small turbulent

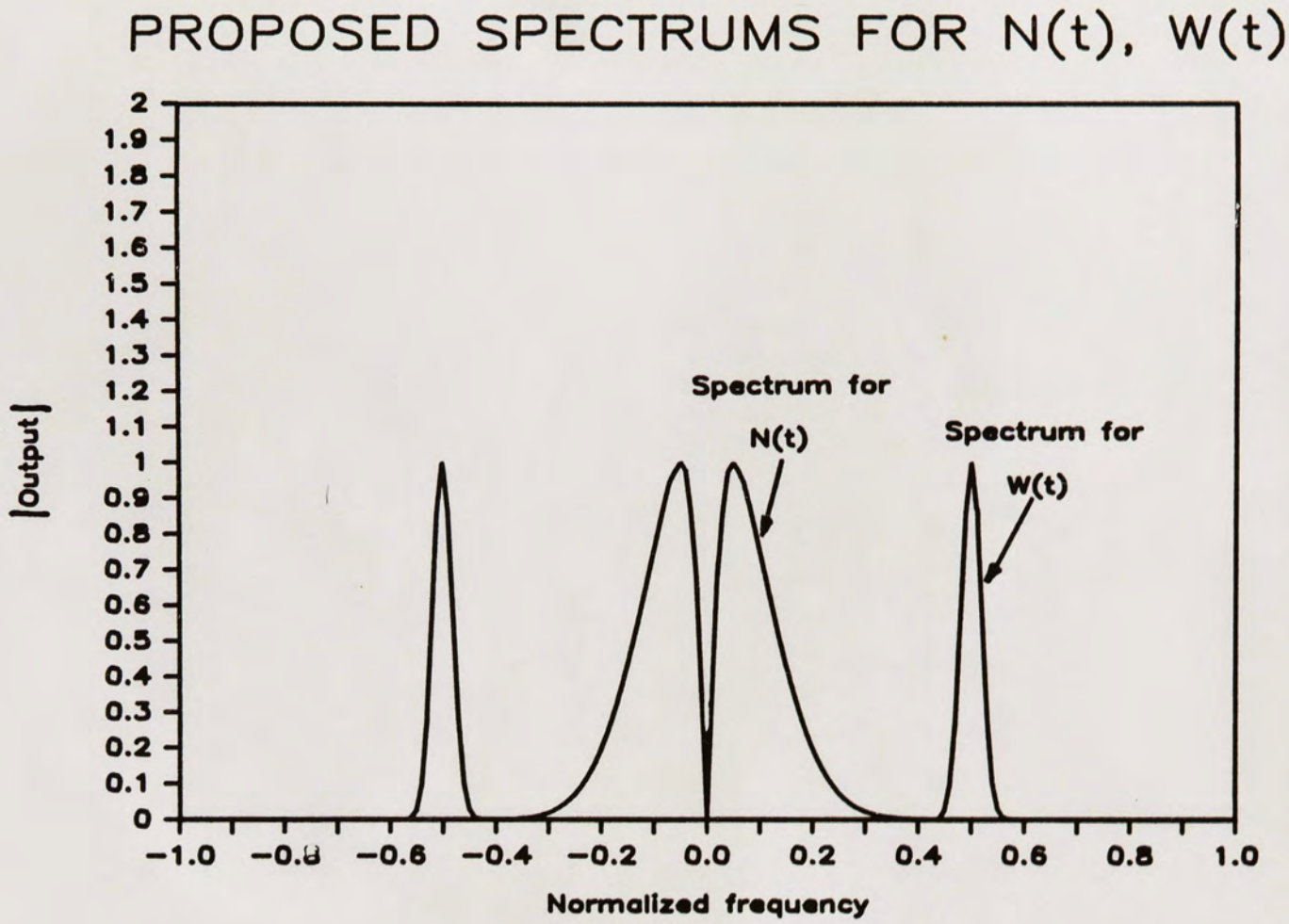

Figure 9. Proposed Spectrum for N(t) and W(t).

eddies are all about the same size. This assumption is not unreasonable based on the experimental data that was taken in the laboratory. In addition, several high speed 16 mm movies of the intensity fluctuations showed that the eddies were all about the same size. For more details on these high speed movie experiments, refer to Appendix D.

To find the spectrum of the product of N(t) with $W(t)^*$ or $N(t)^*$ with W(t), the two spectrums in Figure 9 must be convolved together. From Figure 9 and by graphical convolution, the spectrum for these products would approximately be the spectrum for N(t) shifted up in frequency and distributed symmetrically around the center of the spectrum for W(t). If the bandwidth for the spectrum of N(t) is smaller than half the center frequency for the spectrum of W(t), there will be no overlap in the total spectrum, i.e., no aliasing. The net effect is that the energy in the spectrum for the product of N(t) with $W(t)^*$, or $N(t)^*$ with W(t), will be shifted up in frequency and mainly concentrated about the center frequency for the spectrum of W(t). If the intensity data as described by eq. 9 is lowpass filtered, the two cross product terms will be approximately zero.

Lowpass filtering the intensity fluctuations yields

$$I(t)_{LPF} = A^2 + \left| |N(t)\cdot W(t)|^2 \right|_{LPF} . \qquad (10)$$

In figures 10 and 11, the spectrums for $|N(t)|^2$, $|W(t)|^2$ and $|N(t)\cdot W(t)|^2$ are given. The spectrum for $|N(t)|^2$ is simply the spectrum for N(t) convolved with itself.

Since the spectrum for N(t) is symmetrical about DC, the spectrum for $|N(t)|^2$ is also centered on DC with a bandwidth double that of $|N(t)|$. It should be pointed out that even though the spectrum for W(t) is not centered on DC, part of the spectrum for $|W(t)|^2$ will be centered on DC due to the convolution of W(t) with W(t). Hence, convolving $|N(t)|^2$ with $|W(t)|^2$ yields the spectrum for $|W(t)\cdot N(t)|^2$ given in Figure 11.

By proper lowpass filtering of the proposed spectrum given in Figure 11, the spectrum that remains is approximately the spectrum for $|N(t)|^2$. Hence, the last term in eq. 10 reduces to $|N(t)|^2\cdot k$, where k is an arbitary constant. The lowpass filtered intensity fluctuations are then given by

$$I(t)_{LPF} = A^2 + |N(t)|^2\cdot k \quad . \tag{11}$$

Eq. 11 is simply a deterministic term added to a slowly varying random process that is gamma distributed. To evaluate the constant, the expected value of eq. 11 is taken, yielding

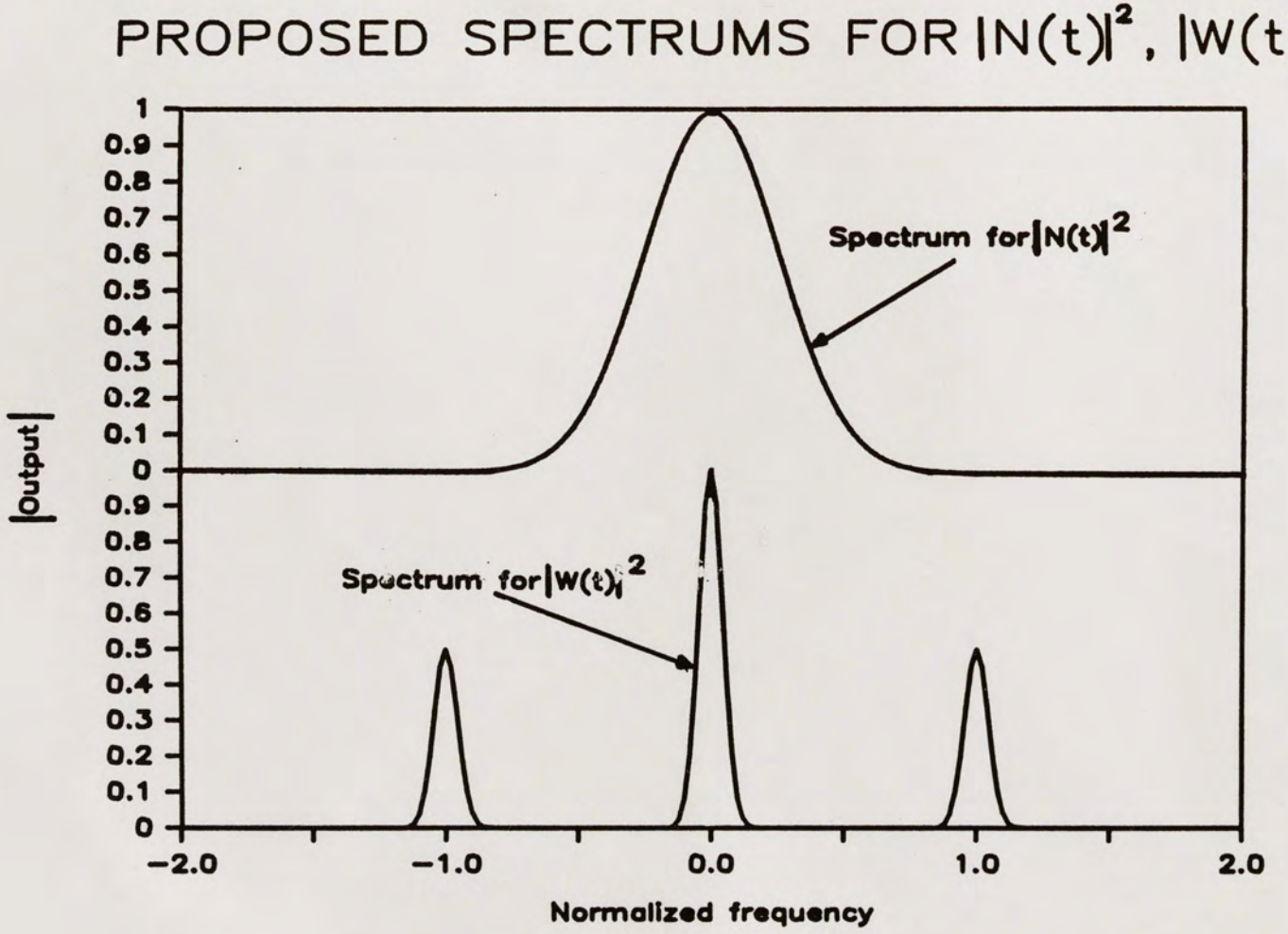

Figure 10. Proposed Spectrum for $|N(t)|^2$ and $|W(t)|^2$.

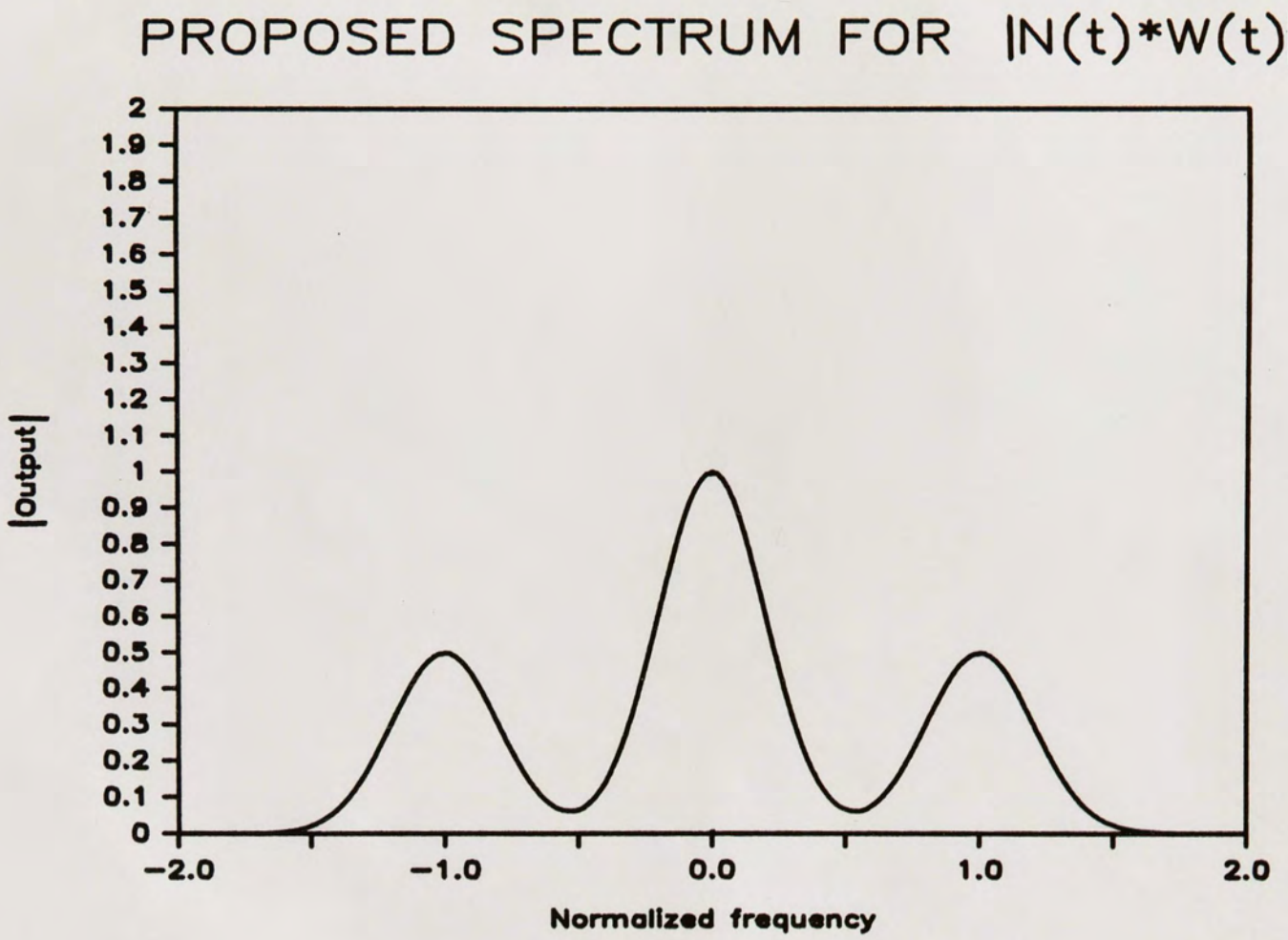

Figure 11. Proposed Spectrum for $|N(t) \cdot W(t)|^2$.

$$E\left[I(t)_{LPF}\right] = A^2 + E\left[|N(t)|^2\right]\cdot k \ . \qquad (12)$$

From eq. C-104, the expected value for the lowpassed intensity fluctuations is given by

$$E\left[I\right] = A^2 + n_o w_o \ , \qquad (13)$$

and immediately yields $k = w_o$. The final form for the lowpass filtered intensity is

$$I(t) = A^2 + w_o |N(t)|^2 \ . \qquad (14)$$

From Appendix C, the statistics for the lowpass filtered I(t) will be gamma distributed. In the derivation of eq. 14, it was assumed that the spectrum of W(t) was much smaller than the spectrum of N(t). This assumption is required if the spectrum for the second term in eq. 10 is to have approximately the same spectrum as N(t), since the convolution of the two variables yields a spectrum that is about the same size as the spectrum of the variable with the largest bandwidth.

The derivation described above is the same type of approach that would be taken if W(t) was a simple deterministic high frequency carrier modulated by a deterministic low frequency signal N(t) that was applied to the input of a square law detector and the output lowpass filtered. In the case of the laser beam

propagation phenomenon, the two terms N(t) and W(t) are not deterministic functions but are random processes.

Experimental data was taken with a single phase screen using the same experimental setup that was used for the single phase screen intensity measurements. Lowpass filtered data was then taken at various distances behind the phase screen. To measure the gamma statistics, the lowpass filter was set to a 20 Hz cutoff frequency. To determine this lowpass filter cutoff, the moments were measured at a distance of 10 feet and the lowpass filter cutoff was adjusted until the experimental moments fit the gamma moments.

To compare the moments for the experimental data with the moments of the gamma distribution, the deterministic part A^2 in eq. 14 was removed from the calculations of the experimental moments. Instead of immediately computing the normalized moments, the moments about the mean intensity were computed and compared with the moments about the mean intensity for the gamma distribution. The nth moment about the mean, $E[X^n]$ is given by

$$E\left[X^n\right] = E\left[(I-\bar{I})^n\right] = \frac{1}{m}\sum_{k=0}^{m}(I_k-\bar{I})^n \ , \qquad (15)$$

where m is the total number of sampled points, I_k is the

kth sample of the fluctuating intensity, and $\bar{I}$ is defined as the mean intensity.

From eq. C-97 describing the moments of the gamma distribution, two parameters are needed to compute the moments, viz., α and n_o. Using eq. 15 along with eq. C-97, α and n_o are related to the moments about the mean by

$$\alpha = \frac{4\ E\left[X^2\right]^3}{E\left[X^3\right]^2} \quad , \tag{16}$$

and

$$n_o = \frac{2\ E\left[X^2\right]^2}{E\left[X^3\right]} \quad . \tag{17}$$

Next the mean, n_o, of the gamma distribution was used to convert the moments about the mean to normalized moments.

Using eqs. 16 and 17 along with the mean, n_o, to remove A^2 in the calculation of the normalized moments resulted in the matching of the mean, the normalized second, and the normalized third moment of the gamma distribution with the experimental normalized moments. Since the first three moments of the gamma distribution were matched identically with the experimental moments, only the normalized fourth and fifth moments were used to compare the theoretical results to the experimental data.

The corrected normalized third, fourth and fifth moments versus the normalized second moment for the lowpass filter data is given in Figure 12. The solid lines are graphs of the normalized moments predicted by the gamma distribution. Figure 13 gives the normalized second moment as a function of distance and shows that the normalized second moment for the lowpass filtered data decreases as the distance behind the phase screen increases. For distances greater than 30 feet, Figure 12 shows an excellent fit between the experimental and the gamma distributed normalized fourth and fifth moments. For distances less than 30 feet, it is believed that one possible cause for the slight error is that the spectrums for either N(t) or W(t) have become large resulting in the overlap of their spectrums, thus making it impossible to separate N(t) from W(t).

Figures 14 and 15 plot the number of modes, α, and the SNR, ρ, respectively, as a function of distance behind the phase screen. It is known that for large propagation distances, the intensity fluctuations can be predicted by the negative exponential distribution [13]. The statistics for the fluctuating variance must therefore eventually approach a constant and the SNR, ρ, must eventually approach zero, if eq. 2 is to yield negative exponential statistics. When ρ is equal to zero, the

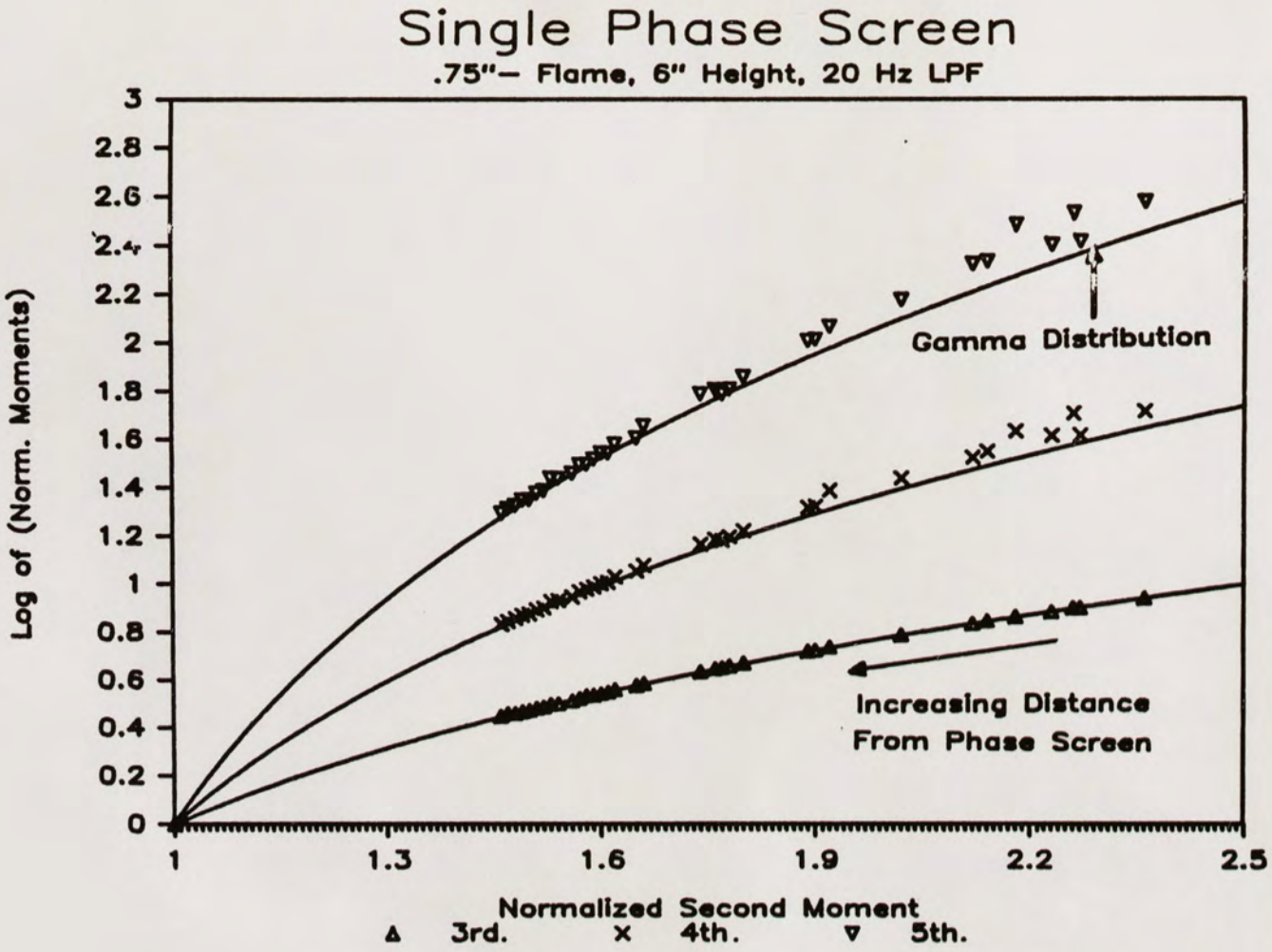

Figure 12. Normalized Moments for the Lowpass Filter Experiment.

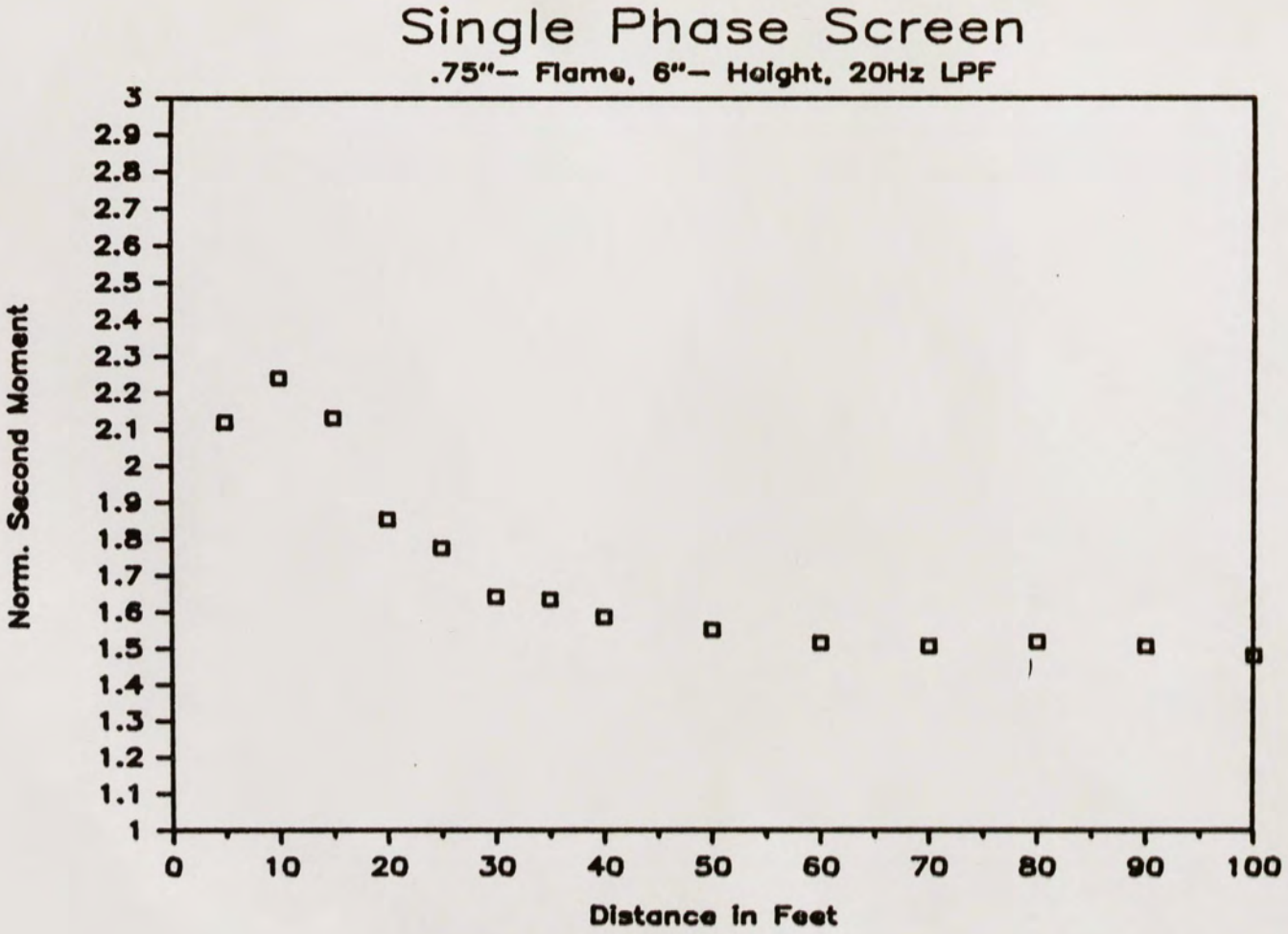

Figure 13. Normalized Second Moment vs. Distance for the Lowpass Filter Experiment.

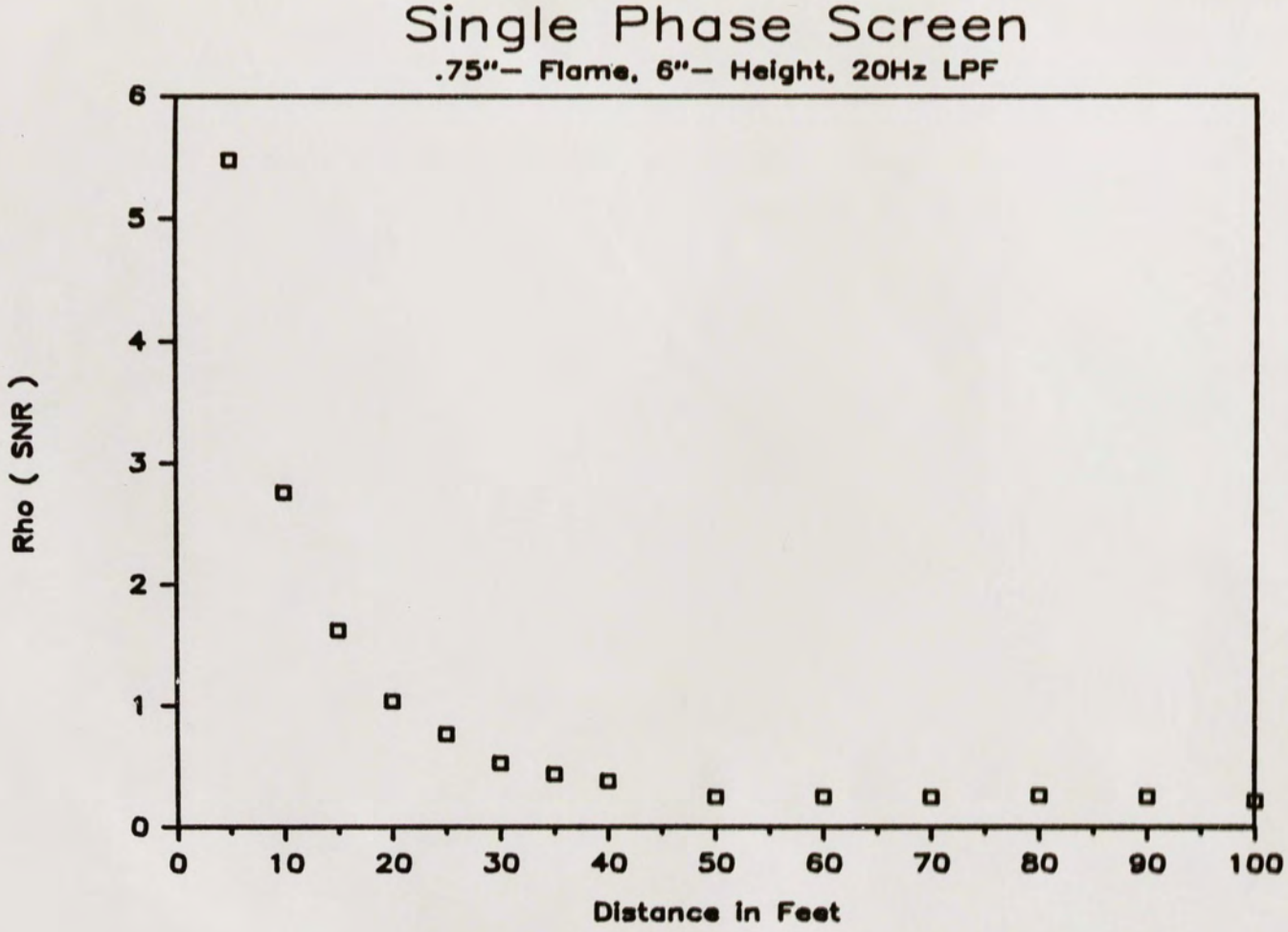

Figure 14. ρ vs. Distance for the Lowpass Filter Experiment.

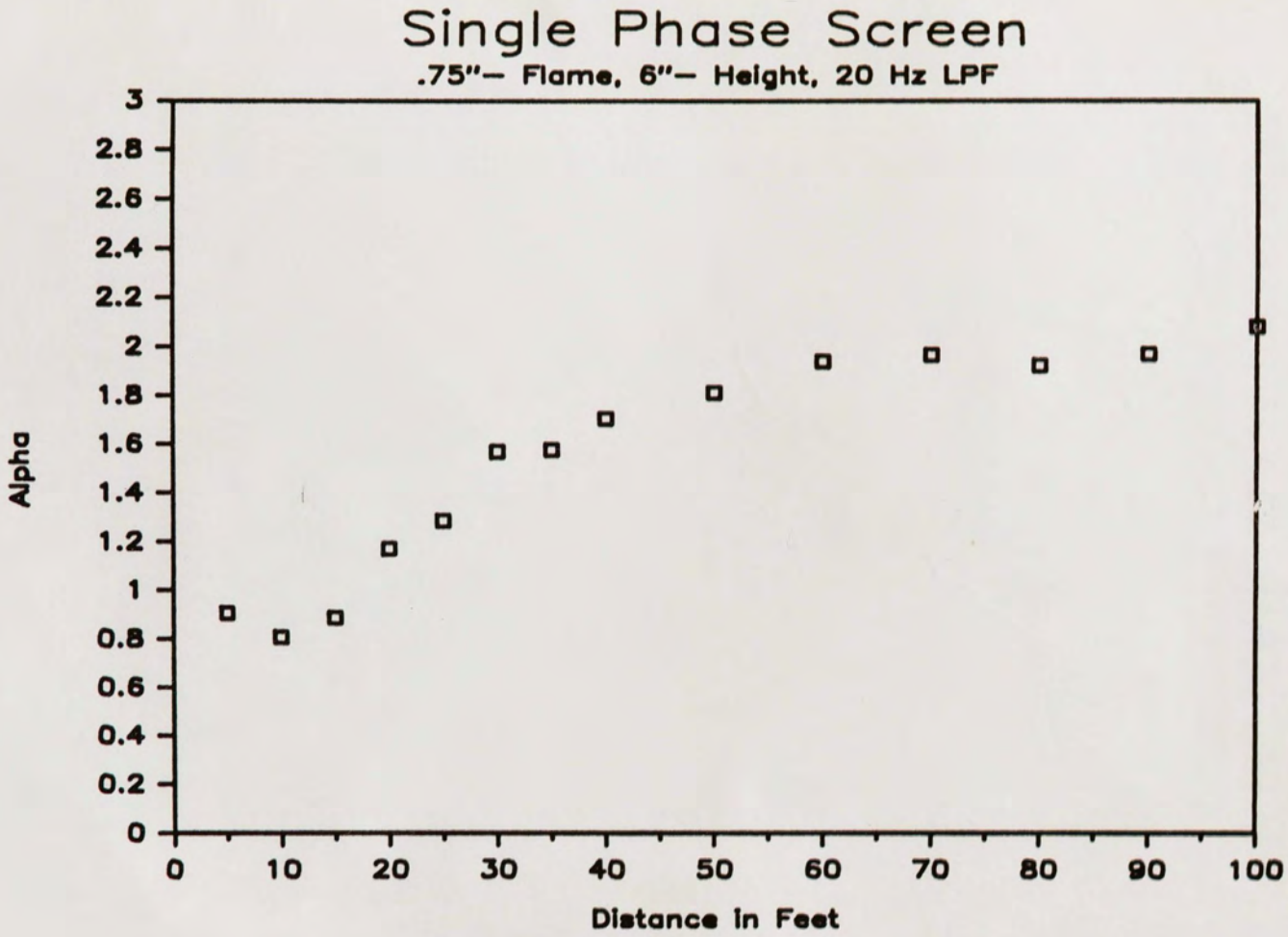

Figure 15. α vs. Distance for the Lowpass Filter Experiment.

conditional statistics for the intensity fluctuations reduce to the negative exponential distribution. With the conditional statistics described by the negative exponential distribution and the distribution for the variance described by a delta function, evaluation of eq. 2 yields a negative exponential distribution for the unconditional intensity statistics.

In the limit as α approaches infinity, the gamma distribution approaches a delta function at n_o. Figure 15 shows that α is monotonically increasing for distances larger than 10 feet. Once the saturation region is reached, α increases very slowly with distance. Hence, the intensity statistics approach the negative exponential distribution very slowly. In addition to α increasing with distance, Figure 14 shows that ρ is decreasing with distance. Since the normalized moments for the intensity statistics are close to unity for short distances, which implies that the intensity fluctuations are small compared to A^2, it is not unreasonable to expect large values for ρ at short distances and for ρ to decrease monotonically with distance.

Since α and ρ are known as a function of distance behind the phase screen (figures 14 and 15), the normalized moments for the HK and the I-K distributions were computed as a function of distance behind the phase

screen. In Figure 16, the normalized second, third, fourth, and fifth moments are plotted as a function of distance for both the HK and I-K distributions. Also, the normalized moments for the single phase screen intensity experiments are shown. Considering the method in which the parameters were chosen, both the HK and the I-K distributions fit the experimental data extremely well. The possible reason that the predicted moments are slightly low is that lowpass filtering truncates part of the spectrum of $|N(t)|^2$, resulting in an incorrect estimate of α and ρ. It should also be noted that an approximation was made to the characteristic function of the HK distribution in deriving the I-K distribution; hence, the similarity of the normalized moments for both distributions is expected.

The last experiment performed involving lowpass filtering the intensity fluctuations was to verify that the moments remained gamma distributed independent of the time over which the data was averaged. In Figure 17, the normalized third, fourth, and fifth moments versus the normalized second moment for a distance of 62 feet behind the phase screen is shown. A distance of 62 feet was chosen because at this distance A^2 was one-fourth of $n_o w_o$, allowing A^2 in eq. 14 to be assumed to be zero. Instead of computing the moments over a time interval of 100

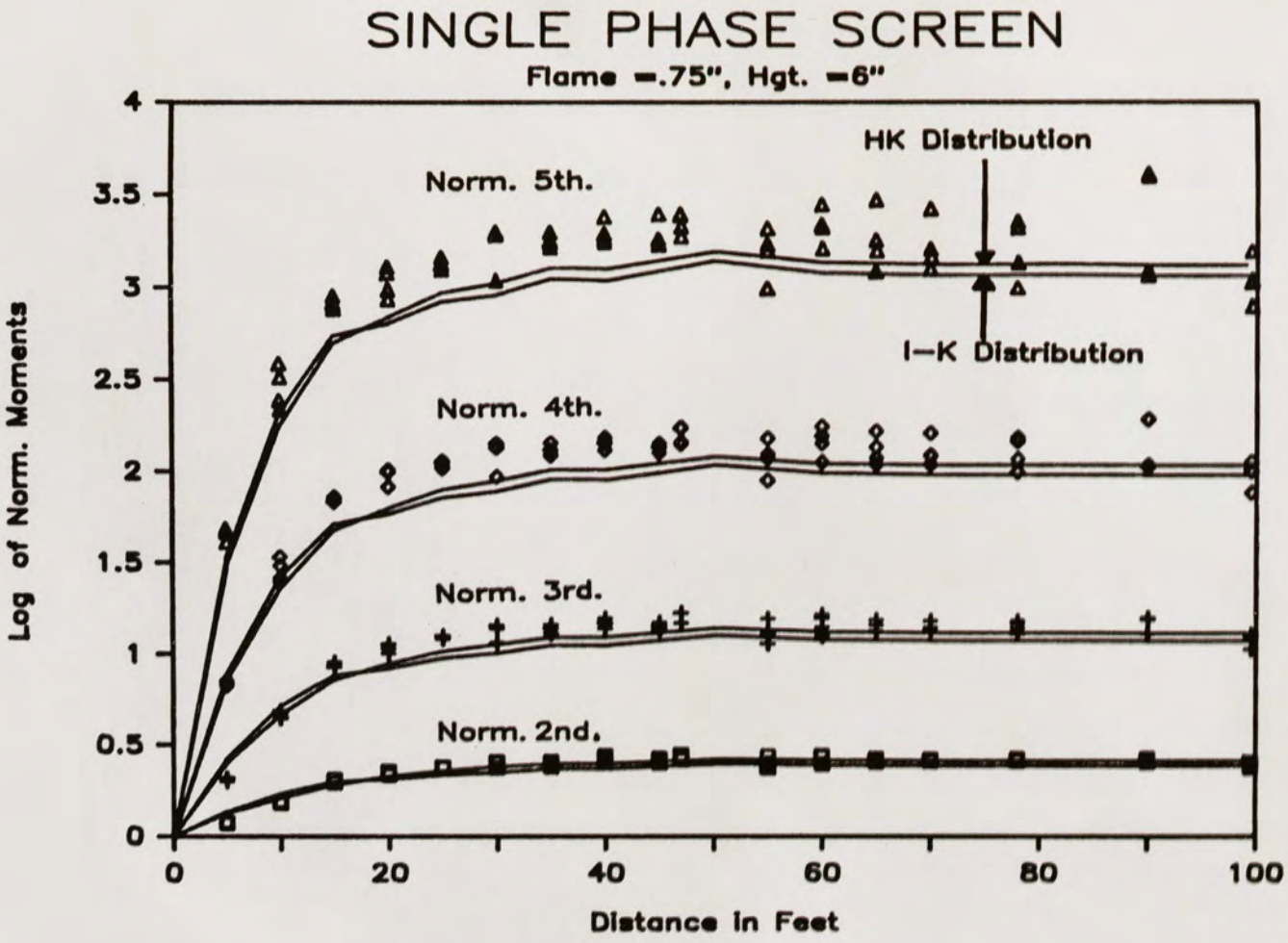

Figure 16. HK and I-K Normalized Moments vs. Distance Using the Lowpass Filter Parameters in Figures 14 and 15.

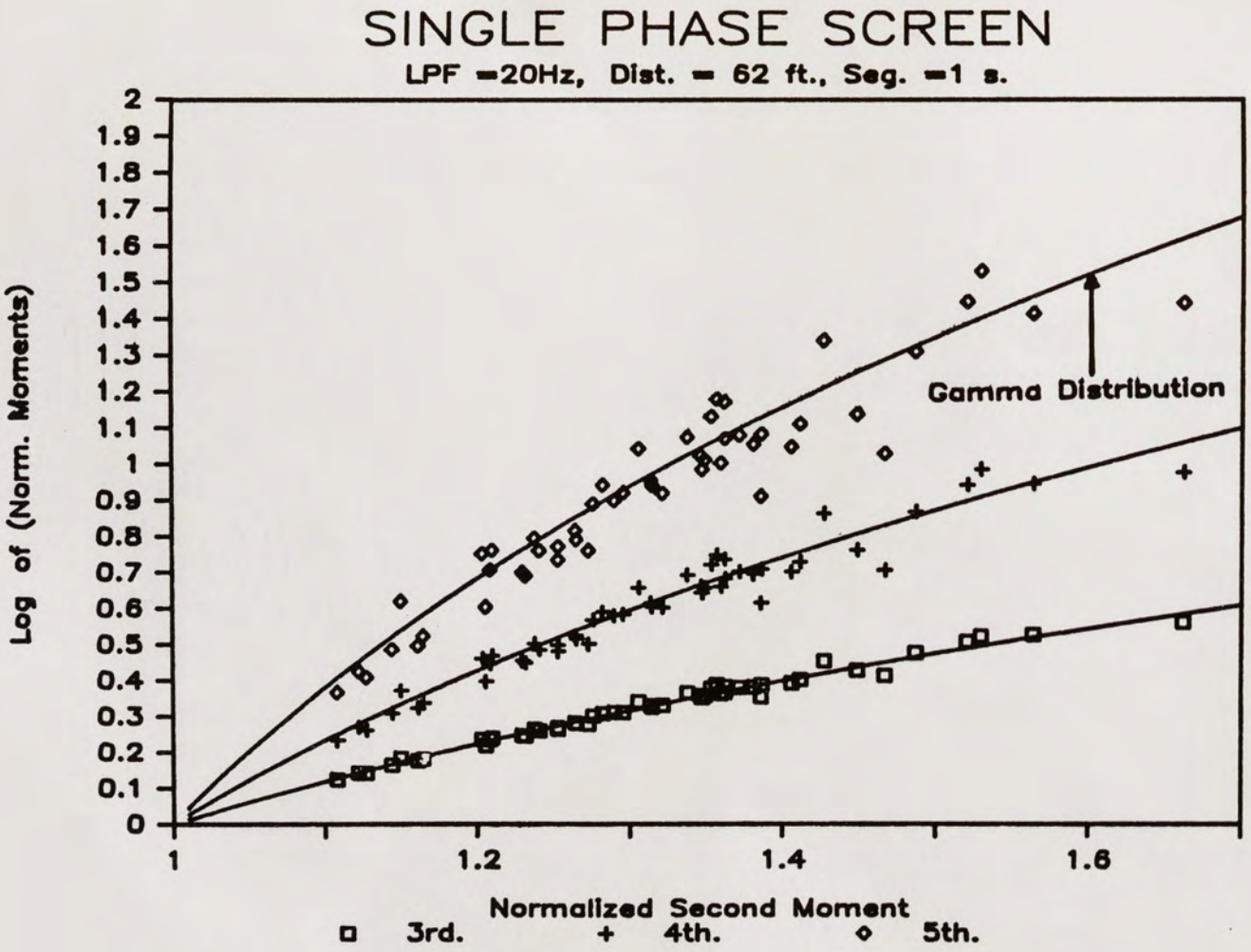

Figure 17. Normalized Moments for the Lowpass Filter Experiment by Segmenting the Data.

seconds as previously done to compute the normalized moments in Figure 12, the 100 seconds of data was divided into 100 one second time interval segments.

The moments for each segment were then computed and compared with moments of the gamma distribution. Except for the additional scatter due to averaging over fewer data points, the experimental moments for the lowpass filter experiment still appears to be gamma distributed. It should be noted that for this experiment, only the experimental normalized second moment was used to determine α in the gamma distribution. Since the computation of the moments for the lowpass filter experiment was independent of the time interval used to compute the moments, it is not unreasonable to assume that the process for $|N(t)|^2$ was stationary.

Rician Statistics

To find the conditional statistics for the intensity fluctuations, the process for the slowly changing variance must be assumed to be a constant. From Appendix C, when $N(t) = n_o$, a constant, the distribution describing the intensity fluctuations will be Rician distributed. One way of measuring the process for a constant variance is to divide the time series data for the intensity fluctuations into small time intervals (bins) in which the variance remains essentially constant.

Next, all segments that have the same variance are grouped together to create a new time series (bins) in which the variance is approximately constant over this new time interval. Next, the normalized moments for each bin are computed and compared with the normalized moments of the Rician distribution. Essentially the distribution of the number of time segments in each bin represents the histogram of the fluctuations in the variance of the random field.

With the use of eq. B-64, the variance b of the Rician distribution, is related to the mean and the second moment of the intensity fluctuations by

$$b = E[I] - \sqrt{2E[I]^2 - 2E[I^2]} \quad . \tag{18}$$

Eq. 18 was used to compute the variance for each time segment. Then all variances that were within one percent of each other were grouped together into the same bin.

The same data that were compiled for the single phase screen intensity experiments were segmented into different segment sizes and the experimental normalized moments were compared to the Rician normalized moments. Figures 18, 19, and 20 illustrate the effect of segment size on the computed experimental normalized moments. For a distance of 10 feet, three different segment times were chosen. The three segment times were 150, 50, and 15 milliseconds.

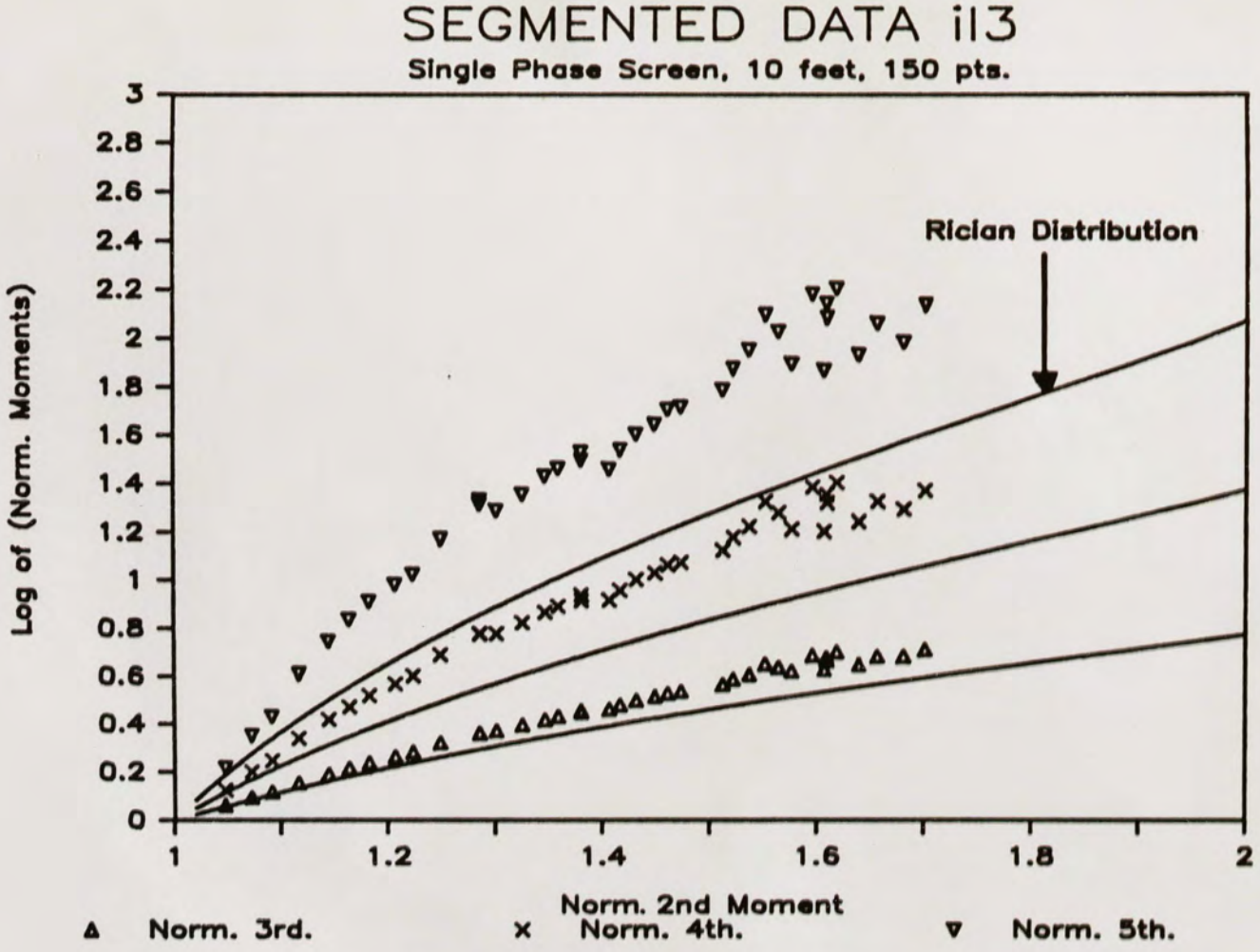

Figure 18. Normalized Moments for a Segment Size of 150 Milliseconds and a Distance of 10 Feet.

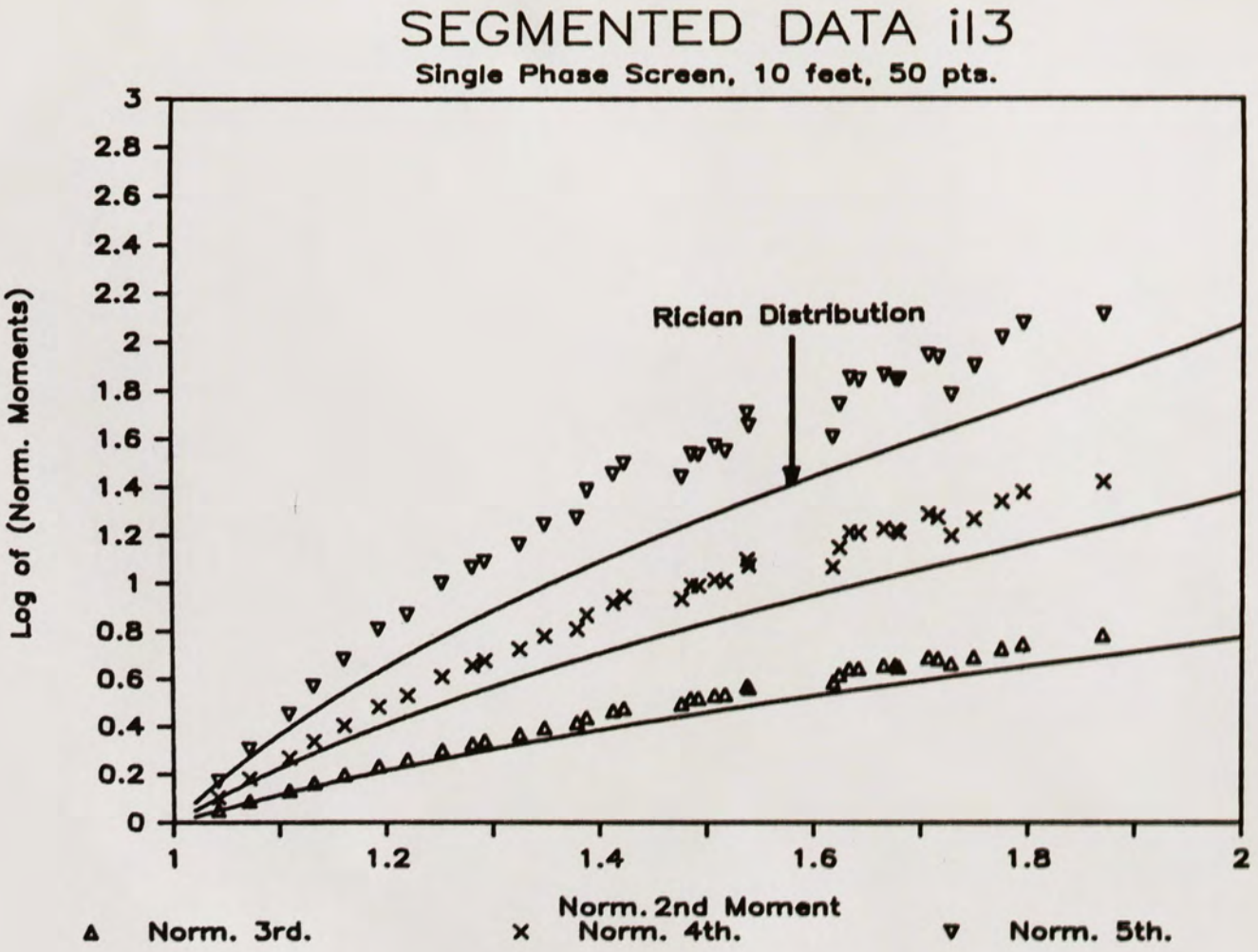

Figure 19. Normalized Moments for a Segment Size of 50 Milliseconds and a Distance of 10 Feet.

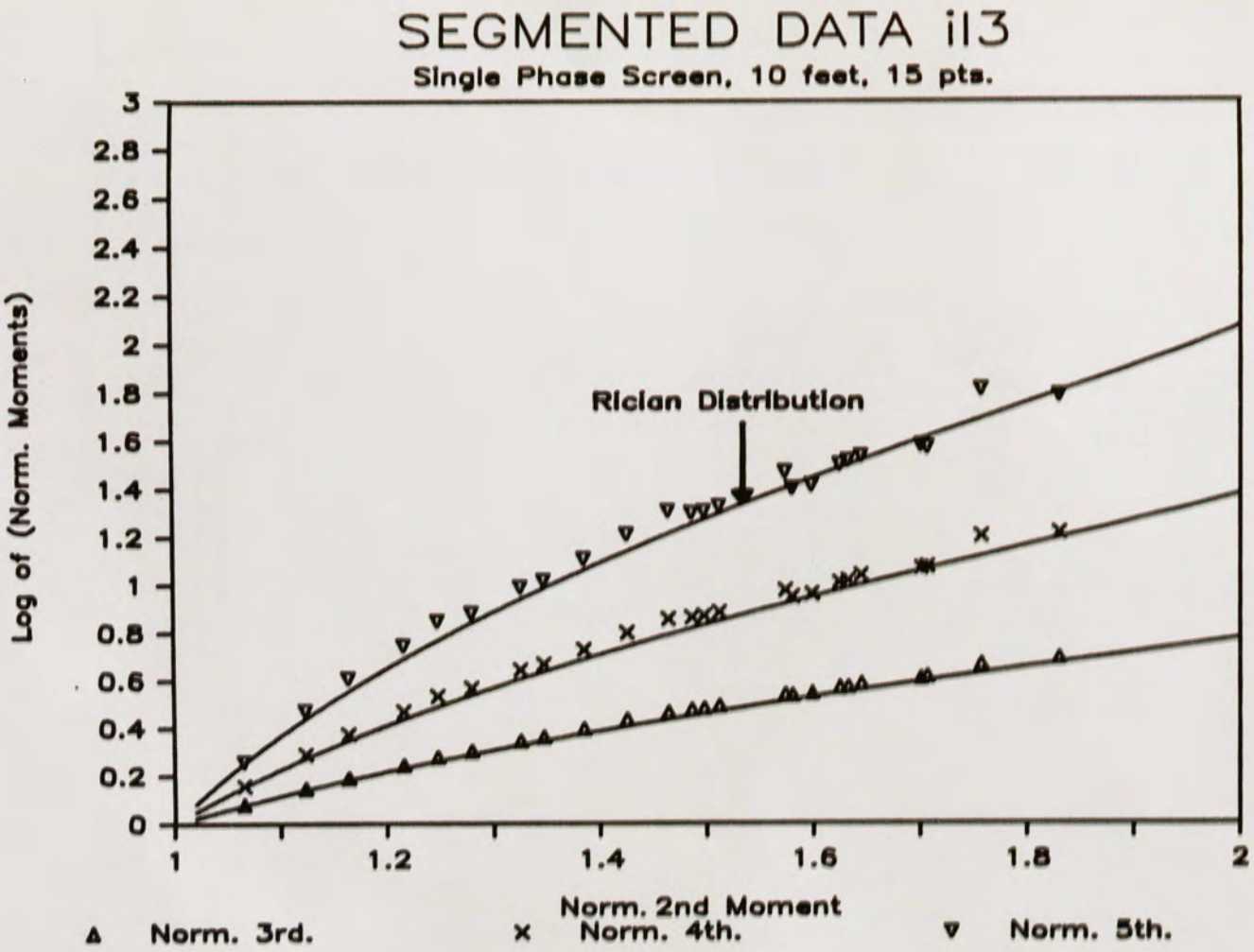

Figure 20. Normalized Moments for a Segment Size of 15 Milliseconds and a Distance of 10 Feet.

For a segment size of 150 milliseconds, the normalized moments lay well above the normalized moments predicted by the Rician distribution. As the segment size decreased to 50 milliseconds, the computed normalized moments moved closer to those of the Rician distribution. Finally, for the segment size of 15 milliseconds, the computed normalized moments matched the normalized moments for the Rician distribution. Only the normalized second moment of the Rician distribution was used to match the experimental moments. The higher order normalized moments for the Rician distribution were determined from the normalized second moment. No data matching technique was used to determine these higher order moments.

Considering that determining the stationary time of the statisitcs with equal time segments was really not completely correct, the normalized moments from the experimental data fit the normalized moments for the distribution extremely well. Figures 21, 22, and 23 compare the segmented experimental normalized moments to the Rician normalized moments for three different distances of 5 feet, 35 feet, and 100 feet, respectively. The segment size required to match the normalized moments increased from 8 milliseconds at a distance of 5 feet to 150 milliseconds at a distance of 100 feet. For short distances, the normalized moments lay very close to unity

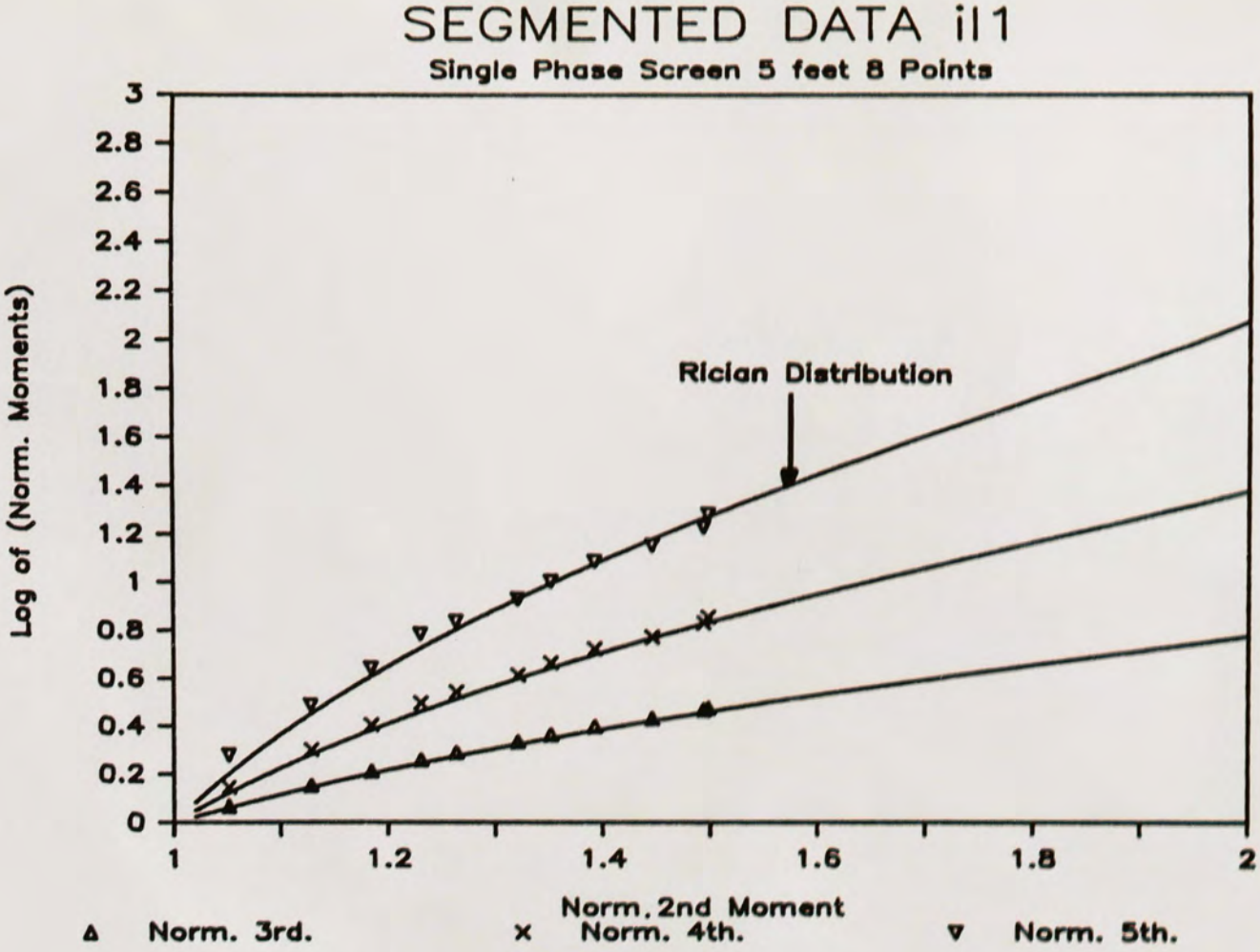

Figure 21. Normalized Moments for a Segment Size of 8 Milliseconds and a Distance of 5 Feet.

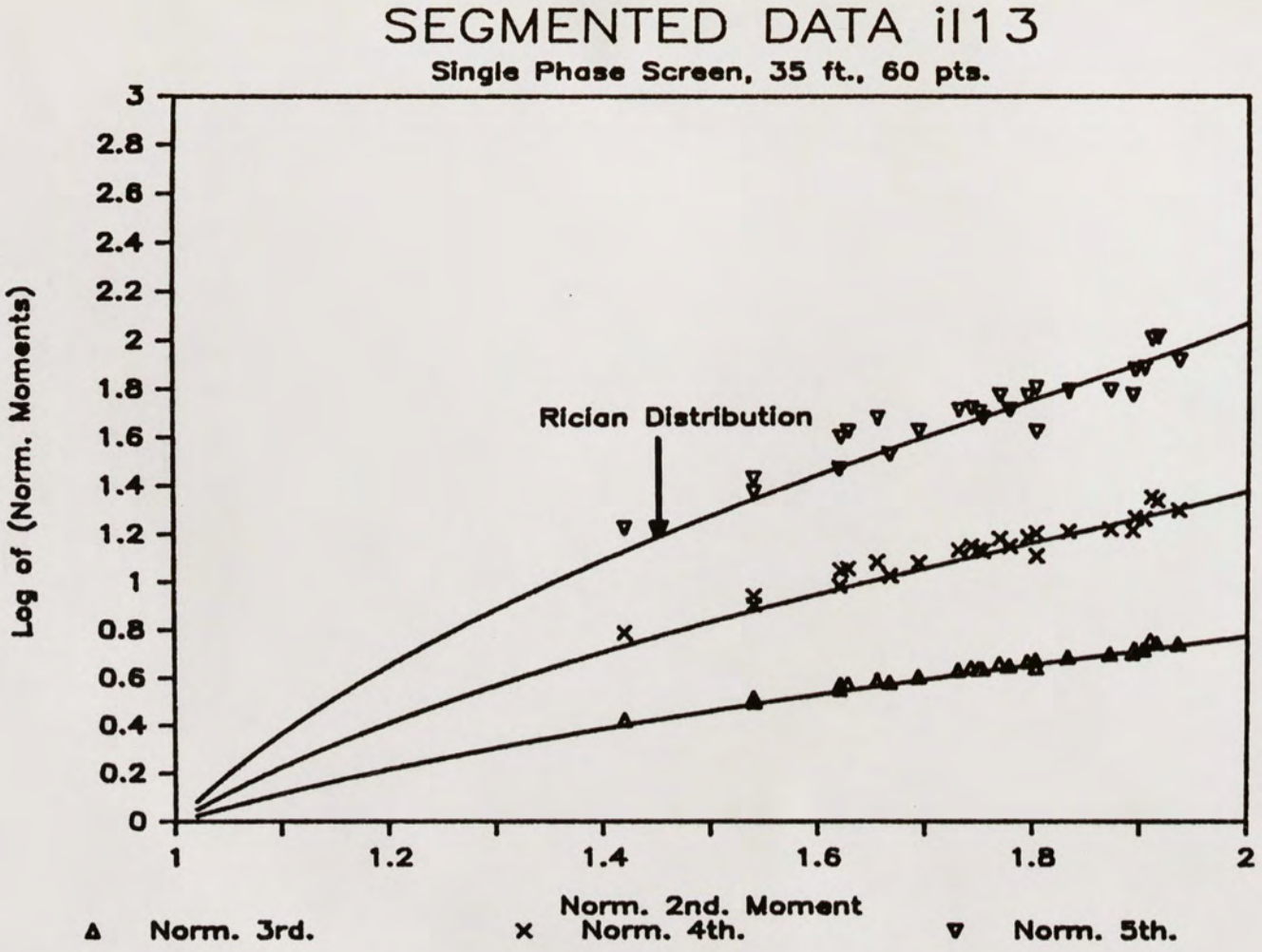

Figure 22. Normalized Moments for a Segment Size of 60 Millseconds and a Distance of 35 Feet.

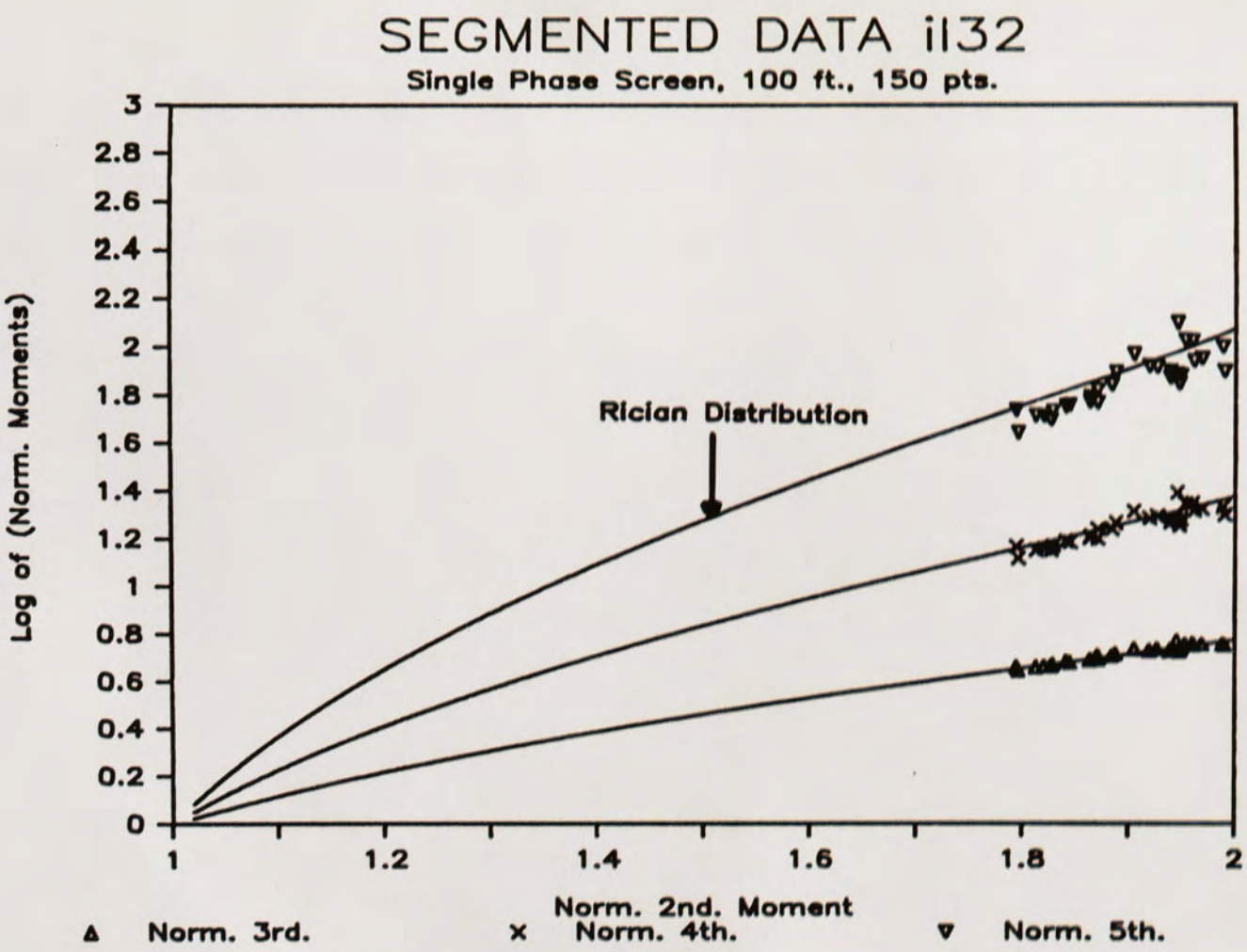

Figure 23. Normalized Moments for a Segment Size of 150 Milliseconds and a Distance of 100 Feet.

as expected, since the intensity fluctuations were small compared to the deterministic part of the intensity. For long propagation lengths, the nth normalized moment approaches the nth normalized moment for the negative exponential distribution, n!.

Figure 24 shows the segment time required to match the normalized moments of the Rician distribution as a function of distance. As the distance behind the phase screen increases, the segment time, i.e., the stationary time, monotonically increases. In the limit as the distance behind the phase screen approaches infinity, the stationary period as given in Figure 24 is also tending toward infinity. This is in agreement with the fact that as the propagation distance becomes infinitely long, the PDF for the slowly changing variance becomes a delta function. The variance for the electric field is no longer varying with time but is a constant which yields an infinite stationary time.

At first the stationary period increases rapidly with distance, but then increases slowly with distance once the focusing region is reached. This is similar to the way the α parameter of the gamma distribution and its normalized moments behave with distance.

Segmenting the data has verified that the conditional statistics for the intensity fluctuations is indeed Rician

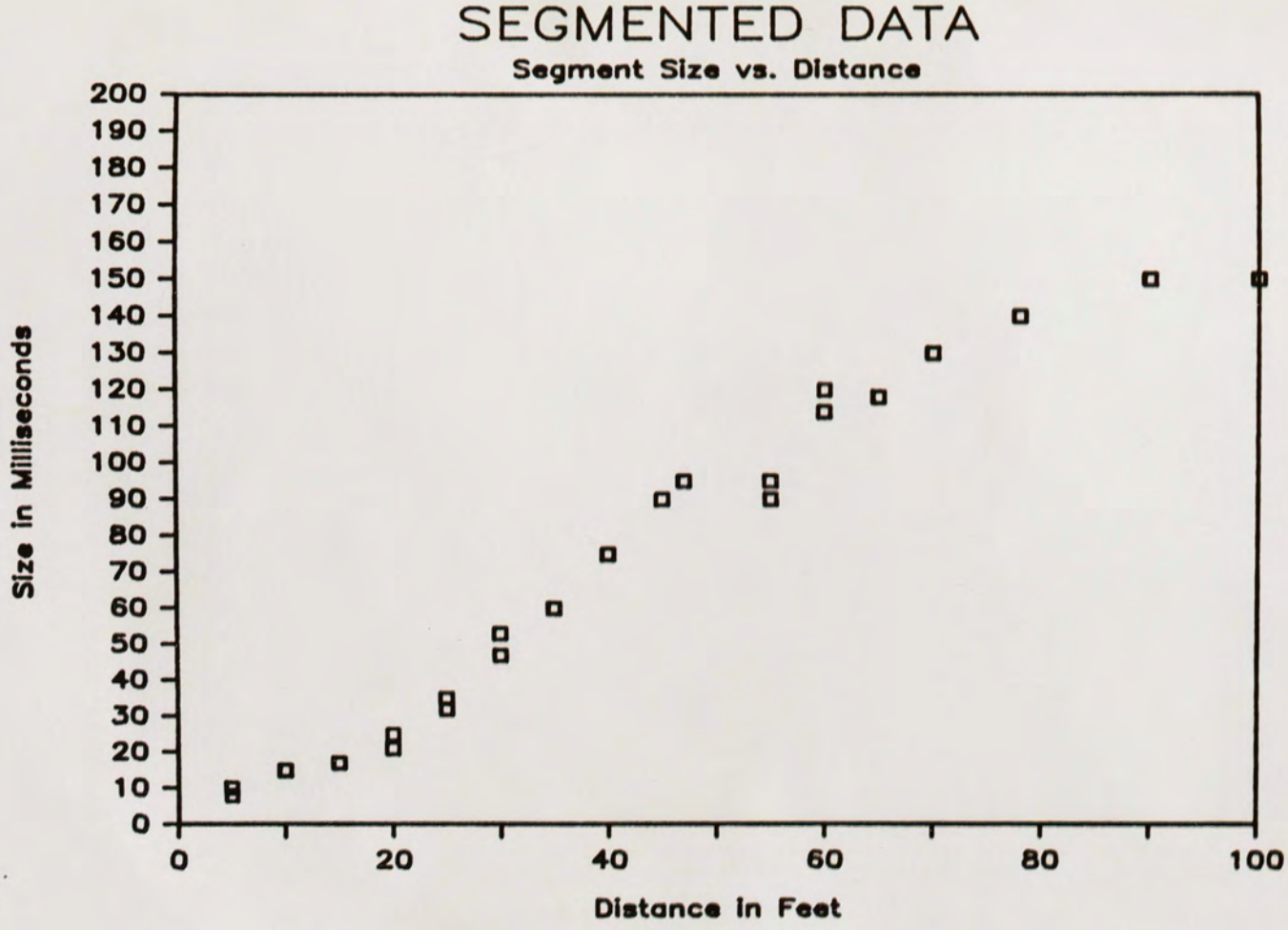

Figure 24. Segment Size vs. Distance.

distributed. Since the statistics of the intensity fluctuations depend on the time interval that is used to compute the moments, the statistics for the intensity fluctuations are assumed to be nonstationary. In dealing with nonstationary data, the length of time that is used to compute the experimental moments becomes important.

For example, the data taken at 100 feet tends to indicate that if a laser transmitter transmitted all of its data within 150 milliseconds, the statistics of the intensity fluctuations would be Rician, not HK distributed. On the other hand, if the time required to transmit the data occurred on the order of minutes, the statistics of the intensity fluctuations could be predicted by the HK distribution.

MULTIPLE PHASE SCREEN INTENSITY EXPERIMENTS

When a laser beam propagates through the atmosphere from ground to space, the turbulence that is encountered along the propagation path is different than the turbulence that is enconutered by laser beam propagating along a homogeneous path parallel to and close to the ground. For the case of a laser beam propagating parallel to the ground, the turbulent conditions that occur are usually continuous along the whole propagation path. The turbulence that is encountered along the ground-space path appears in thin shear layers separated by large distances. Within these shear layers a thin sheet (relative to the entire path length) of high turbulent conditions exist. Each shear layer encountered by the laser beam acts like a thin phase screen that randomly modulates the phase of the laser beam. Since each shear layer is separated by large distances, the random phase induced by each shear layer causes some intensity fluctuations to develop before the next shear layer is encountered.

This type of atmospheric condition can be modeled in the laboratory by several propane burners separated by a

distance of several feet. Each burner acts like a thin shear layer introducing random phase fluctuations into the laser beam. The block diagram for the multiple phase screen experiments is shown in Figure 25. Two experiments were performed, one for the case of two phase screens and the other for the case of three phase screens. The phase screens were separated by a distance of 20 feet to simulate the large separation distances between shear layers in the actual atmosphere. This allowed for the development of some intensity fluctuations between each phase screen. So that each burner generated approximately the same turbulent conditions, the distance from the phase screen to the optical axis of the collimator for all the phase screens was set to 6 inches; the flame heights for all of the burners were set at .75 inches.

For the separation distance of 20 feet between the burners, the intensity fluctuations due to the previous phase screen were almost fully developed. In addition, with the burners being separated by this distance, the intensity fluctuations induced by each burner could be assumed to be independent. Also, for the three phase screen intensity experiments the distance between all the phase screens was set equal so as to reduce the number of unknown variables in the experiment.

MULTIPLE PHASE SCREEN BLOCK DIAGRAM

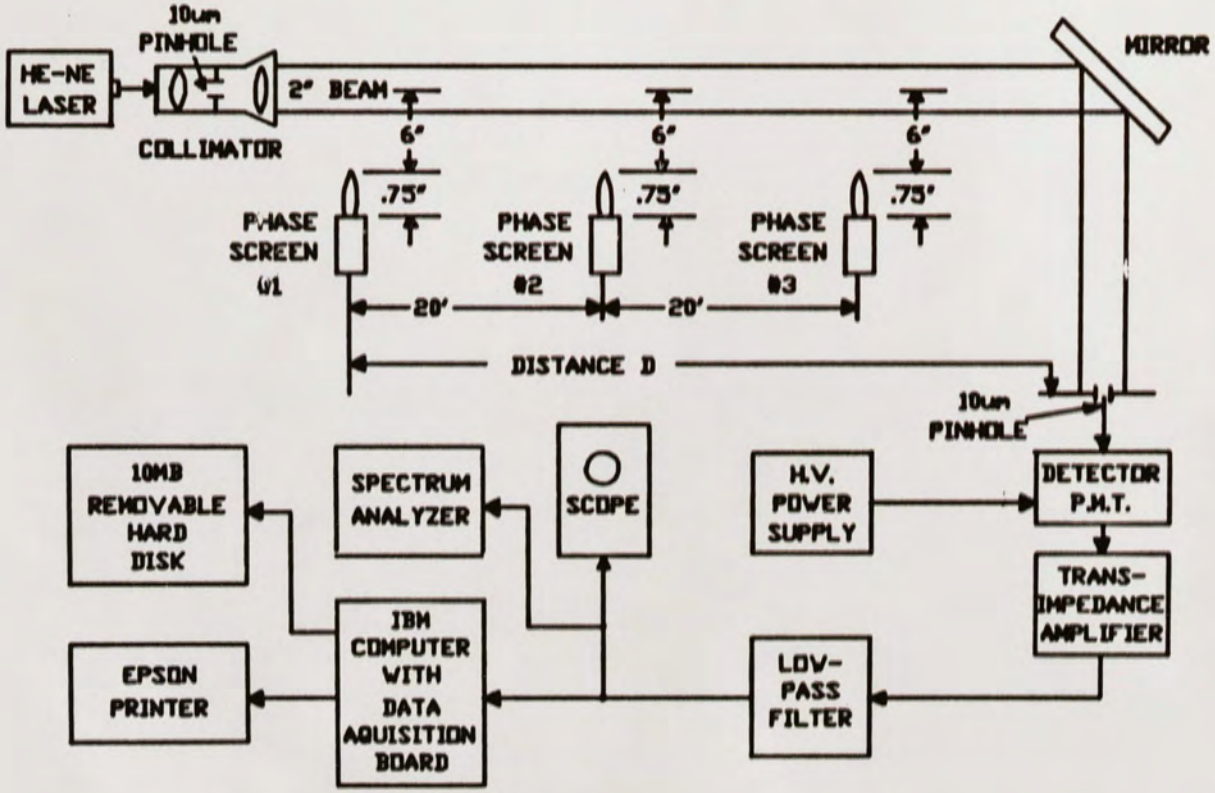

Figure 25. Block Diagram for the Multiple Phase Screen Intensity Experiments.

Except for some preliminary experiments that were performed at the University of Central Florida in April of 1985, there has been very little theoretical or experimental work completed for a laser beam propagating through multiple phase screens [14]. The experiments that were performed in April of 1985 used a converging laser beam along with two phase screens separated by a short distance of 9 inches. The intensity experiments that are presented here used a two inch collimated laser beam that was assumed to be a plane wave, and multiple phase screens that were separated by distances of 20 feet.

The first experiment measured the normalized moments as a function of distance for two phase screens using eq. 7. The normalized moments were then computed for 100,000 sampled data points. A sample size of 100,000 points corresponds to a sample time of 100 seconds. A plot of the normalized moments as a function of distance behind the phase screens is given in Figure 26. The distances shown are measured from the position of the first phase screen. The solid line is an estimate of the normalized moments using the extended range model to predict the parameters α and ρ in the I-K distribution with an inner scale of .006 meters [20]. An equivalent strengh of turbulence parameter, C_n^2, in this model, was computed from the value of the normalized second moment measured at a

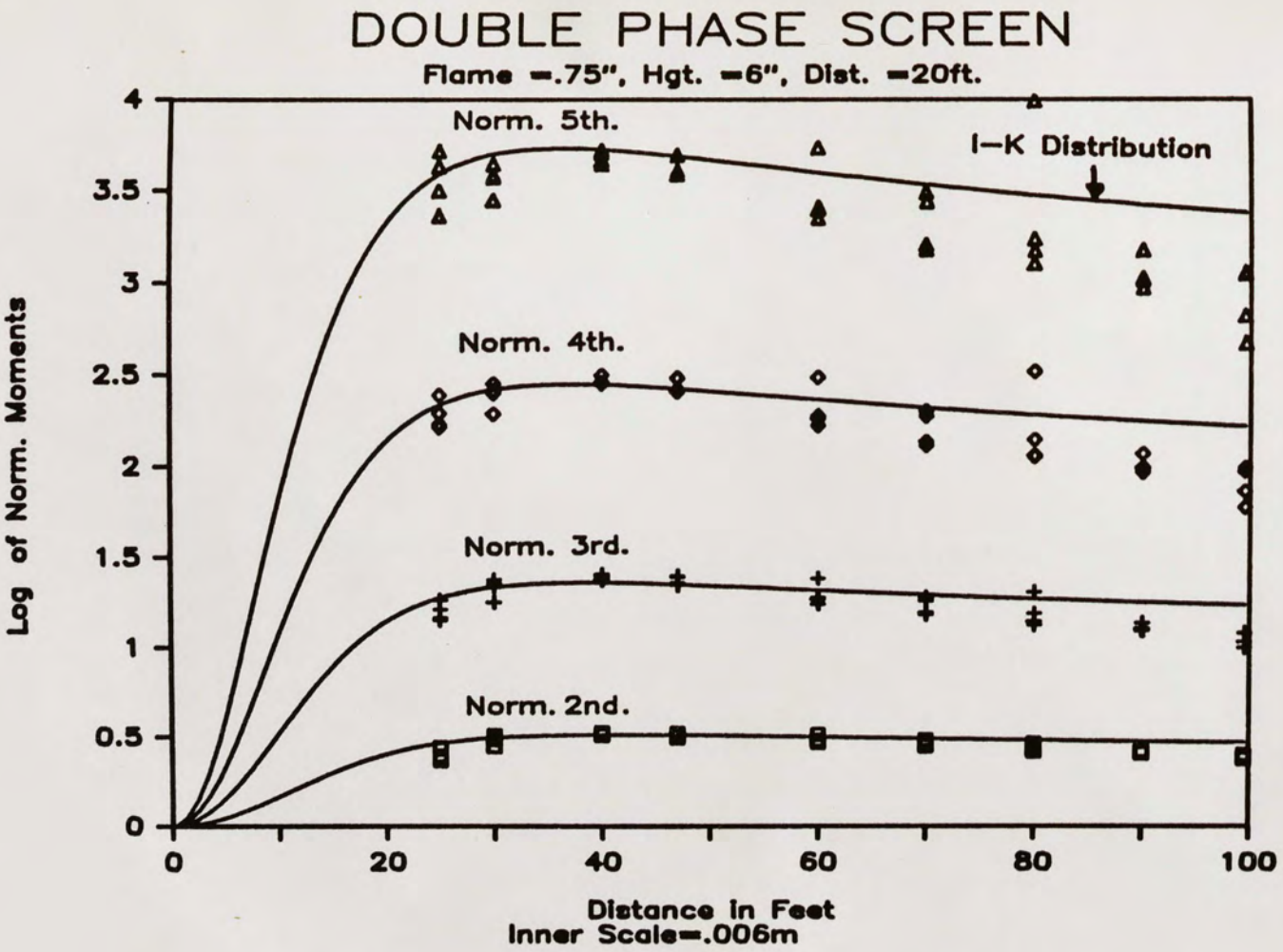

Figure 26. Normalized Moments for a Double Phase Screen as a Function of Distance.

distance of 10 feet behind the first phase screen as shown in Figure 4.

The reason that the normalized moments for the extended turbulence model does not fit the experimental normalized moments very well is that the normalized second moment for a distance of 10 feet was used to compute the equivalent strength of turbulence parameter, C_n^2. By using this normalized second moment to compute C_n^2, the value that is obtained for C_n^2 is due solely to one phase screen. Hence, the effects of the other phase screens are ignored. The extended turbulence model uses C_n^2 to predict the α and ρ parameters in the I-K distribution as a function of distance behind the phase screen.

To compute C_n^2 from the normalized second moment, the normalized second moment must be measured in the weak turbulence region. In other words, ρ must be much larger than one. To compute C_n^2 due to both phase screens, the normalized second moment used must be measured behind the second phase screen. From Figure 26, the normalized moments for the intensity fluctuations indicate that the level of turbulence is very strong. For a distance of 5 feet behind the second phase screen, the measured normalized moments are already in the focusing region. The normalized moments measured due to both phase screens cannot be used in the extended range model to predict the

parameters for the I-K distribution. Hence, for multiple phase screens separated by large distances as compared to the location of the saturation region, there is no way to predict C_n^2 due to all of the phase screens.

Comparing Figure 4 with Figure 26, the normalized moments in the saturation region have increased with the addition of the second phase screen. In addition, the two plots show that the location of the focusing region at 50 feet has not moved. For the single phase screen experiment, the normalized moments decreased slowly with distance once the focusing region was reached. On the other hand, the normalized moments for the double phase screen experiment decrease more rapidly with distance once the focusing region was reached. For a distance of 100 feet, the value of the normalized moments for the double phase screen experiment is about the same as the normalized moments for the single phase screen experiment. In comparing Figure 4 with Figure 26, it was concluded that the addition of the second phase screen only raised the normalized moments in the focusing region.

Plots of the spectrum for intensity fluctuations for distances of 25 feet and 100 feet are given in figures 27 and 28, repectively. The spectrums shown in figures 27 and 28 are very similar to the spectrums taken for the single phase screen experiment. Again, two power law

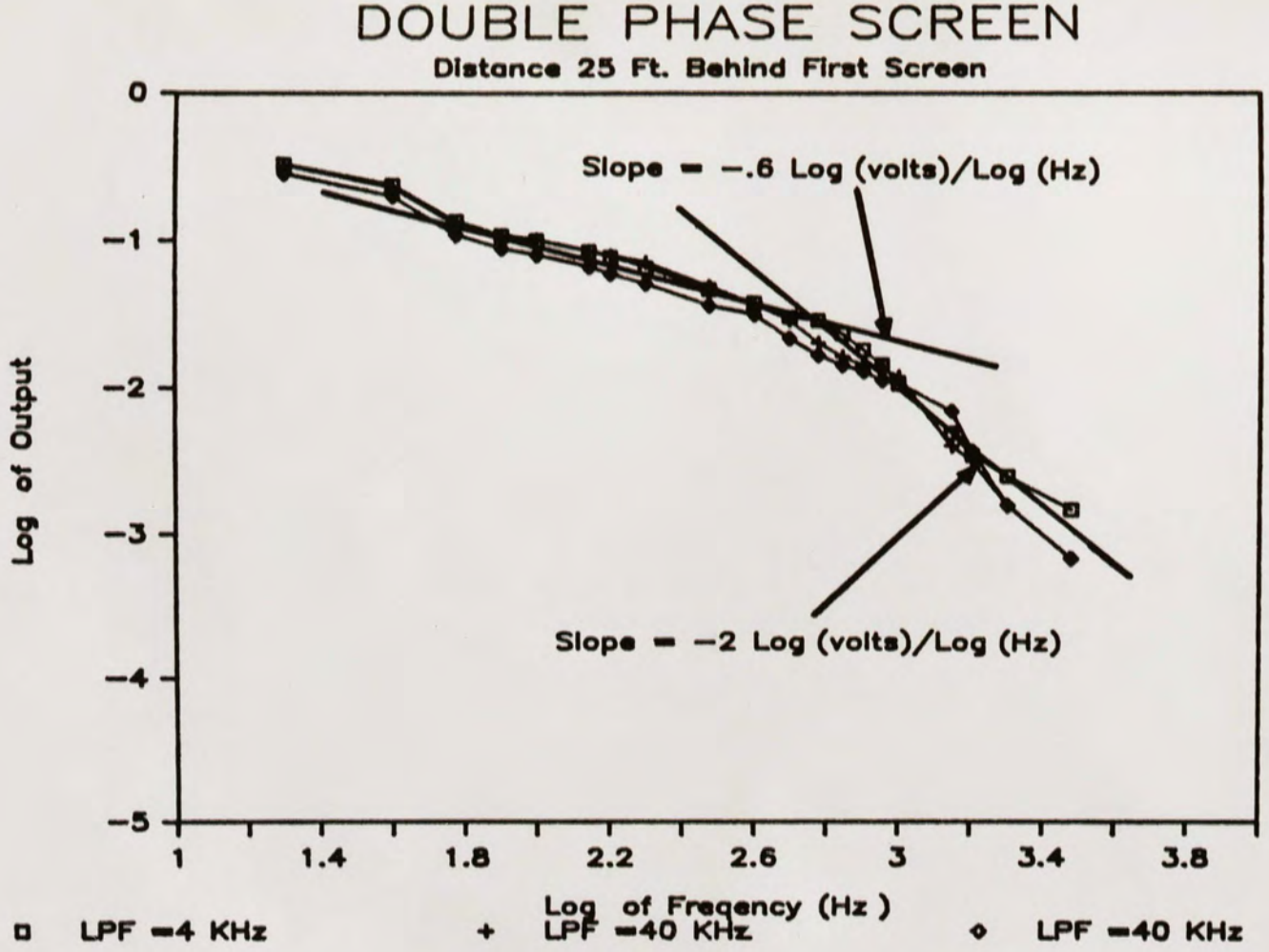

Figure 27. Spectrum Data for a Double Phase Screen for a Distance of 25 Feet.

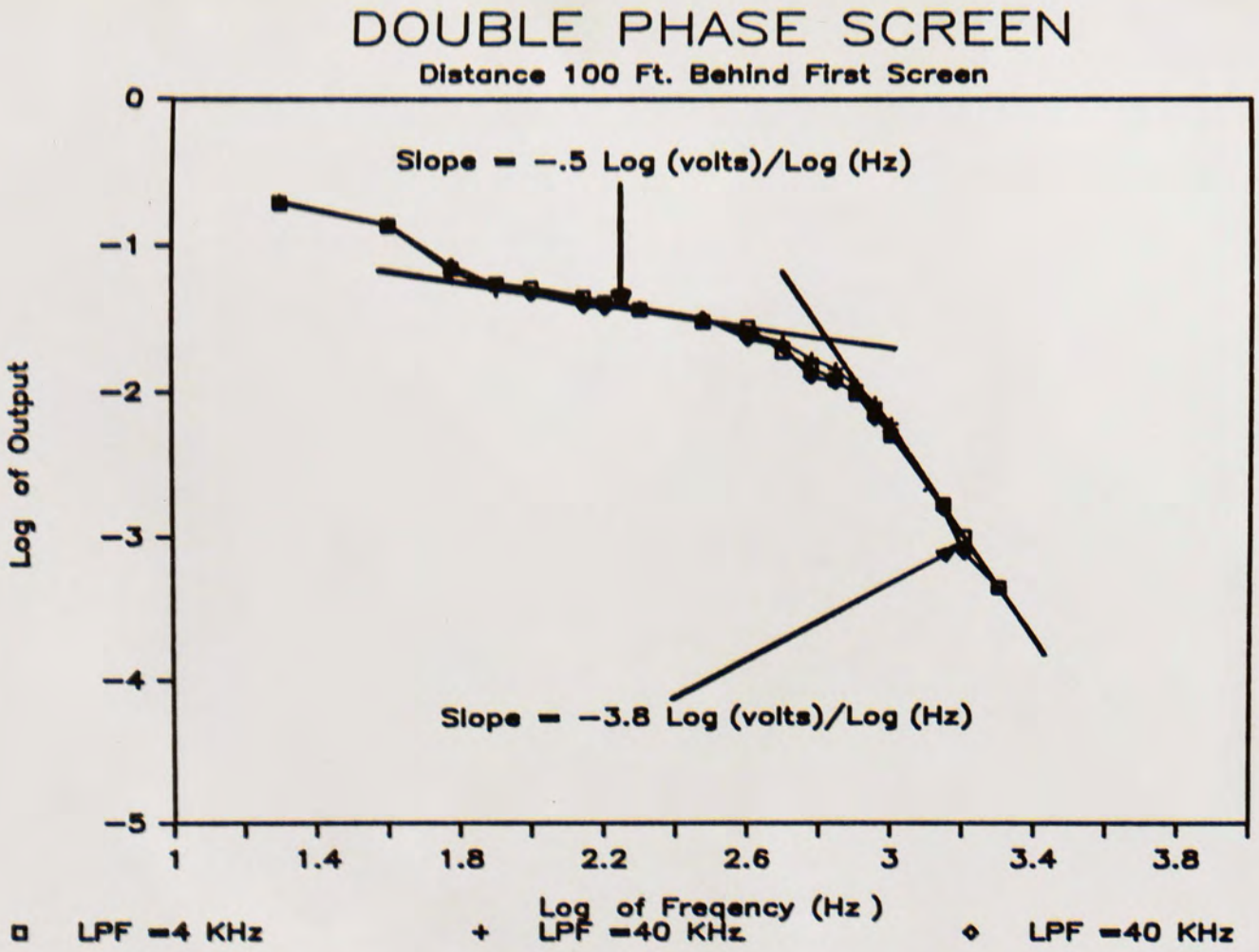

Figure 28. Spectrum Data for a Double Phase Screen for a Distance of 100 Feet.

regions can be seen in the spectrums. In particular, the spectrum for the double phase screen experiment taken at a distance of 100 feet is almost identical to the spectrum for the single phase screen experiment taken at 100 feet. This is not unreasonable to expect, since the moments for both these experiments at this distance are about the same.

A plot of the normalized moments as a function of distance for the triple phase screen experiment is given in Figure 29. From Figure 29, the normalized moments indicate that intensity fluctuations due to three phase screens is well into the saturation region. In other words, the normalized moments are monotonically decreasing with distance behind the third phase screen. Assuming that the addition of the third phase screen did not move the location of the focusing region, all data taken for the triple phase screen experiments were for distances beyond the focusing region. Again, the normalized moments in Figure 29 are approximately the same as the normalized moments for the single phase screen experiment at a distance of 100 feet. Hence, for distances greater than 100 feet, the normalized moments seem to be independent of the number of phase screens through which the laser beam propagates.

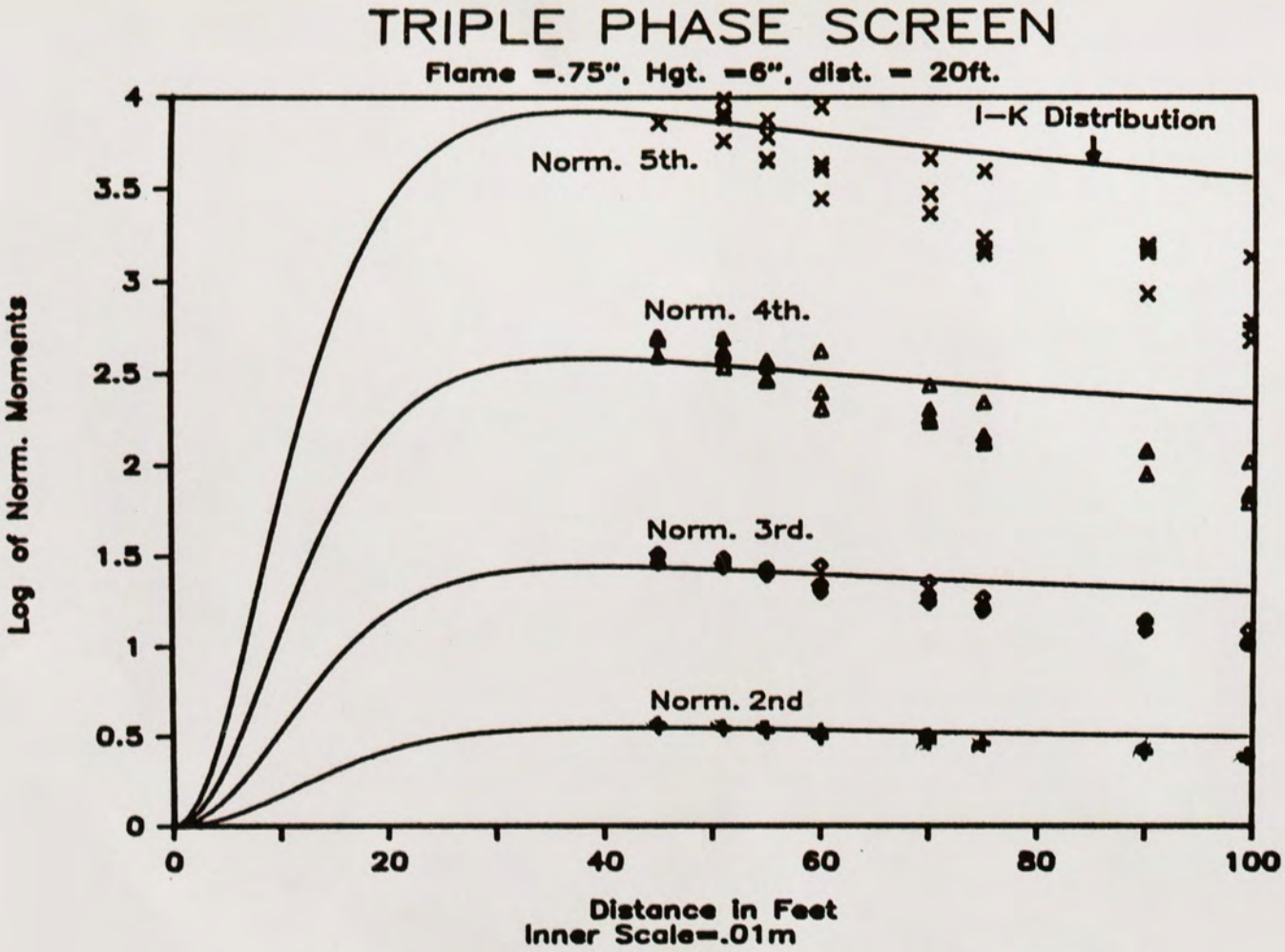

Figure 29. Normalized Moments for a Triple Phase Screen as a Function of Distance.

In figures 30 and 31, the spectrum for distances of 45 and 100 feet are given. Again, two power law regions are seen in the spectrums. The spectrum for a distance of 100 feet is identical to the spectrums taken for the single phase screen and the double phase screen experiments at the same distance of 100 feet.

The plot of the normalized moments versus the normalized second moment for the single, double, and triple phase screen experiments is shown in Figure 32. The normalized moments for the single phase screen experiment is marked by a square symbol; for the double phase screen experiment by a cross symbol; for the triple phase screen experiment by a diamond symbol. Figure 32 shows that by placing multiple phase screens in the laser propagation path, the statistical distribution of the intensity fluctuations does not change, but rather only the level of the intensity fluctuations appears to increase with more phase screens. For long propagation distances, the level of the intensity fluctuations are independent of the number of phase screens encountered by the laser beam. In other words, once the distance behind the phase screens is in the far field, the number of phase screens no longer affects the intensity statistics.

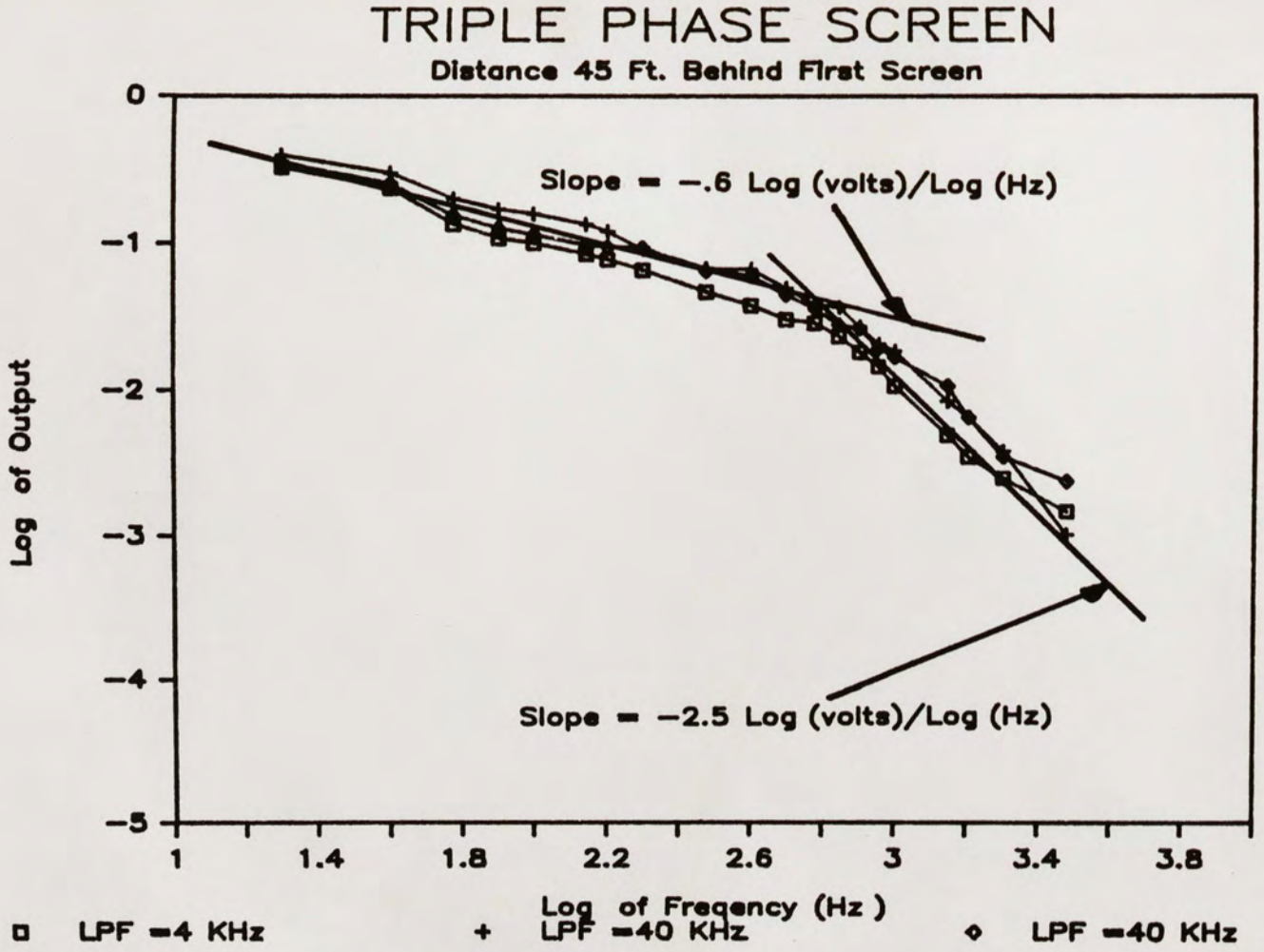

Figure 30. Spectrum Data for a Triple Phase Screen for a Distance of 45 Feet.

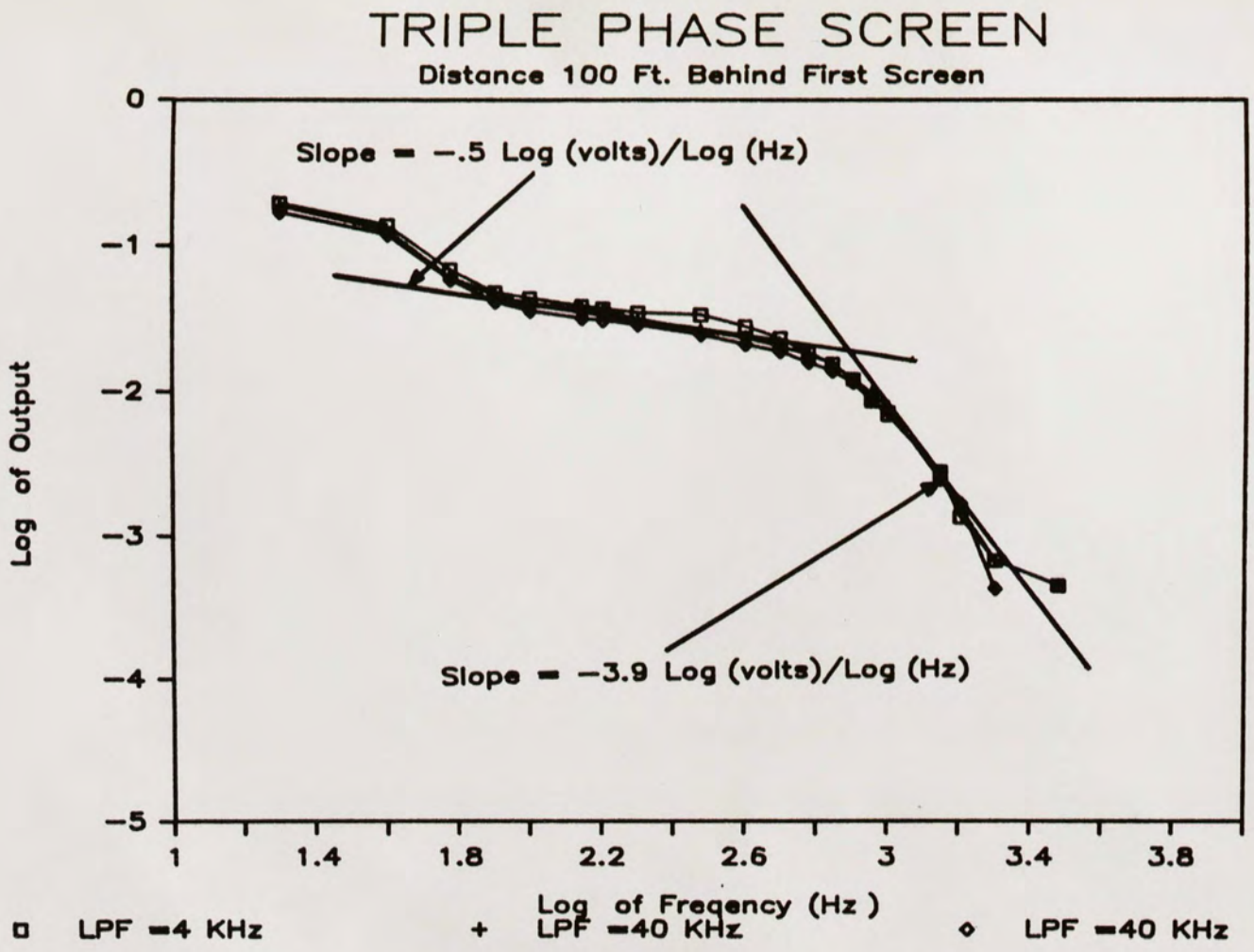

Figure 31. Spectrum Data for a Triple Phase Screen for a Distance of 100 Feet.

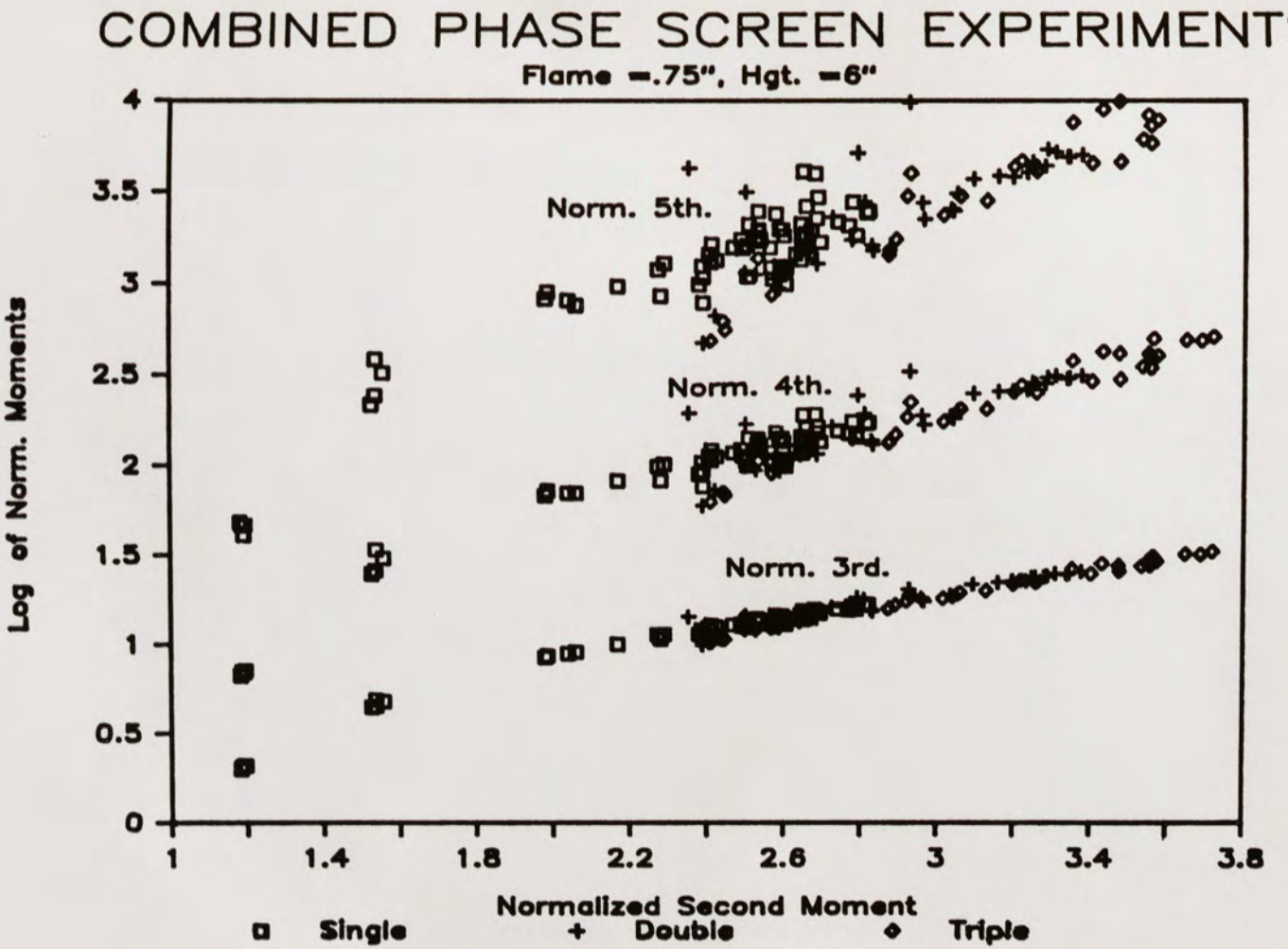

Figure 32. Comparison of the Normalized Moments for the Single, Double, and Triple Phase Screens.

COMPUTER SIMULATION OF THE K DISTRIBUTION

To verify the concept that nonstationary statistics are derivable from a modulation process, a computer simulation program was written to simulate the K distribution. Jakeman has shown that the K distribution predicts the random fluctuations for a nonstationary process that contains only noise [11]. In the development of the K distribution, the nonstationary process was shown to be the modulation of a fast fluctuating random process with a slowly varying random process [17]. The slowly varying process was used to model the slowly fluctuating variance of the fast process. The process for the K distribution as described by eq. C-1 is

$$U(t) = N(t) \cdot W(t) \ , \tag{19}$$

where W(t) is the fast-varying process and N(t) is the slow-varying process.

The intensity is simply the magnitude squared of eq. 19 and is given by

$$I(t) = |N(t)|^2 \cdot |W(t)|^2 \ . \tag{20}$$

From Appendix C, the slow-varying process, $|N(t)|^2$, was assumed to be gamma distributed while the process for W(t) was assumed to be zero mean Gaussian distributed. Immediately, the fast process describing $|W(t)|^2$ is found to be negative exponential distributed. By assuming the process for $|N(t)|^2$ is gamma distributed and the process for $|W(t)|^2$ is negative exponential distributed, the underlying assumption is that both processes are derivable from Gaussian processes. The PDF for the K distribution is given by eq. A-5 as

$$p(I) = \frac{2I^{(\alpha-1)/2}}{\Gamma(\alpha)} \left[\frac{\alpha}{n_o w_o}\right]^{(\alpha+1)/2} K_{\alpha-1}(2\sqrt{I\alpha/n_o w_o}) \quad , \quad (21)$$

where α is the effective number of scatters (modes) given in the gamma distribution. In addition, n_o is the variance for the slow process $|N(t)|^2$, and w_o is the variance for the fast process $|W(t)|^2$.

To reduce the complexity of the computer simulation program, α was set to unity in eq. 21. With α set to unity, the gamma distribution describing the slow process $|N(t)|^2$ reduces to a negative exponential distribution. When α equals unity, the PDF for the K distribution is

$$p(I) = \frac{2}{n_o w_o} K_o(2\sqrt{I/n_o w_o}) \quad . \quad (22)$$

To simulate the statistics described by eq. 22, two

independent negative exponential distributions were used, one for $|N(t)|^2$ and the other for $|W(t)|^2$. The only difference between the two negative exponential distributions was their spectrums. The spectrum for $|N(t)^2|$ was centered around DC and contained low frequencies, while the spectrum for W(t) was a bandpass filter spectrum centered on a higher frequency.

To generate the two negative exponential distributed processes, the output of two spectrally filtered zero mean Gaussian distributed noise generators were used. One of the noise generators were spectrally filtered to match the proposed spectrum for N(t) shown in Figure 9, while the other noise generator was spectrally filtered to match the proposed spectrum for W(t) shown in Figure 9. To generate these two negative exponential distributed processes from Gaussian distributed noise processes, the following equation was used

$$Z = X^2 + Y^2 \ , \tag{23}$$

where the random variable Z is negative exponential distributed and the random variables X and Y are two independent zero mean Gaussian distributed processes with the same variances.

For the case of the computer simulation, the two negative exponential distributed processes, i.e., the fast

varying process and the slow varying process, were generated from the two spectrally filter Gaussian noise generators by sampling each noise generator twice. The four random samples that were obtained from the spectrally filtered noise generators were labeled $N_1(t)$, $N_2(t)$, $W_1(t)$ and $W_2(t)$, respectively. Using equation 23 twice, the two negative exponential distributed processes were defined by

$$n = (N_1^2 + N_2^2) \tag{24}$$

and

$$w = (W_1^2 + W_2^2) \quad , \tag{25}$$

where n is the slowly varying and w is the fast varying negative exponential distributed processes.

The process predicted by eq. 22 is given by

$$I = n \cdot w \quad , \tag{26}$$

where the processes n and w are defined in eqs.24 and 25.

In Figure 33, the block diagram for the simulation of the K distribution is given. To generate N(t), one of the outputs of the white noise generators was lowpass filtered at 20 Hz and its DC value was removed. The lowpass filter cutoff of 20 Hz was chosen because for this cutoff, the normalized moments for the lowpass filter experiments agreed with the normalized moments for the gamma

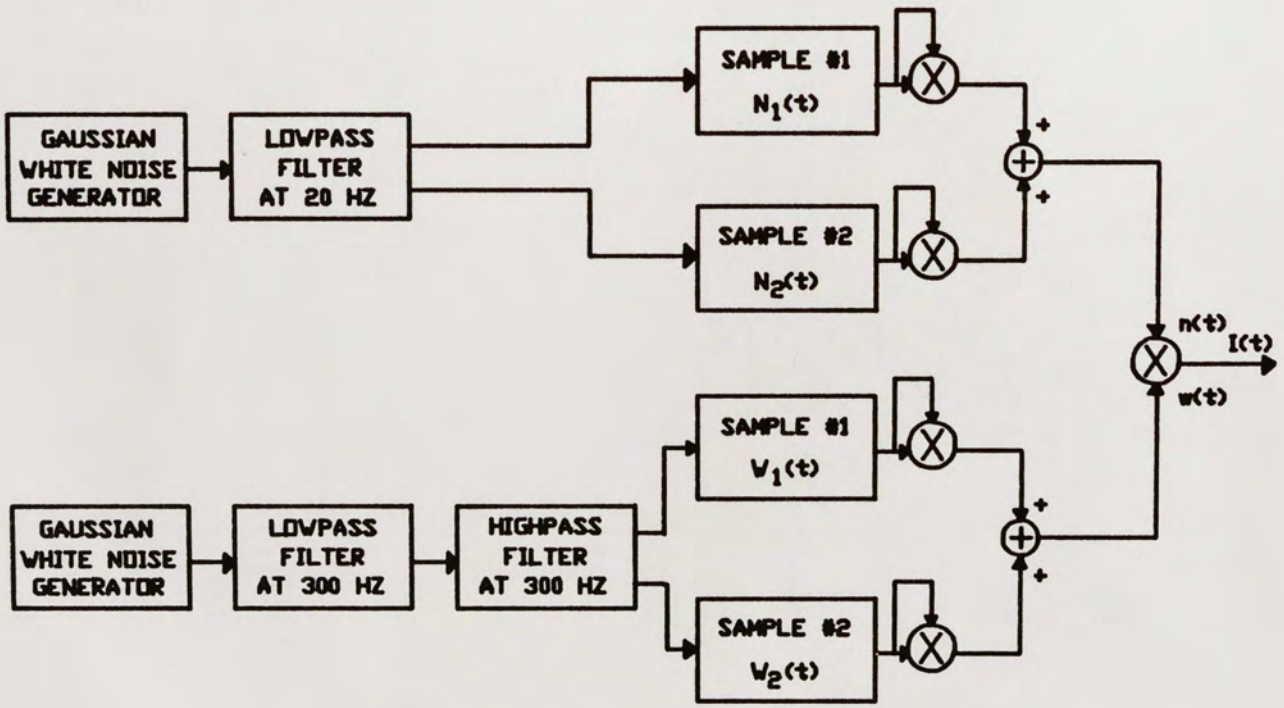

Figure 33. Block Diagram for the Computer Simulation of the K Distribution for $\alpha = 1$.

distribution. Two independent time samples were then taken from the output of the lowpass filter to generate $N_1(t)$ and $N_2(t)$. The output of the other white noise generator was bandpass filtered around a center frequency of 300 Hz by using a lowpass filter and a highpass filter cascaded together. Likewise, $W_1(t)$ and $W_2(t)$ were generated by two independent time samples taken from the bandpass filtered Gaussian noise.

In Figure 34, the time series plot for $N_1(t)$ and $W_1(t)$ is given. From Figure 34, $N_1(t)$ can be seen to be slowly varying compared to $W_1(t)$. A plot of $N_2(t)$ and $W_2(t)$ yielded very similar plots. The time series plot for $N_1(t)$ and $W_1(t)$ showed that their processes are stationary, since their mean, variances and spectrums were not changing with time.

The output I(t) was generated by using eq. 24 and the four time series $N_1(t)$, $N_2(t)$, $W_1(t)$ and $W_2(t)$. The time series plot for I(t) is given in Figure 35. The intermittant conditions seen in time series plots for nonstationary data can also be seen in Figure 35. Since the output of the computer simulation appeared to be intermittant, it is reasonable to conclude that the simulated output was nonstationary [15]. Hence, the modulation of two random stationary noise processes has led to the generation of a nonstationary process.

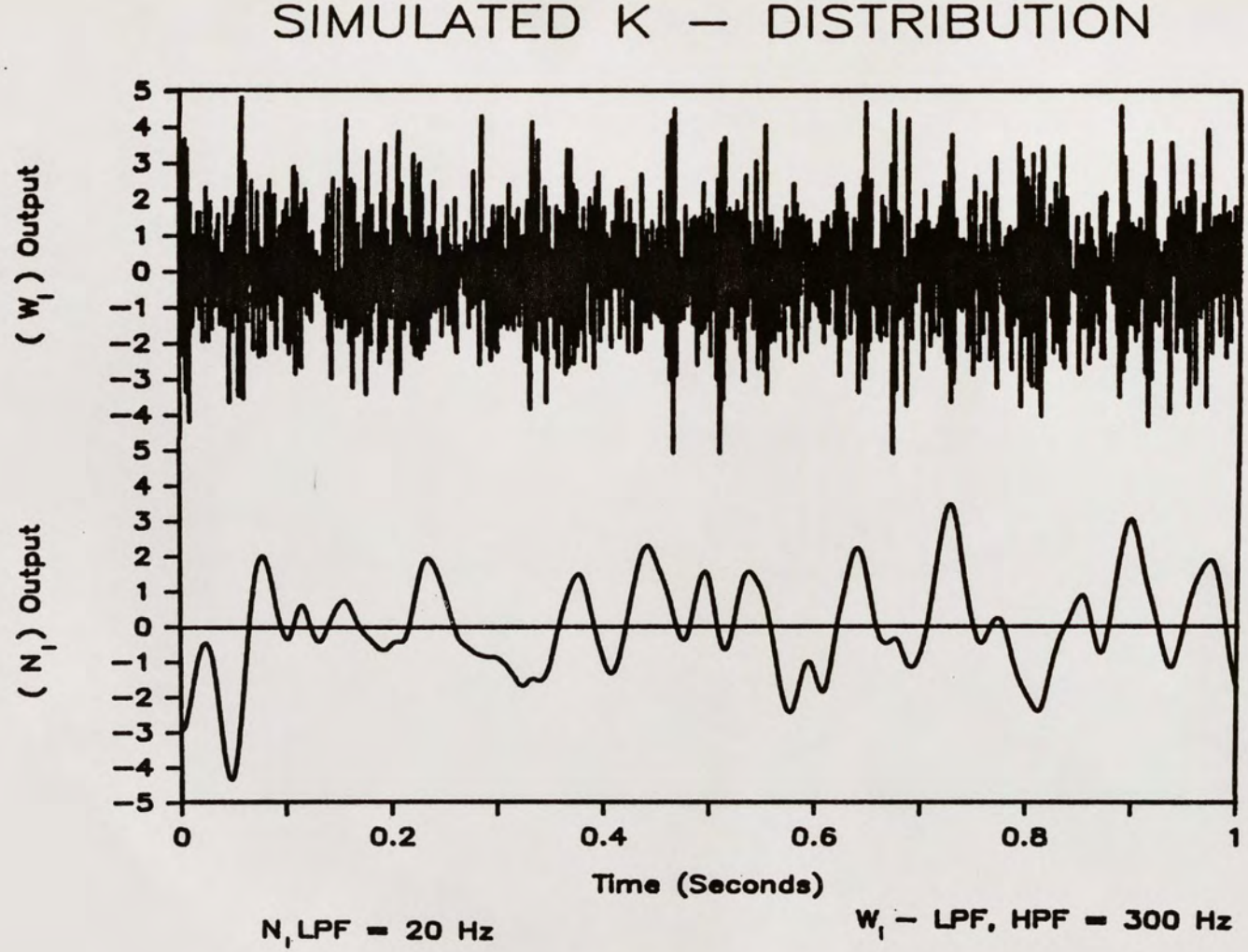

Figure 34. Time Series Plot for $N_1(t)$ and $W_1(t)$.

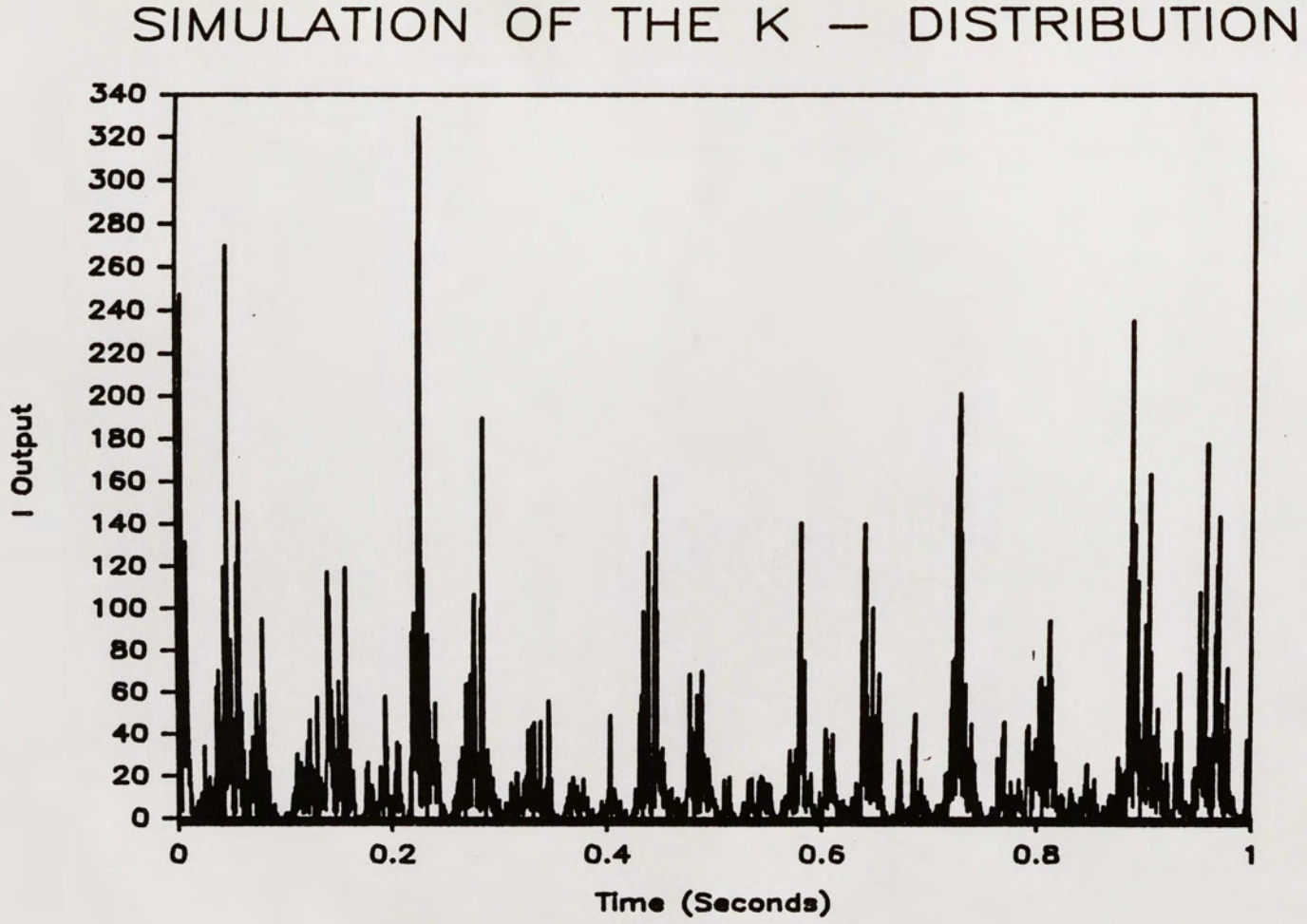

Figure 35. Time Series Plot for I(t).

The normalized moments for the simulation output were then computed and compared with the normalized moments of the K distribution for the case when α was equal to unity. The normalized moments of the simulation output were slightly low in comparison with the normalized moments of the K distribution. Considering that the normalized moments were computed from only one sample set of 2000 points, a large scatter in the normalized moments was expected. In addition, the total length of time that the normalized moments were computed over was only one second. This time interval that the normalized moments were computed over, is somewhat short a time period to obtain a good estimate of the normalized moments.

A Fast Fourier Transform (FFT) program was used to compute the spectrums for $N_1(t)$, $W_1(t)$, and $I(t)$. The spectrums for $N_1(t)$ and $W_1(t)$ are given in figures 36 and 37, respectively. Since the filter that was used was a non-ideal filter, the spectrum for $N_1(t)$ shows that most of its energy is contained within a span of 40 Hz. The sidelopes that are seen in Figure 36 are due to the lowpass filter, not the truncation of the time series that is normally seen in Fast Fourier Transform plots. The spectrum of $W_1(t)$ yields a center frequency of approximately 325 Hz and a bandwidth that is approximately 125 Hz wide.

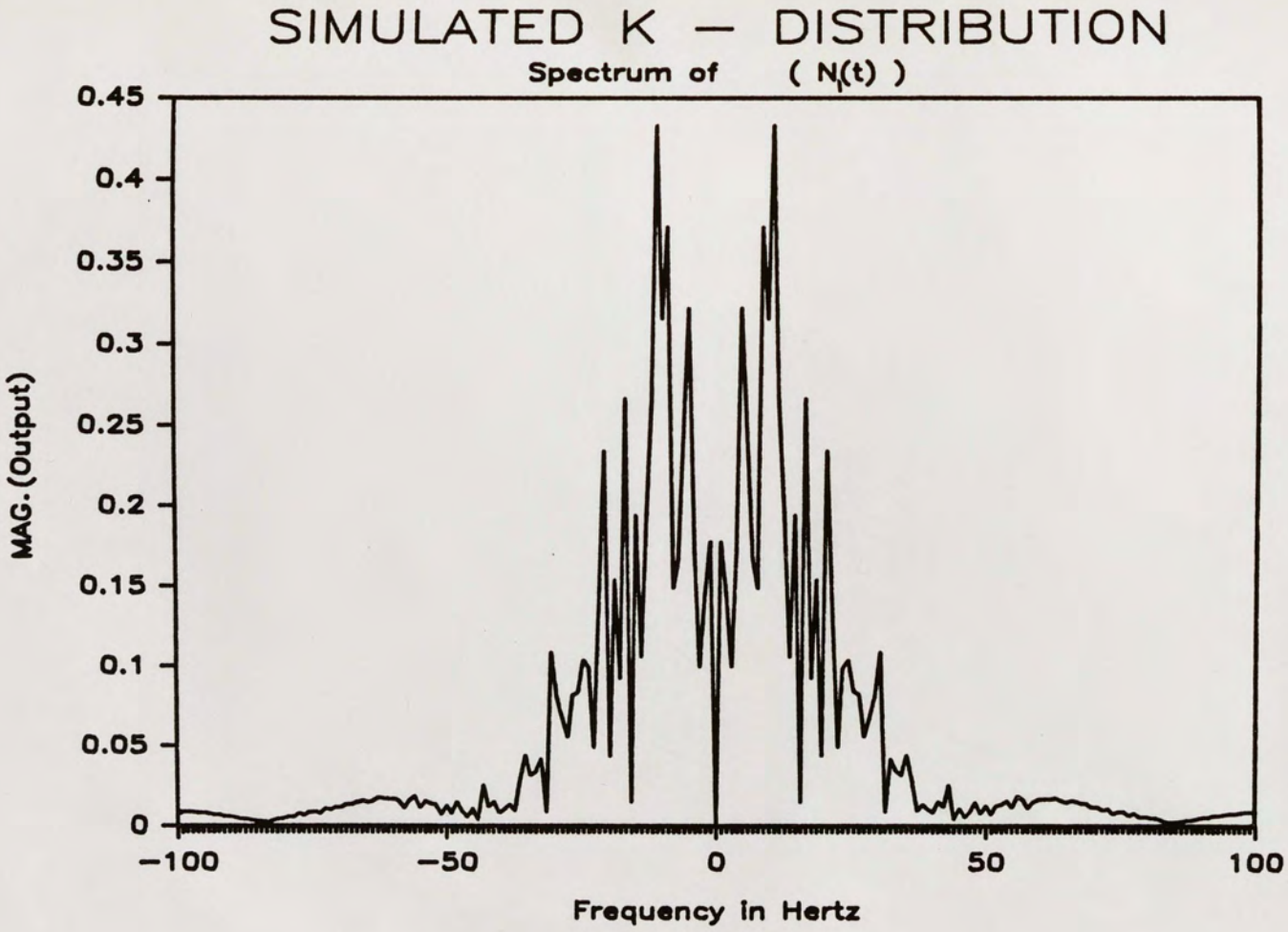

Figure 36. Spectrum for $N_1(t)$.

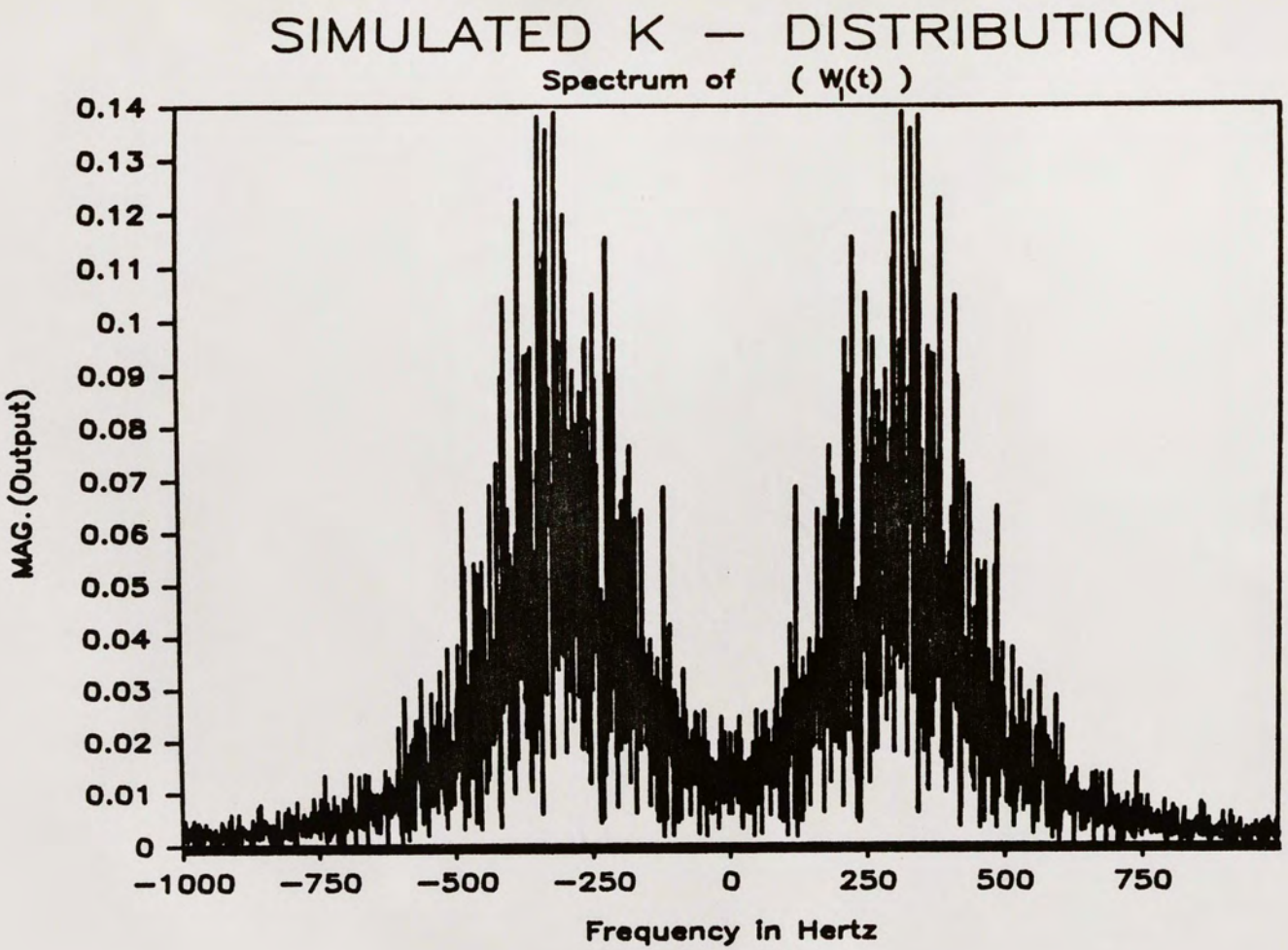

Figure 37. Spectrum for $W_1(t)$.

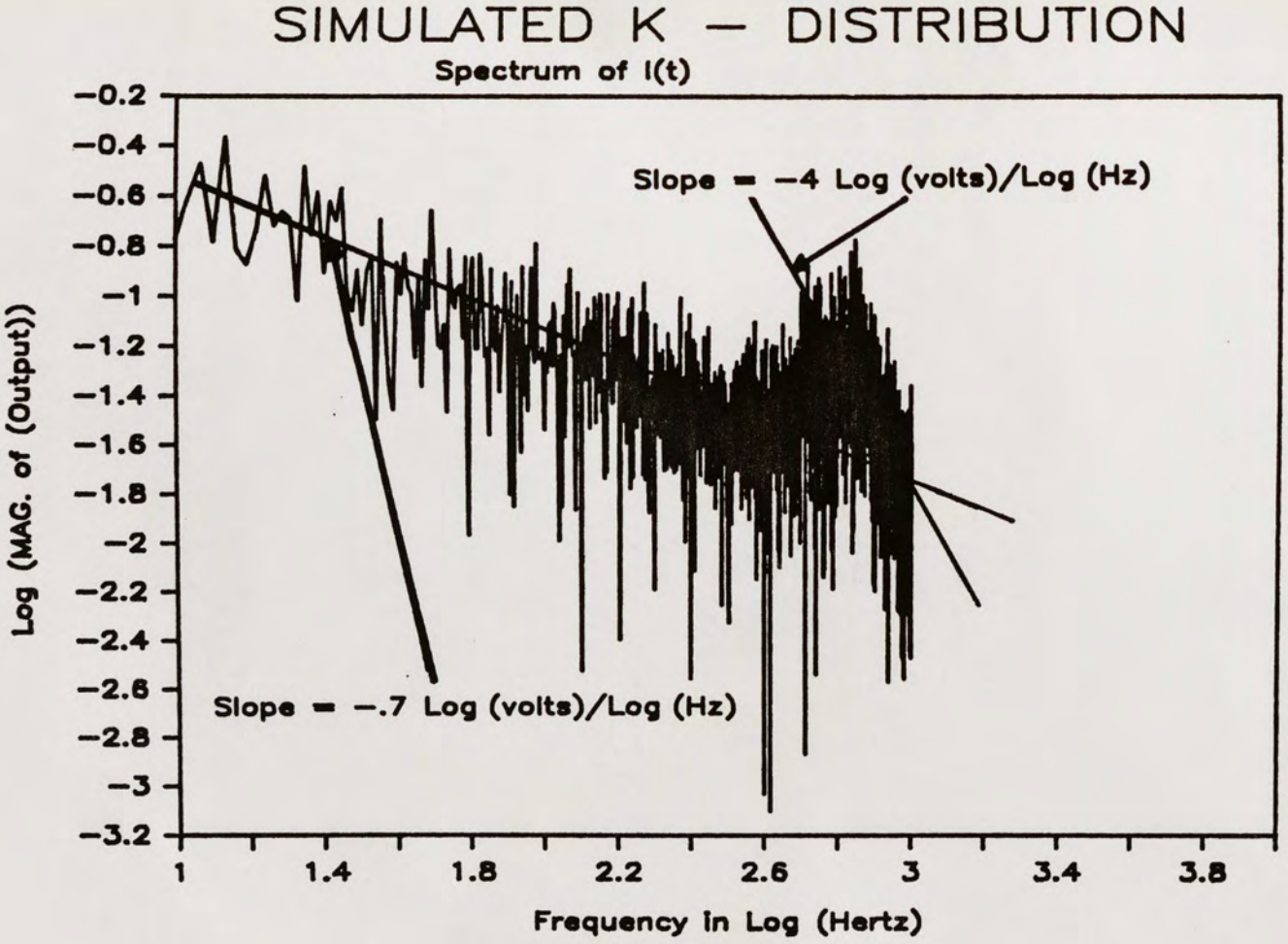

Figure 38. Spectrum for I(t).

The spectrum for the simulation output, I(t), is given in Figure 38. The spectrum for I(t) was plotted on a log-log plot so that comparisons with the spectrums of the single phase screen experimental data could be made. One surprising thing is that the spectrum contained two power law regions similar to the actual data spectrum given in Figure 8 at a distance of 100 feet for the single phase screen experiments. The low frequency power law region has a slope that is approximately -.7 log(volts)/ log(Hz) while the other power law region has a slope of approximately -4 log(volts)/log(Hz).. The slopes for the spectrum of the actual intensity data were -.6 log(volts) /log(Hz) and -4 log(volts)/log(Hz), respectively. The comparison of the two slopes from the computer simulation with the slopes for the actual data were surprisingly in good agreement with each other.

Finally, it is interesting to note that the bump that is seen in Figure 38 was also seen in some of the spectrums of single phase screen experimental data although not as pronounced. The bump occurred at about the same location where the two power law regions met. From the computer simulation and the knowledge of the spectrums for N(t) and W(t), it was concluded that the bump will be predominately large whenever the spectrum for N(t) is narrow enough so that there is very little or no

overlap between the spectrums of the two processes N(t) and W(t) during the convolution process to obtain I(t).

It should be mentioned that the only other attempt to generate K distributed noise on a computer used the Fokker-Plank equations to generate the nonstationary process described by the K distribution. The Fokker-Plank equations are a set of differential equations used to describe random processes [21]. By using Gaussian statistics to generate the K distribution via a modulation process, standard communication theory can be used to gain further insight into the underlying processes. In addition, the mathematics required to generate the K distributed noise in this manner is much more straight forward and only requires the use of the transformation of random variables.

CONCLUSION

This dissertation presented both an experimental and a theoretical analysis for a laser beam propagating through random phase screens. The theoretical analysis showed that a nonstationary process could be modeled as a modulation process derivable from stationary Gaussian statistics. The HK distribution, which has been proposed for the intensity statistics for a laser beam propagating through the open atmosphere, was used to predict the statistics for a laser beam propagating through random phase screens. The HK distribution contains both a random part plus a deterministic part. The noise term is the result of a fast varying process that is Gaussian distributed, which is modulated by a slowly fluctuating process that is gamma distributed. For the case when the deterministic term is zero, the HK distribution reduces to the K distribution. It was also shown that the I-K distribution can be obtained from an approximation to the characteristic function of the HK distribution.

The derivation of the HK distribution assumed that the underlying process was the modulation of a Gaussian stationary noise process by another Gaussian process.

The net result was that the process describing the electric field was nonstationary because the variance was now changing with time. The method of handling the multiplication of two noise processes was to set one of the processes equal to a constant, and then find the conditional statistics due to the other process. Once the conditional statistics were known, the statistics due to both processes were then computed.

The first experiment measured the normalized moments for a laser beam propagating through a single phase screen. Next, the measured normalized second moment for a short distance behind the phase screen was used to predict the parameters α and ρ in the I-K distribution using the extended range model. The normalized moments for the intensity data were then compared to the extended range model predictions for the normalized moments. The predicted normalized moments agreed reasonably well with the experimental normalized moments. On the other hand, when multiple phase screens were used, the extended turbulence model did not match the normalized moments of the experimental data as well. This indicated that possibly another method for picking the parameters in the I-K distribution should be found, if the extended range model is to be used to predict the normalized moments for

fluctuations in the intensity for a laser beam propagating from ground to space, i.e., multiple phase screens.

Since the HK distribution was derived as a compound distribution from both the gamma distribution and the Rician distribution, the next experiment verified that these two distributions were indeed the correct distributions. Since the slowly varying random process was gamma distributed, lowpass filtering the intensity data yielded normalized moments that match the normalized moments for the gamma distribution. For short distances behind the phase screen, there exists a slight error between the actual experimental normalized moments and the normalized moments for the gamma distribution. One possible cause is the spectrum of the slowly varying process has increased in size and overlaps the spectrum for the fast varying process. This makes it impossible to separate the two processes by lowpass filtering the intensity fluctuations. The parameters α and ρ were then computed as a function of distance from the lowpass filter data. Next, the computed values of α and ρ were used to compute the normalized moments for both the HK and I-K distributions as a function of distance behind the phase screen. The normalized moments for both the HK and the I-K distributions agreed with the experimental normalized moments.

Next, the intensity data was segmented into small time intervals in which the variance b was approximately constant. Then each time segment that had a variance that was within a one percent difference was combined together to form bins. The normalized moments for each of these bins were then computed and were shown to be in agreement with the normalized moments for the Rician distribution. Segmenting the data this way removed the slowly fluctuating variance from the experimental intensity data.

It is interesting to note that when the lowpass filter intensity data was segmented into small time intervals, the statistics for the small time interval remained gamma distributed. On the other hand, when the unfiltered intensity data was segmented into smaller time intervals, the statistics for the intensity fluctuations changed from the HK distribution to the Rician distribution. Therefore, since the computed normalized moments for the unfiltered intensity data depended on the time interval in which the normalized moments were computed over, the unfiltered intensity fluctuations were considered nonstationary.

A computer program was written to simulate the K distribution from two zero mean Gaussian noise processes for the special case when α was unity. Since the underlying process in the derivation of the K distribution

was assumed to be the modulation of a fast varying random process by a slowly varying random process, a spectrum for both processes was proposed. The proposed spectrum assumed the fast varying process was located about some center frequency with a small bandwidth, while the slowly varying process was assumed to be centered around DC with a much wider bandwidth than the fast varying process. In addition, the proposed spectrums were used in the argument to describe how lowpass filtering the intensity fluctuations yielded normalized moments that matched the normalized moments for the gamma distribution.

The computer simulation generated a time series plot that looked similar to the time series plot for the case of a laser beam propagating through a phase screen. The intermittant fluctuation conditions could be seen in both plots, implying that the time fluctuations were indeed nonstationary. The normalized moments were then computed and compared with the normalized moments for the K distribution. These experimental moments lay below those for the K distribution. Since the normalized moments were computed from only one sample of 2,000 points, the error in the normalized moments is probably due to the scatter in estimating the normalized moments.

Next, the spectrum of the computer simulation output was computed using a Fast Fourier Transform program. The

Once the derivation of the spectrums is understood, the next area of study should be to simulate, via a computer, both the K and HK distributions from Gaussian processes in two dimensions. The goal of the simulation would be to measure the autocorrelation function from the actual intensity fluctuations, and to use this data in the computer simulation to generate a two-dimensional picture that simulates the actual intensity fluctuations. Once the computer can simulate the actual intensity fluctuations, work in the area of digital signal processing to remove these random fluctuations should be performed.

APPENDICES

APPENDIX A

SUMMARY OF PROBABILITY DENSITY FUNCTIONS

Gamma: $(0 < b < \infty)$

$$p(b) = \frac{b^{\alpha-1}}{\Gamma(\alpha)} \left[\frac{\alpha}{b_o} \right]^{\alpha} e^{-\alpha b/b_o} \qquad \text{(A-1)}$$

where b_o is the mean.

Gaussian: $(-\infty < x < \infty)$

$$p(x) = \frac{1}{\sqrt{2\pi b}} e^{-(x-A)^2/2b} \qquad \text{(A-2)}$$

where b is the variance and A is the mean.

HK: $(0 \leq V < \infty)$

$$p(I) = \left[\sqrt{I}\right]^{-1} \left[\frac{\alpha A\sqrt{I}}{b_o}\right]^{\alpha} \sum_{k=0}^{\infty} \frac{2(1-\alpha+2k)\Gamma(1-\alpha+k)^2}{\Gamma(1-\alpha)\Gamma(\alpha)k!k!A} E_{2k} \qquad \text{(A-3)}$$

where E_{2k} is defined as

$$E_{2k} = \begin{cases} K_{1-\alpha+2k}(2A\sqrt{\alpha/b_o})\ I_{1-\alpha+2k}(2\sqrt{I\alpha/b_o}) & \text{for } A^2 > I \\ I_{1-\alpha+2k}(2A\sqrt{\alpha/b_o})\ K_{1-\alpha+2k}(2\sqrt{I\alpha/b_o}) & \text{for } I > A^2 \end{cases}$$

I-K: $(0 \leq I < \infty)$

$$p(I) = 2\left[\frac{\sqrt{I}}{A}\right]^{\alpha-1}\left[\frac{\alpha}{b_o}\right] \cdot \begin{cases} K_{\alpha-1}(2A\sqrt{\alpha/b_o})\, I_{\alpha-1}(2\sqrt{\alpha I/b_o}) & \text{for } A^2 > I \\ I_{\alpha-1}(2A\sqrt{\alpha/b_o})\, K_{\alpha-1}(2\sqrt{\alpha I/b_o}) & \text{for } I > A^2 \end{cases} \quad \text{(A-4)}$$

K: $(0 \leq I < \infty)$

$$p(I) = \frac{2I^{(\alpha-1)/2}}{\Gamma(\alpha)}\left[\frac{\alpha}{b_o}\right]^{(\alpha+1)/2} K_{\alpha-1}(2\sqrt{I\alpha/b_o}) \quad \text{(A-5)}$$

M: $(0 \leq R < \infty)$

$$p(R) = \frac{2R^{2\alpha-1}}{\Gamma(\alpha)}\left[\frac{\alpha}{b_o}\right]^{\alpha} e^{-\alpha R^2/b_o} \quad \text{(A-6)}$$

Negative Exponential: $(0 \leq b < \infty)$

$$p(b) = \frac{1}{b_o} e^{-b/b_o} \quad \text{(A-7)}$$

where b_o is the mean of b.

Rayleigh: $(0 \leq R < \infty)$

$$p(R) = \frac{R}{b} e^{-R^2/(2b)} \quad \text{(A-8)}$$

where the mean is $\sqrt{b\pi/2}$.

Rician: $(0 \leq R < \infty)$

$$p(R) = \frac{2R}{b} e^{-(R^2+A^2)/b} I_o(2AR/b) \qquad \text{(A-9)}$$

Uniform: $(-\pi < x \leq \pi)$

$$p(x) = \frac{1}{2\pi} \qquad \text{(A-10)}$$

APPENDIX B

STATIONARY STATISTICS DERIVED FROM GAUSSIAN PROCESSES

Many random phenomena in nature can be derived from Gaussian statistics. One of the main reasons that the Gaussian distribution is so widely used in modeling random phenomena is because the central limit theorem applies to the physics behind the problem [4]. The central limit theorem, when applicable, eliminates the need to know the underlying process of the individual parts of the physical problem. If the physical problem is the result of many independent contributors that are all random, the PDF of the whole process will be Gaussian distributed.

Gaussian statistics can be described by three variables: the mean A, the variance σ^2, and the auto-correlation function $R(\tau)$. From the auto-correlation function, the spectrum of the process can be found by using the Wiener-Khintchine theorem [4]. The Gaussian PDF is given by

$$p(x) = \frac{1}{\sigma\sqrt{2\pi}} e^{-(x-A)^2/2\sigma^2} , \qquad (B-1)$$

where x is defined in the range $(-\infty < x < \infty)$. From the Gaussian PDF, several well known PDFs can be derived

through various nonlinear transformations, which include the Rayleigh distribution, the negative exponential distribution, the gamma distribution, the m distribution, and the Rician distribution.

Rayleigh Distribution

The Rayleigh distribution can be derived directly from a complex Gaussian process. A complex Gaussian process is of the form

$$Z = X + iY \ , \tag{B-2}$$

where X and Y are independent real Gaussian variables. Assuming that X and Y have equal variances and that both variables have zero mean, the PDFs for X and Y are

$$p(X) = \frac{1}{\sigma\sqrt{2\pi}} e^{-X^2/2\sigma^2} \ , \qquad (-\infty < X < \infty) \tag{B-3}$$

$$p(Y) = \frac{1}{\sigma\sqrt{2\pi}} e^{-Y^2/2\sigma^2} \ , \qquad (-\infty < Y < \infty) \tag{B-4}$$

where σ^2 is the variance of the random variables X and Y. Since X and Y are independent, their joint PDF is simply the product

$$p(X,Y) = p(X) \cdot p(Y) \ . \tag{B-5}$$

Using eqs. B-3, B-4 and B-5, the joint PDF for X and Y become

$$p(X,Y) = \frac{1}{\sigma^2 2\pi} e^{-(X^2+Y^2)/2\sigma^2} . \qquad \text{(B-6)}$$

Eq. B-2 can be rewritten in the terms of a magnitude and angle using polar notation

$$R \cdot e^{i\theta} = X + iY , \qquad \text{(B-7)}$$

where $R^2 = X^2 + Y^2$ and $\theta = \tan^{-1}\left[\frac{Y}{X}\right]$.

The joint PDF for R and θ is given by

$$p(R,\theta) = p(X,Y) \cdot J , \qquad \text{(B-8)}$$

where J is the Jacobian of transformation defined by

$$J = \begin{vmatrix} \frac{\partial X}{\partial R} & \frac{\partial X}{\partial \theta} \\ \frac{\partial Y}{\partial R} & \frac{\partial Y}{\partial \theta} \end{vmatrix} . \qquad \text{(B-9)}$$

Since,

$$X = R \cdot \cos(\theta) , \qquad \text{(B-10)}$$

$$Y = R \cdot \sin(\theta) , \qquad \text{(B-11)}$$

the Jacobian becomes

$$J = \begin{vmatrix} \cos(\theta) & -R \cdot \sin(\theta) \\ \sin(\theta) & R\cos(\theta) \end{vmatrix} = R. \qquad \text{(B-12)}$$

Combining eqs. B-6, B-10, B-11, and B-12 with eq. B-8, the joint PDF for R and θ becomes

$$p(R,\theta) = \frac{1}{\sigma^2 2\pi} R \cdot e^{-R^2/2\sigma^2}. \qquad (0 \leq R < \infty) \qquad \text{(B-13)}$$

Integrating $p(R,\theta)$ over the range of R leads to the PDF for θ. Performing this integration, the PDF for θ is

$$p(\theta) = \int_0^{\infty} p(R,\theta)\, dR, \qquad \text{(B-14)}$$

or

$$p(\theta) = \frac{1}{2\pi}. \qquad \text{(B-15)}$$

From eq. B-15, that the PDF of the phase θ is uniformly distributed over some 2π interval. For a zero mean, the interval will be from $-\pi \leq \theta < \pi$. The PDF for the magnitude R can be found by using the relation

$$p(R) = \int_{-\pi}^{\pi} p(R,\theta)\, d\theta, \qquad \text{(B-16)}$$

which yields

$$p(R) = \frac{R}{\sigma^2} e^{-R^2/2\sigma^2} \qquad (0 \leq R < \infty), \qquad \text{(B-17)}$$

where eq. B-17 is the Rayleigh PDF. One example of a physical situation in which Rayleigh statistics occur is finding the probability of hitting a two-dimensional target with a projectile [4; 18].

Negative Exponential Distribution

The easiest way to derive the negative exponential PDF is to start with the Rayleigh PDF and then make the transformation of variables $E = R^2$. Doing so gives

$$p(E) = \frac{1}{2\sigma^2} e^{-E/2\sigma^2} \qquad (0 \leq E < \infty) , \quad \text{(B-18)}$$

which is the negative exponential PDF. Thus, if a random process is Rayleigh distributed, the square of the process will always be negative exponential distributed.

Gamma Distribution

The gamma is the exact distribution for a sum of n independent variables, all of which have the same mean value and are governed by the negative exponential distribution. An equation defining such a process is

$$G = \sum_{k=1}^{n} E_k , \quad \text{(B-19)}$$

where each E_k is a negative exponential random variate.

To find the PDF for G, n convolutions have to be performed [18]. Another way of finding the PDF for G is to first express its characteristic function as the product of the characteristic functions of each E_k. The PDF of G is then found by taking the inverse Fourier Transform of the characteristic function.

Assuming that each E_k has the same negative exponential PDF, the characteristic function for the kth element is

$$C_{E_k}(U) = \int_{-\infty}^{\infty} p(E_k) \cdot e^{iUE_k} \, dE_k \, , \qquad \text{(B-20)}$$

where each E_k has the PDF

$$p(E_k) = \frac{1}{2\sigma^2} e^{-E_k/2\sigma^2} \qquad (0 \leq E < \infty). \qquad \text{(B-21)}$$

Performing the integration in eq. B-20, the characteristic function for the kth element is

$$C_{E_k}(U) = \frac{1}{(1-iU2\sigma^2)} \, . \qquad \text{(B-22)}$$

Performing n products of Eq.B-22 with itself, the characteristic function for the gamma PDF, $C_G(U)$, becomes

$$C_G(U) = \frac{1}{(1-iU2\sigma^2)^n} \, . \qquad \text{(B-23)}$$

The PDF for G can be found by the inverse Fourier Transform relation

$$p(G) = \frac{1}{2\pi} \int_{-\infty}^{\infty} C_G(U) \, e^{-iUG} \, dU \, . \qquad \text{(B-24)}$$

The substitution of eq. B-23 into eq. B-24 yields

$$p(G) = \frac{G^{n-1}}{\Gamma(n)} \left[\frac{1}{2\sigma^2} \right]^n e^{-G/2\sigma^2} \quad (0 \leq G < \infty) , \quad \text{(B-25)}$$

which is known as the gamma distribution. It is interesting to note that when n equals unity, the gamma PDF reduces to the negative exponential PDF.

The m distribution is related to the gamma distribution by the transformation $M = \sqrt{G}$. Performing this transformation and using

$$p(M) = P(G) \cdot \left| \frac{\partial G}{\partial M} \right| , \quad \text{(B-26)}$$

the PDF for the m distribution is given as

$$p(M) = \frac{2M^{2n-1}}{\Gamma(n)} \left[\frac{1}{2\sigma^2} \right]^n e^{-M^2/2\sigma^2} \quad (0 \leq M < \infty). \quad \text{(B-27)}$$

It should be noted that the Rayleigh distribution is the special case of the the m distribution for n equal to unity.

Rician Distribution

Thus far, all of the PDFs that have been derived in this appendix have been based on the assumption that the original process was Gaussian distributed with mean zero. This is the usual assumption when dealing with noise processes alone. For the case of Gaussian noise plus a deterministic part, the same techniques for transformation

of random variables can be used to determine the PDF of several related distributions.

Let the process be defined by

$$Ve^{i\upsilon} = Ae^{i\phi} + Re^{i\eta} , \qquad \text{(B-28)}$$

where $Ae^{i\phi}$ is the deterministic part and $Re^{i\eta}$ is the random part. Assuming that the random part is complex Gaussian distributed, it has been shown that R becomes Rayleigh distributed and η is uniformly distributed. Rewriting eq. B-28,

$$Ve^{i(\upsilon-\phi)} = A + Re^{i(\eta-\phi)} \qquad \text{(B-29)}$$

and letting $\psi = \upsilon-\phi$ and $\theta = \eta-\phi$, eq. B-29 reduces to

$$Ve^{i\psi} = A + Re^{i\theta} . \qquad \text{(B-30)}$$

Since η is uniform and ϕ is a constant, θ remains uniformly distributed but is now centered around the interval $-(\pi+\phi) \leq \theta < (\pi-\phi)$. For mathematical convenience and without any loss to generality, ϕ will be set to zero in the analysis to follow.

The joint PDF for V and ψ can be related to the joint PDF for R and θ by

$$p(V,\psi) = p(R,\theta)\cdot J , \qquad \text{(B-31)}$$

where J is the Jacobian of transformation. To find the Jacobian, the first step is to separate eq. B-30 into its real and imaginary parts. This yields two independent equations of the form

$$V \cdot \sin(\psi) = R \cdot \sin(\theta) \tag{B-32}$$

and

$$V \cdot \cos(\psi) = A + R \cdot \cos(\theta) \ . \tag{B-33}$$

Solving eqs. B-32 and B-33 for R and θ gives

$$R^2 = A^2 + V^2 - 2AV \cdot \cos(\psi) \tag{B-34}$$

and

$$\tan(\theta) = \frac{V \cdot \sin(\psi)}{V \cdot \cos(\psi) - A} \ . \tag{B-35}$$

The Jacobian for the transformation as described by eq. B-30 is

$$J = \begin{vmatrix} \frac{\partial R}{\partial V} & \frac{\partial R}{\partial \psi} \\ \frac{\partial \theta}{\partial V} & \frac{\partial \theta}{\partial \psi} \end{vmatrix} \ . \tag{B-36}$$

Using eqs. B-34 and B-35 along with eq. B-36, and after some algebra, the Jacobian of transformation becomes

$$J = \frac{V}{R} \ . \tag{B-37}$$

Returning to eq. B-31 and substituting eqs. B-34 and B-37, the joint PDF for V and ψ assumes the form

$$p(V,\psi) = \frac{V}{2\pi\sigma^2} e^{-(V^2 + A^2 - 2AV\cdot\cos(\psi))/2\sigma^2} . \qquad (B\text{-}38)$$

To find the marginal PDF for V, the random variable ψ is integrated over the interval 0 to 2π using the following equation,

$$p(V) = \int_0^{2\pi} p(V,\psi)\, d\psi . \qquad (B\text{-}39)$$

Combining eqs. B-38 and B-39, the PDF for V becomes

$$p(V) = \frac{V}{2\sigma^2\pi} e^{-(V^2+A^2)/2\sigma^2} \int_0^{2\pi} e^{AV\cdot\cos(\psi)/\sigma^2} d\psi . \qquad (B\text{-}40)$$

Using the identity from page 376 of reference [22]

$$I_o(x) = \frac{1}{2\pi} \int_0^{2\pi} e^{x\cdot\cos(\theta)}\, d\theta, \qquad (B\text{-}41)$$

the PDF for V becomes

$$p(V) = \frac{V}{\sigma^2} e^{-(V^2+A^2)/2\sigma^2} I_o\left[\frac{AV}{\sigma^2}\right] \quad 0 \le V < \infty . \qquad (B\text{-}42)$$

Eq. B-42 is known as the Rician PDF. A more common form that occurs in optics is obtained by making the substitution $I = V^2$, where I is the intensity of the field. The PDF for I is

$$p(I) = \frac{1}{2\sigma^2} e^{-(I+A^2)/2\sigma^2} I_o\left[\frac{A\sqrt{I}}{\sigma^2}\right] . \qquad (B-43)$$

Eq. B-43 is known as the modified Rician PDF. The Rician statistic is very common in real optical systems where the noise contains both a deterministic part and a random part. If eq. B-30 is used to model the electric field of an optical process, the output of the detector, which is proportional to $|Ve^{i\psi}|^2 = V^2$, will be Rician distributed and given by eq. B-43. For A equal to zero, the Rician PDF defined by eq. B-43 reduces to the negative exponential PDF.

Gamma Moments

Since the gamma and Rician PDFs are used in the development of nonstationary statistics derived from complex Gaussian processes, their moments are also of interest. That is, by knowing the theoretical moments, experimental data can be easily compared with such moments to verify theoretical models. Starting with eq. B-25 and making the substitutions $2\sigma^2 = b_o/\alpha$ and $\alpha = n$, the gamma PDF becomes

$$p(G) = \frac{G^{\alpha-1}}{\Gamma(\alpha)} \left[\frac{\alpha}{b_o}\right]^{\alpha} e^{-G\alpha/b_o} , \qquad (B-44)$$

which conveniently makes the mean of the gamma

distribution a constant b_o independent of α. This substitution is strictly for mathematical convenience, since only normalized moments are of interest.

The nth moment is defined as the expected value

$$E\left[G^n\right] = \int_{-\infty}^{\infty} G^n \cdot p(G)\, dG. \qquad \text{(B-45)}$$

Substituting eq. B-44 into eq. B-45, and rearranging terms, eq. B-45 becomes

$$E\left[G^n\right] = \frac{1}{\Gamma(\alpha)} \left[\frac{\alpha}{b_o}\right]^{\alpha} \int_0^{\infty} G^{n+\alpha-1}\, e^{-G\alpha/b_o}\, dG. \qquad \text{(B-46)}$$

Letting $U = G\alpha/b_o$, $dU = \alpha/b_o\, dG$, and using the identity from page 255 of reference [23],

$$\Gamma(m) = \int_0^{\infty} t^{m-1}\, e^{-t}\, dt, \qquad \text{(B-47)}$$

the moments for the gamma distribution are

$$E\left[G^n\right] = \left[\frac{b_o}{\alpha}\right]^n \frac{\Gamma(n+\alpha)}{\Gamma(\alpha)} . \qquad \text{(B-48)}$$

Using the identity from page 256 of reference [23],

$$\frac{\Gamma(n+\alpha)}{\Gamma(\alpha)} = (n-1+\alpha)(n-2+\alpha)\ldots(\alpha) , \qquad \text{(B-49)}$$

the gamma moments are given by

$$E\left[G^n\right] = \left[\frac{b_o}{\alpha}\right]^n (n-1+\alpha)(n-2+\alpha)\ldots(\alpha). \qquad \text{(B-50)}$$

For the case when n = 1, the mean for the gamma distribution reduces to b_o. From the gamma moments given by eq. B-50, the normalized moments are easily found. The normalized moments are found by dividing eq. B-50 by the mean b_o to the nth power. A nice feature of computing normalized moments is the comparison with experimental data is then much easier, since normalizing the moments by the mean value essentially makes the mean value unity. The normalized moments for the gamma distribution are defined as

$$\frac{E\left[G^n\right]}{E\left[G\right]^n} = \frac{(n-1+\alpha)(n-2+\alpha)\ldots(\alpha)}{(\alpha)^n} . \qquad \text{(B-51)}$$

Rician Moments

The Rician moments are of interest because the Rician distribution will be used in the derivation of the HK distribution model of nonstationary statistics. The Rician moments are defined as

$$E\left[I^n\right] = \int_{-\infty}^{\infty} I^n \, p(I) \, dI . \qquad \text{(B-52)}$$

Using the definition for the Rician PDF defined in

eq. B-43, along with substituting $b = 2\sigma^2$, the moments can be written as

$$E\left[I^n\right] = \frac{1}{b}\, e^{-A^2/b} \int_0^\infty I^n\, e^{-I/b}\, I_o\left[\frac{2A\sqrt{I}}{b}\right] dI. \qquad \text{(B-53)}$$

Using the identity from page 720 of reference [22]

$$\frac{\Gamma(u+v+1/2)}{\Gamma(2v+1)}\, \beta^{-1}\, e^{\beta^2/2\alpha}\, \alpha^{-u}\, M_{-u,v}\left(\frac{\beta^2}{\alpha}\right) =$$

$$\int_0^\infty x^{u-1/2}\, e^{-\alpha x}\, I_{2v}(2\beta\sqrt{x})\, dx\ , \qquad \text{(B-54)}$$

where $M_{-u,v}(x)$ is the Whittaker's function, and setting $v = 0$, $u-1/2 = n$ $\beta = A/b$ and $\alpha = 1/b$, the integral in eq. B-53 yields,

$$E\left[I^n\right] = n!\, \left[\frac{\sqrt{b}}{A}\right] b^n\, e^{-A^2/2b}\, M_{-n-1/2,0}(A^2/b)\ . \qquad \text{(B-55)}$$

Using the identity from page 1059 of reference [22],

$$M_{\lambda,-u}(z) = z^{-u+1/2}\, e^{-z/2}\, {}_1F_1(-u-\lambda+1/2;-2u+1;z), \qquad \text{(B-56)}$$

where ${}_1F_1(u;x;z)$ is the degenerate hypergeometric function, the Rician moments are then given by

$$E\left[I^n\right] = e^{-A^2/b}\, n!\, b^n\, {}_1F_1(n+1;1;A^2/b)\ . \qquad \text{(B-57)}$$

Making the substitution from page 1058 of reference [22]

$$ {}_1F_1(\alpha;y;z) = e^z \; {}_1F_1(y-\alpha;y;-z) \; , \qquad \text{(B-58)} $$

with $\alpha = -n$, $y = 1$, and $z = -A^2/b$, eq B-57 reduces to

$$ E\left[I^n\right] = n! \; b^n \; {}_1F_1(-n;1,-A^2/b) \qquad \text{(B-59)} $$

Recognizing that the degenerate hypergeometric function for the special case defined by eq. B-59 is related to Laguerre polynomials by the identity from page 1037 of reference [22] as

$$ L_n(x) = {}_1F_1(-n;1;x) \; . \qquad \text{(B-60)} $$

Using eq. B-60 and the relationship from page 1037 of reference [22]

$$ L_n(x) = \sum_{m=0}^{n} (-1)^m \begin{bmatrix} n \\ n-m \end{bmatrix} \frac{x^m}{m!} \; , \qquad \text{(B-61)} $$

yields the moments for the Rician distribution

$$ E\left[I^n\right] = n! \; b^n \sum_{m=0}^{n} \begin{bmatrix} n \\ n-m \end{bmatrix} \frac{(A^2/b)^m}{m!} \; . \qquad \text{(B-62)} $$

By setting $n = 1$, the mean is given as

$$ E(I) = b(1+A^2/b) \; , \qquad \text{(B-63)} $$

where A^2/b is the ratio of the intensity of the deterministic part of the signal to the intensity of the

noise part of the signal. Hence, this ratio is simply the signal to noise power ratio. Defining $\rho = A^2/b$ as the signal to noise power ratio and using eq. B-63, the normalized moments for the Rician distribution in terms of ρ are

$$\frac{E\left[I^n\right]}{E\left[I\right]^n} = \frac{n!}{(1+\rho)^n} \sum_{m=0}^{n} \begin{bmatrix} n \\ n-m \end{bmatrix} \frac{\rho^m}{m!} . \qquad \text{(B-64)}$$

APPENDIX C

NONSTATIONARY STATISTICS DERIVED FROM COMPOUND GAUSSIAN PROCESSES

Recently, it has been observed that several physical phenomena could not be modeled with stationary Gaussian statistics. Fluctuations in the intensity of a laser beam as it propagates through the atmosphere, and fluctuations in the return signal of radar echo off the sea's surface, are two such examples of physical processes that appear nonstationary for short time intervals [8; 9; 10; 11; 12; 13; 14]. Attempts to use the various PDFs that were derived for stationary statistics failed. The experimental time series data for both the laser propagation and the radar echo problems revealed that the variance of the electric field was varying with time. From this fact, researchers concluded that both problems were nonstationary random processes.

Nonstationary processes must be handled differently than stationary processes. There are three parameters which determine a Gaussian process, the mean, the variance, and the autocorrelation function. If any of the three factors are changing with time, the Gaussian process

may be considered nonstationary. For both physical examples mentioned, it is believed that the variance of the electric field is changing with time.

One approach in modeling nonstationary processes in which the variance is changing with time, is to assume that the process is the result of two noise processes modulating each other. The modulation of two noise processes is simply the multiplication of the two noise processes yielding a short term nonstationary process [15; 16; 17]. So that the same techniques used for stationary processes can be used for this product process, it is assumed that one of the noise processes is initially held constant. Then the conditional statistics due solely to the "free" noise process is computed. Next, the unconditional statistics are computed by averaging the conditional statistics with the statistic of the noise process which was initially held fixed.

Several PDFs have been derived using conditional statistics [11; 12; 13; 19]. The K distribution was derived for the radar echo problem by averaging a negative exponential PDF with a gamma PDF. The gamma PDF was used to model the slowly varying fluctuations in the variance of the electric field, while the negative exponential PDF was used to model the conditional field. The HK PDF was derived for the laser beam propagation problem by assuming

that the conditional electric field was Rician distributed and then averaging this PDF with a gamma PDF. The gamma PDF was used to model the fluctuations in the variance of the electric field.

K Distribution

The K distribution is derivable from two zero mean complex Gaussian processes, one modulating the other. To gain further insight into the laser beam propagation problem, the K distribution will be derived for the intensity statistics. Assuming an electric field of the form

$$U(t) = N(t) \cdot W(t), \tag{C-1}$$

where N(t) is assumed to be slowly varying with time, and W(t) is assumed to be rapidly varying with time.

A more common form for the field appearing in the literature is [12; 13]

$$U(t) = R(t)e^{i\phi(t)}. \tag{C-2}$$

Assuming that W(t) is the sum of independent modes, which was previously called scatterers in the literature, [13], W(t) can then be written in the form

$$W(t) = \sum_{k=1}^{m} r_k(t) \cdot e^{i\phi_k(t)} . \tag{C-3}$$

Since each $r_k e^{\phi_k}$ is the result of a large number of rays, each mode is assumed to be complex Gaussian with a zero mean. In addition, each mode is also assumed to be completely independent of all other modes.

Defining σ_k^2 as the variance for both the real and imaginary parts of the kth mode, the variance for the kth mode is just the sum of the variance from both the real and imaginary parts and is given by

$$E\left[r_k^2\right] = 2\sigma_k^2 \quad . \tag{C-4}$$

Since the mean of W is zero, the variance of W simply equals the second moment of W. Using eq. C-3, the variance of W is

$$\sigma_w^2 = E\left[\sum_{k=1}^{m} \sum_{j=1}^{m} r_k r_j \, e^{i(\phi_k - \phi_j)} \right]$$

$$= E\left[\sum_{k=1}^{m} r_k^2 \right] + E\left[\sum_{\substack{k=1 \\ j \neq k}}^{m} \sum_{j=1}^{m} r_k e^{i\phi_k} \, r_j e^{-i\phi_j} \right] . \tag{C-5}$$

Switching the order of the expected value and the summation in the second term of eq. C-5, because the modes are independent, the expected value of the kth mode with the jth mode is

$$E\left[r_k e^{i\phi_k} \, r_j e^{-i\phi_j}\right] = E\left[r_k e^{i\phi_k}\right] E\left[r_j e^{-i\phi_j}\right] . \tag{C-6}$$

Since the expected value of $r_k e^{i\phi_k}$ is zero, the second term in eq. C-5 is zero. Interchanging the order of the expected value with the summation in the first term of eq. C-5, and using the results of eq. C-4, the variance for W becomes

$$\sigma_w^2 = \sum_{k=1}^{m} 2\sigma_k^2 \quad . \tag{C-7}$$

Since each mode is from the same physical process, it is not unreasonable to assume that the variance for each mode is approximately the same. Letting

$$\sigma_k^2 = \sigma^2 \quad , \tag{C-8}$$

the variance for W then reduces to

$$\sigma_w^2 = w_o = 2m\sigma^2 \quad . \tag{C-9}$$

Rewriting the fast varying process W as a complex variable, since it is the sum of m independent variables that are each complex and Gaussian distributed, yields

$$W(t) = r(t)e^{i\phi(t)} \quad , \tag{C-10}$$

where r is Rayleigh distributed and ϕ is uniformly distributed. Substituting eq. C-10 into eq. C-1 a new form for the electric field in terms of a magnitude and a

phase angle is

$$U(t) = N(t)r(t)e^{i\phi(t)} \quad . \tag{C-11}$$

To find the PDF for the electric field U, N(t) is held fixed and the conditional PDF for the electric field is computed [16]. Once the conditional PDF for the field is known, the unconditional PDF for the electric field or intensity is obtained by averaging on the PDF for the process of N [18]. Setting N(t) = c, a constant, eq. C-11 describing the electric field becomes

$$U(t) = cr(t)\ e^{i\phi(t)} \quad . \tag{C-12}$$

Using eq. C-2, the joint PDF of the field in terms of R,ϕ is given by

$$p(R,\phi) = p(r,\phi)\cdot J \quad . \tag{C-13}$$

Since W is complex Gaussian, $p(r,\phi)$ is given by eq. B-13

$$p(r,\phi) = \frac{r}{2m\sigma^2\pi}\ e^{-r^2/2m\sigma^2} \quad . \tag{C-14}$$

Using the Jacobian of transformation

$$J = \begin{vmatrix} \frac{\partial r}{\partial R} & \frac{\partial r}{\partial \phi} \\ \frac{\partial \phi}{\partial R} & \frac{\partial \phi}{\partial \phi} \end{vmatrix} \quad , \tag{C-15}$$

and the variable which is defined as

$$R \cdot e^{i\phi} = cr \cdot e^{i\phi} , \qquad \text{(C-16)}$$

yields

$$r = R/c , \qquad \text{(C-17)}$$

and

$$J = \frac{1}{c} . \qquad \text{(C-18)}$$

The conditional PDF for the field in terms R and ϕ is

$$p(R,\phi|c) = \frac{R}{c^2 m\sigma^2 2\pi} e^{-R^2/c^2 m 2\sigma^2} . \qquad \text{(C-19)}$$

Integrating ϕ over the interval $-\pi$ to π, the conditional PDF for the magnitude of the electric field reduces to the Rayleigh PDF

$$p(R|c) = \frac{R}{c^2 m\sigma^2} e^{-R^2/2c^2 m\sigma^2} . \qquad \text{(C-20)}$$

The conditional PDF for the intensity can be found by making the transformation $I = |U^2|$, which implies that $I = R^2$. Performing the transformation, the conditional PDF for the intensity is

$$P(I|c) = \frac{1}{2c^2 m\sigma^2} e^{-I/2c^2 m\sigma^2} . \qquad \text{(C-21)}$$

Eq. C-21, is the negative exponential PDF, and the

conditional variance of the field is

$$\sigma_U^2 = 2c^2 m\sigma^2 \quad . \tag{C-22}$$

From the above derivation, the slowly varying term N(t) manifests itself as a slowly changing variance. Since the variance of the electric field is varying with time, the process for the electric field is taken to be nonstationary. Defining b as the slowly varying variance, and replacing c by N(t), the time dependent variance of the field becomes

$$b = 2m\sigma^2 N(t)^2 = w_o N(t)^2 \quad . \tag{C-23}$$

The number of modes, m, could just as likely have been replaced by the average number of modes, M_o, and $N^2(t)$ used to describe the slow variations in these modes. This is the continuous analog of the negative bimomial distribution for the arrival of photons that Jakeman proposed [11]. Andrews and Phillips proposed that the total number of modes can be replaced by the effective number of modes, α, enabling α to be a continuous variable [12; 13]. In the limit, the negative binomial PDF which is used to describe the discrete photon arrival process reduces to the gamma PDF for continuous processes. Since the effective number of modes is a continuous process, the

PDF for the fluctuations in the variance of the electric field is chosen to be gamma distributed.

Using eqs. C-21 and C-23 and $n = N(t)^2$, the conditional PDF for the intensity is

$$p(I|n) = \frac{e^{-I/nw_o}}{nw_o} . \qquad \text{(C-24)}$$

Letting n_o define the average of the slowly varying process, and using eq. A-1 for the gamma PDF, the PDF for the time dependent variance becomes

$$p(n) = \frac{n^{\alpha-1}}{\Gamma(\alpha)} \left[\frac{\alpha}{n_o}\right]^{\alpha} e^{-\alpha n/n_o} . \qquad \text{(C-25)}$$

Using,

$$P(I) = \int_0^{\infty} p(I|n)\, p(n)\, dn , \qquad \text{(C-26)}$$

and substituting eqs. C-24 and C-25 into eq. C-26, the unconditional PDF for the intensity is

$$p(I) = \left[\frac{\alpha}{n_o}\right]^{\alpha} \frac{1}{\Gamma(\alpha)} \int_0^{\infty} \frac{n^{\alpha-2}}{w_o} e^{-(I/nw_o+\alpha n/n_o)}\, dn . \qquad \text{(C-27)}$$

Using the identity from page 340 [384] of reference [22]

$$2\left[\frac{b}{a}\right]^{v/2} K_v(2\sqrt{ab}) = \int_0^{\infty} x^{v-1} e^{-ax-b/x}\, dx , \qquad \text{(C-28)}$$

with $v = \alpha-1$, $a = \alpha/n_o$, and $b = I/w_o$, the unconditional

PDF for the intensity reduces to

$$p(I) = \frac{2}{\Gamma(\alpha)} \left[\frac{\alpha}{n_o w_o}\right]^{\frac{\alpha+1}{2}} I^{\frac{\alpha-1}{2}} K_{\alpha-1}\left[2\sqrt{\alpha I / n_o w_o}\right] , \qquad (C\text{-}29)$$

which is known as the K distribution.

The K distribution, as defined by eq. C-29, has been used to predict the statistics of a laser beam propagating through the atmosphere under strong turbulent conditions. For this case, the resulting statistics are considered to be in the saturation region. The K distribution also provides good predictions for the statistics of the twinkling of star light and for the statistics of the return signal for radar echo off the sea's surface.

HK Distribution

Like the K distribution, the HK distribution is also derivable from a complex Gaussian process. The HK distribution was originally proposed by Jakeman, but Link derived the HK PDF [19]. Link computed the HK PDF as an infinite sum of I and K Bessel functions. In the derivation of the HK distribution, Link assumed that the process was compound containing a nonstationary random part plus a deterministic part.

The nonstationary fluctuations in the electric field can be modeled as a modulation of a slowly varying random process with a fast varying random process. An equation

defining the electric field is

$$U(t) = Ae^{i\theta} + N(t)\cdot W(t) \ , \qquad \text{(C-30)}$$

where N(t) is the slowly varying process and W(t) is the fast varying process. Both N(t) and W(t) are assumed to be derivable from stationary complex Gaussian statistics. $Ae^{i\theta}$ is a complex constant making up the deterministic part of the electric field. For ease of notation and without any loss of generality, θ will be set to zero yielding an equation for the electric field as

$$U(t) = A + N(t)\cdot W(t) \ . \qquad \text{(C-31)}$$

Assuming that the fast process W(t) is composed of the sum of m independent modes, then W(t) can be written as a sum as in eq. C-3. Applying the Central Limit Theorem to the assumption that each mode is due to the sum of a large number of rays, the conditional joint PDF for R and ϕ is given by eq. C-19. Then the process for the electric field is simply

$$U = A + R\, e^{i\phi} \ . \qquad \text{(C-32)}$$

Rewriting eq. C-32 in terms of a magnitude and a phase

$$U = Ve^{i\psi} = A + Re^{i\phi} \qquad \text{(C-33)}$$

and then taking the expected value to find the mean of the electric field, i.e.,

$$E\left[Ve^{i\psi}\right] = E\left[A\right] + E\left[Re^{i\phi}\right] = A \ . \qquad \text{(C-34)}$$

The expected value of V^2 is given by

$$E\left[V^2\right] = E\left[A^2\right] + E\left[R^2\right] + A\,E\left[Re^{-i\phi}\right] + A\,E\left[Re^{i\phi}\right] \ , \qquad \text{(C-35)}$$

which immediately reduces to

$$E\left[V^2\right] = A^2 + E\left[R^2\right] \ , \qquad \text{(C-36)}$$

since the mean value of the random portion of the field is zero. Using eq. C-22, $E\left[R^2\right] = 2c^2 m\sigma^2$ and the identity that the variance of the random portion of the field is equal to the second moment minus the mean of the electric field squared, the conditional variance for the electric field is thus given by

$$\sigma_U^2 = 2c^2 m\sigma^2 \ , \qquad \text{(C-37)}$$

which is the same variance as that found for the K distribution. Replacing c^2 by $N^2(t)$, the time dependent variance is

$$b = 2\,N(t)^2 m\sigma^2 = w_o N(t)^2 \ . \qquad \text{(C-38)}$$

Again, the slowly varying process manifests itself as a

slowly changing variance making the process for the electric field appear nonstationary.

Using the conditional joint PDF for R and ϕ from eq. C-19 and the slowly varying variance given in eq. C-38, the conditional PDF for the random part of the electric field is

$$p(R,\phi|n) = \frac{R}{\pi n w_o} e^{-R^2/nw_o} . \qquad (C-39)$$

Using eq. C-33, and recalling the derivation of the Rician distribution given in Appendix B, yields the conditional PDF for the magnitude of the electric field

$$p(V|n)= \frac{2V}{nw_o} e^{-(V^2+A^2)/nw_o} I_o(2AV/nw_o) . \qquad (C-40)$$

Making the substitution $I = V^2$ and performing the transformation of variables, the conditional PDF for the intensity fluctuations is

$$p(I|n) = \frac{e^{-(I+A^2)/nw_o}}{nw_o} I_o(2A\sqrt{I}/nw_o) . \qquad (C-41)$$

Based on the same physical assumptions that were used in the development of the K distribution, the PDF for the variance of the electric field is given by the gamma PDF

$$p(n) = \frac{n^{\alpha-1}}{\Gamma(\alpha)} \left[\frac{\alpha}{n_o}\right]^{\alpha} e^{-\alpha n/n_o} , \qquad (C-42)$$

where α is the effective number of modes and n_o is the average of the slowly varying process. The unconditional PDF for the intensity fluctuations is then found using

$$p(I) = \int_0^\infty p(I|n)\, p(n)\, dn \ . \qquad \text{(C-43)}$$

Combining eqs. C-41, C-42, and C-43, the unconditional PDF for the intensity is

$$p(I) = \left[\frac{\alpha}{n_o}\right]^\alpha \frac{1}{\Gamma(\alpha) w_o} \int_0^\infty n^{\alpha-2}\ e^{-\alpha n/n_o}\ e^{-(I+A^2)/nw_o}$$

$$\cdot\ I_o(2A\sqrt{I}/nw_o)\ dn \ . \qquad \text{(C-44)}$$

Using the identity from page 375 of reference [23]

$$I_o(z) = \sum_{k=0}^{\infty} \frac{(z/2)^{2k}}{(k!)^2} \ , \qquad \text{(C-45)}$$

and reversing the order of integration and the summation, eq. C-44 yields

$$p(I) = \left[\frac{\alpha}{n_o}\right]^\alpha \frac{1}{\Gamma(\alpha)} \sum_{k=0}^{\infty} \frac{(A^2 I)^k}{(k!)^2} \cdot \left[\frac{1}{w_o}\right]^{2k+1}$$

$$\cdot \int_0^\infty n^{\alpha-2-2k}\ e^{-\alpha n/n_o - (I+A^2)/nw_o}\ dn \ . \qquad \text{(C-46)}$$

The integral in eq. C-46 can be evaluated using eq. C-28 to give

$$p(I) = \left[\frac{\alpha}{n_o}\right]^{\alpha} \frac{2}{\Gamma(\alpha)} \sum_{k=0}^{\infty} \frac{(A^2 I)^k}{(k!)^2} \left[\sqrt{(I+A^2)n_o/w_o\alpha}\right]^{\alpha-1-2k}$$

$$\cdot K_{\alpha-1-2k}\left[2\sqrt{(I+A^2)\alpha/n_o w_o}\right] \cdot \left[\frac{1}{w_o}\right]^{2k+1} . \qquad \text{(C-47)}$$

Rewriting eq. C-47 in a different form using $K_v(z) = K_{-v}(z)$ from page 375 of reference [23]

$$p(I) = \frac{2}{\Gamma(\alpha)} \sum_{k=0}^{\infty} \frac{(A^2 I)^k}{(k!)^2} \; 2^{2k+1-\alpha} \left[\frac{\alpha}{n_o w_o}\right]^{2k+1}$$

$$\cdot \frac{K_{2k+1-\alpha}\left[2\sqrt{(I+A^2)\alpha/n_o w_o}\right]}{\left[2\sqrt{(I+A^2)\alpha/n_o w_o}\right]^{2k+1-\alpha}} . \qquad \text{(C-48)}$$

Using the identity from page 126 of reference [24]

$$\frac{K_v\left[a\sqrt{I+A^2}\right]}{\left[a\sqrt{I+A^2}\right]^v} = 2^v \Gamma(v) \sum_{n=0}^{\infty} \frac{(v+n)}{(a^2 A\sqrt{I})^v} \; G_{n+v} \; C_n^v(0) \qquad \text{(C-49)}$$

where $C_n^v(z)$ is the Gegenbauer polynomial, a is any constant and

$$G_{n+v} = \begin{cases} I_{v+n}(aA) \quad K_{v+n}(a\sqrt{I}) & I > A^2 \\ I_{v+n}(a\sqrt{I}) \; K_{v+n}(aA) & I \leq A^2 \end{cases} . \qquad \text{(C-50)}$$

For $v = 2k+1-\alpha$, and $a = 2\sqrt{\alpha/n_o w_o}$, eq. C-48 becomes

$$p(I) = \left[\frac{\alpha}{n_o w_o}\right]^{\alpha} \frac{2(A\sqrt{I})^{\alpha-1}}{\Gamma(\alpha)} \sum_{k=0}^{\infty} \sum_{n=0}^{\infty} \frac{\Gamma(2k+1-\alpha)(2k+1-\alpha+n)}{(k!)^2}$$

$$\cdot E_{n+2k} \cdot C_n^{2k+1-\alpha}(0) \ , \qquad \text{(C-51)}$$

where

$$E_{n+2k} =$$

$$\begin{cases} I_{n+2k+1-\alpha}\left[2\sqrt{A^2\alpha/n_o w_o}\right] K_{n+2k+1-\alpha}\left[2\sqrt{I\alpha/n_o w_o}\right] & I > A^2 \\ I_{n+2k+1-\alpha}\left[2\sqrt{I\alpha/n_o w_o}\right] K_{n+2k+1-\alpha}\left[2\sqrt{A^2\alpha/n_o w_o}\right] & I \leq A^2 \end{cases} , \qquad \text{(C-52)}$$

and from page 777 of reference [23] the Gegenbauer polynomial evaluated at zero is

$$C_n^a(0) = \begin{cases} 0 & n \text{ odd} \\ \dfrac{(-1)^{n/2}\,\Gamma(a+n/2)}{\Gamma(a)\,(n/2)!} & n \text{ even} \end{cases} . \qquad \text{(C-53)}$$

Using eqs. C-52 and C-53, the unconditional PDF for the intensity fluctuations is

$$p(I) = \left[\frac{\alpha}{n_o w_o}\right]^{\alpha} \frac{2(A\sqrt{I})^{\alpha-1}}{\Gamma(\alpha)} \sum_{k=0}^{\infty} \sum_{n=0}^{\infty} \frac{(2k+1-\alpha+2n)\ \Gamma(2k+1-\alpha+n)}{k!k!\ n!}$$

$$\cdot (-1)^n E_{2n+2k} \ . \qquad \text{(C-54)}$$

Making the substitution m = n+k and writing the k summation from zero to infinity, even though all terms for k > m are zero, yields

$$P(I) = \left[\frac{\alpha}{n_o w_o}\right]^{\alpha} \frac{2(A\sqrt{I})^{\alpha-1}}{\Gamma(\alpha)}$$

$$\cdot \sum_{m=0}^{\infty} \sum_{k=0}^{\infty} \frac{(-1)^{m-k}(2m+1-\alpha)\Gamma(k+1+m-\alpha)}{k!k!\ (m-k)!} E_{2m} \quad . \qquad (C-55)$$

Using the identity $\Gamma(a+1) = a\Gamma(a)$ from page 256 of reference [23] eq. C-55 becomes

$$p(I) = \left[\frac{\alpha}{n_o w_o}\right]^{\alpha} \frac{2(A\sqrt{I})^{\alpha-1}}{\Gamma(\alpha)} \sum_{n=0}^{\infty} \frac{(2n+1-\alpha)\ \Gamma(1-\alpha+n)(-1)^n}{n!} E_{2n}$$

$$\cdot \sum_{k=0}^{\infty} \frac{(-n)_k\ (n-\alpha+1)_k}{k!k!}, \qquad (C-56)$$

where $(a)_k$ is the pochhammer symbol. It is defined from page 256 of reference [23] as

$$(a)_k = a(a+1)(a+2)(a+3)\ldots(a+k-1) \ , \qquad (C-57)$$

Using the identities

$$\frac{(-n)_k}{k!} = (-1)^k \begin{bmatrix} n \\ k \end{bmatrix} \ , \qquad (C-58)$$

and

$$(1-a+n)_k = \frac{\Gamma(1-a+n+k)}{\Gamma(1-a+n)} \ . \qquad (C-59)$$

and the identity from page 1039 of reference [22] for the Hypergeometric function

$$ {}_2F_1(a,g;y;z) = \sum_{k=0}^{\infty} \frac{(a)_k (g)_k}{(y)_k} \frac{z^k}{k!} , \qquad \text{(C-60)} $$

with a = -n, g = (1-α+n), y = 1 and z = 1 yields

$$ P(I) = \left[\frac{\alpha}{n_o w_o}\right]^{\alpha} \frac{2(A\sqrt{I})^{\alpha-1}}{\Gamma(\alpha)} \sum_{n=0}^{\infty} \frac{(2n+1-\alpha)\ \Gamma(1+n-\alpha)(-1)^n}{n!} E_{2n} $$

$$ \cdot\ {}_2F_1(-n,1+n-\alpha;1;1) . \qquad \text{(C-61)} $$

Using the identity from page 1042 of reference [22]

$$ {}_2F_1(a,g;y;1) = \frac{\Gamma(y)\ \Gamma(y-a-g)}{\Gamma(y-a)\ \Gamma(y-g)} \qquad \text{(C-62)} $$

with a = -n, g = 1+n-α and y = 1, eq. 61 reduces to

$$ p(I) = \left[\frac{\alpha}{n_o w_o}\right]^{\alpha} \frac{2(A\sqrt{I})^{\alpha-1}}{\Gamma(\alpha)} \sum_{n=0}^{\infty} \frac{(2n+1-\alpha)\ \Gamma(\alpha)\Gamma(1+n-\alpha)}{n!\ \Gamma(1+n)\Gamma(\alpha-n)} (-1)^n E_{2n} . \qquad \text{(C-63)} $$

Using the identity from page 256 of reference [23]

$$ \Gamma(a) = (a-1)\ \Gamma(a-1) \qquad \text{(C-64)} $$

to yield

$$ \frac{(-1)^n \Gamma(\alpha)}{\Gamma(\alpha-n)} = \frac{\Gamma(1+n-\alpha)}{\Gamma(1-\alpha)} , \qquad \text{(C-65)} $$

and substituting eq. C-65 into eq. C-63, the unconditional PDF for the intensity fluctuations is

$$p(I) = \left[\frac{\alpha}{n_o w_o}\right]^{\alpha} \frac{2(A\sqrt{I})^{\alpha-1}}{\Gamma(\alpha)} \sum_{n=0}^{\infty} \frac{(2n+1-\alpha)\Gamma(1-\alpha+n)^2}{n!n!\ \Gamma(1-\alpha)} E_{2n} \ , \tag{C-66}$$

where

$$E_{2n} = \begin{cases} I_{2n+1-\alpha}(2A\sqrt{\alpha/n_o w_o})\ K_{2n+1-\alpha}(2\sqrt{I\alpha/n_o w_o}) & I > A^2 \\ I_{2n+1-\alpha}(2\sqrt{I\alpha/n_o w_o})\ K_{2n+1-\alpha}(2A\sqrt{\alpha/n_o w_o}) & I \leq A^2 \end{cases} . \tag{C-67}$$

Eq. C-67 was originally derived by Link and was appropriately named the HK distribution [19]. For A = 0, the HK distribution reduces to the K distribution as described by eq. C-29. Because of the complexity of the HK distribution, only the moments had previously been computed.

I-K Distribution

Since the HK distribution is an infinite sum of I and K Bessel functions, the complexity of the PDF makes its use complex. Because of the complexity of the HK distribution, Andrews and Phillips developed the I-K distribution as a simplified version of the HK distribution [12; 13]. There are several ways to derive the I-K distribution as a simplified alternative to the HK PDF, one of which is to assume that the conditional statistic is a generalized Rician PDF and the PDF for the changing variance is negative exponential distributed.

Another method of deriving the I-K distribution is to make an approximation to the characteristic function for the HK PDF. Both methods were originally derived by Andrews and Phillips and result in a PDF that is a single product of I and K Bessel Functions [12; 13].

The derivation that will be presented here will be to approximate the characteristic function for the HK PDF. The characteristic function for the intensity PDF is defined as

$$C_I(U) = E\left[e^{iUI}\right] = \int_0^\infty e^{iUI}\, p(I)\, dI \ . \qquad \text{(C-68)}$$

Since the intensity is described by the expression

$$I = R^2 + A^2 + 2AR\cos(\phi) \ , \qquad \text{(C-69)}$$

the characteristic function defined in eq. C-68 becomes

$$C_I(U) = \int_{-\pi}^{\pi} \int_0^\infty e^{iU(R^2+A^2+2AR\cos(\phi))}\, p(R,\phi)\, dR\, d\phi \ . \qquad \text{(C-70)}$$

Using eq. C-39

$$p(R,\phi|n) = \frac{R}{nw_o\pi}\, e^{-R^2/nw_o} \ , \qquad \text{(C-71)}$$

which is the conditional joint PDF for R and ϕ, and

$$p(R,\phi) = \int_0^\infty p(R,\phi|n)\ p(n)\ dn\ , \qquad (C\text{-}72)$$

the unconditional joint PDF for R and ϕ is

$$p(R,\phi) = \frac{R}{\pi\Gamma(\alpha)} \left[\frac{\alpha}{n_o}\right]^\alpha \int_0^\infty \frac{n^{\alpha-2}}{w_o}\ e^{-R^2/nw_o - \alpha n/n_o}\ dn\ , \qquad (C\text{-}73)$$

where p(n) is the gamma PDF defined by eq. A-1. Making the substitution $n = n_o R^2/x$ and combining eq. C-73 with eq. C-70, yields

$$C_I(U) = \int_{-\pi}^{\pi} \int_0^\infty \frac{R^{2\alpha-1}}{\pi\ \Gamma(\alpha) n_o w_o} \int_0^\infty \left[\frac{\alpha}{x}\right]^\alpha e^{-x/n_o w_o - \alpha R^2/x}\ dx$$

$$\cdot\ e^{iU(R^2+A^2+2AR\cos(\phi))}\ dR\ d\phi\ . \qquad (C\text{-}74)$$

Defining L as

$$L = \frac{1}{\pi\ \Gamma(\alpha) n_o w_o} \int_0^\infty \left[\frac{\alpha}{x}\right]^\alpha e^{-x/n_o w_o}\ dx\ , \qquad (C\text{-}75)$$

and changing the order of integration in eq. C-74, the characteristic function becomes

$$C_I(U) = L \int_0^\infty e^{iUA^2 + (iU-\alpha/x)R^2}\ R^{2\alpha-1}$$

$$\cdot \int_{-\pi}^{\pi} e^{iU2AR\cos(\phi)}\ d\phi\ dR\ . \qquad (C\text{-}76)$$

Using the identity from page 360 of [23]

$$J_o(z) = \frac{1}{2\pi} \int_0^{2\pi} e^{izcosx}\, dx \ , \qquad \text{(C-77)}$$

eq. C-76 reduces to

$$C_I(U) = L2\pi \int_0^{\infty} e^{iUA^2+(iU-\alpha/x)R^2}\, R^{2\alpha-1}\, J_o(2UAR)\, dR \ . \qquad \text{(C-78)}$$

The integral in eq. C-78 can be evaluated with the use of the identity from page 716 of reference [22]

$$\frac{g^v\, \Gamma(v/2+u/2+1/2)}{2^{v+1}a^{(u+v+1)/2}\Gamma(v+1)}\, {}_1F_1((v+u+1)/2;v+1;-g^2/4a)$$

$$= \int_0^{\infty} x^u\, e^{-ax^2}\, J_v(gx)\, dx \ , \qquad \text{(C-79)}$$

with a = -(iU-α/x), v = 0, u= 2α-1, and g = U2A, yielding

$$C_I(U) = \frac{L\ \pi\ \Gamma(\alpha)\ e^{iUA^2}}{(-1)^{\alpha}(iU-\alpha/x)^{\alpha}}\, {}_1F_1(\alpha;1;A^2U^2/(iU-\alpha/x)) . \qquad \text{(C-80)}$$

Using the identity from page 1058 of reference [22],

$${}_1F_1(a,y;z) = e^z\, {}_1F_1(y-a;y;-z) \qquad \text{(C-81)}$$

and eq. C-75, the characteristic function is

$$C_I(U) = \frac{e^{iUA^2}}{n_o w_o} \int_0^{\infty} \left[\frac{\alpha}{x}\right]^{\alpha} e^{-x/n_o w_o}\, \frac{e^{U^2A^2/(iU-\alpha/x)}}{(\alpha/x-iU)^{\alpha}}$$

$$\cdot\ {}_1F_1(1-\alpha,1;U^2A^2/(\alpha/x-iU))\, dx \ . \qquad \text{(C-82)}$$

For the case of weak turbulence, the number of modes, α, is small and the confluent hypergeometric function ${}_1F_1(\ )$ can be approximated by unity. On the other hand, for α large, the SNR, $A^2/n_o w_o$, is small, which implies that A is approximately zero and the ${}_1F_1(\ )$ is again about equal to unity. Since the ${}_1F_1(\ )$ is approximately unity for both the weak and strong turbulent conditions, Andrews and Phillips approximated ${}_1F_1(\ )$ as a constant equal to 1 for all turbulent conditions. Approximating the ${}_1F_1(\ )$ function by unity for all conditions of turbulence, the characteristic function becomes

$$C_I(U) = \frac{e^{iUA^2}}{n_o w_o} \int_0^\infty \left[\frac{\alpha}{x}\right]^\alpha e^{-x/n_o w_o} \frac{e^{-A^2U^2/(\alpha/x-iU)}}{(\alpha/x-iU)^\alpha}\, dx \ . \quad \text{(C-83)}$$

Dividing U^2 by $(\alpha/x-iU)$ in the one exponential function leads to

$$\frac{U^2}{(\alpha/x-iU)} = iU + \alpha/x - \frac{\alpha^2/x^2}{(\alpha/x-iU)} \ , \quad \text{(C-84)}$$

and substituting this result into eq. C-83, yields

$$C_I(U) = \frac{1}{n_o w_o} \int_0^\infty \left[\frac{\alpha}{x}\right]^\alpha e^{-x/n_o w_o - A^2\alpha/x} \cdot \frac{e^{\alpha^2A^2/x^2(\alpha/x-iU)}}{(\alpha/x-iU)^\alpha}\, dx \ . \quad \text{(C-85)}$$

Now that the characteristic function for the intensity PDF has been simplified, the next step is to find the inverse Fourier transform of the characteristic function so that the approximate PDF for the intensity can be found. The PDF is given by

$$p(I) = \frac{1}{2\pi} \int_0^{\infty} e^{-iUI} \, C_I(U) \, dU \, . \qquad \text{(C-86)}$$

Combining eqs. C-85 and C-86 along with the substitution $p = \alpha/x - iU$, yields

$$P(I) = \frac{1}{n_o w_o 2\pi i} \int_0^{\infty} \int_{\alpha/x - i\infty}^{\alpha/x + i\infty} \frac{e^{Ip} \, e^{A^2\alpha^2/x^2 p}}{p^{\alpha}} \, dp$$

$$\cdot \left[\frac{\alpha}{x}\right]^{\alpha} e^{-x/n_o w_o - \alpha A^2/x - I\alpha/x} \, dx \, . \qquad \text{(C-87)}$$

Recognizing that the integral over p is simply the inverse Laplace transform of $e^{A^2\alpha^2/x^2 p}/p^{\alpha}$, and using the identity from page 1026 of reference [23],

$$\mathcal{L}^{-1}\left\{\frac{e^{k/p}}{p^u}\right\} = \left[\frac{x}{k}\right]^{\frac{u-1}{2}} I_{u-1}(2\sqrt{kx}) \, , \qquad \text{(C-88)}$$

where $I_a(x)$ is the modified Bessel function. The PDF for the intensity is

$K = \frac{A^2\alpha^2}{x^2}$, $u = \alpha$ $\left[\frac{Ix^2}{A^2\alpha^2}\right]^{\frac{\alpha-1}{2}} I_{\alpha-1}\left(2\sqrt{\frac{A^2\alpha^2 I}{x^2}}\right)$

$\left[\frac{x}{A\alpha}\right]^{\alpha-1}\left[I\right]^{\frac{\alpha-1}{2}} I_{\alpha-1}\left(2\frac{A\alpha}{x}\sqrt{I}\right)$

$$p(I) = \left[\frac{\sqrt{I}}{A}\right]^{\alpha-1} \frac{1}{n_o w_o} \int_0^\infty \frac{\alpha}{x} e^{-x/n_o w_o - \alpha(A^2+I)/x}$$

$$\cdot I_{\alpha-1}(2A\alpha\sqrt{I}/x)\, dx \,. \qquad \text{(C-89)}$$

From page 725 of reference [22]

$$\int_0^\infty e^{-x/2-(a^2+b^2)/2x} I_v(ab/x) \frac{dx}{x}$$

$$= \begin{cases} 2I_v(a)\, K_v(b) & a < b \\ 2I_v(b)\, K_v(a) & a > b \end{cases}, \qquad \text{(C-90)}$$

with a change a variable $t = x/2n_o w_o$ and $v = \alpha-1$, $a = 2A\sqrt{\alpha/n_o w_o}$, and $b = 2\sqrt{\alpha I/n_o w_o}$, the PDF for the intensity is

$$p(I) = \frac{2\alpha}{n_o w_o} \left[\frac{\sqrt{I}}{A}\right]^{\alpha-1}$$

$$\cdot \begin{cases} I_{\alpha-1}(2A\sqrt{\alpha/n_o w_o})\, K_{\alpha-1}(2\sqrt{\alpha I/n_o w_o}) & I > A^2 \\ I_{\alpha-1}(2\sqrt{\alpha I/n_o w_o})\, K_{\alpha-1}(2A\sqrt{\alpha/n_o w_o}) & I \leq A^2 \end{cases}.$$

(C-91)

Eq. C-91 was named by Andrews and Phillips as the I-K distribution.

The moments for the I-K distribution agree with the experimental moments for a laser beam propagating through the atmosphere [13]. Since the I-K PDF has a closed form solution, the I-K PDF is a more attractive PDF in comparison with the HK PDF. When A equals zero, it is

interesting to note that the I-K PDF reduces to the K distribution. For the case when α equal one, the I-K PDF is identical to the HK PDF.

K Moments

The statistical mth moment of the K distribution can be computed by taking the expected value of the random variable raised to the mth power. There are two easy ways of computing the moments for the K distribution. The most common method is to compute the moments using

$$E\left[I^m\right] = \int_0^\infty I^m \, p(I) \, dI, \tag{C-92}$$

where p(I) is given by the K distribution. The other method requires taking the expected value of the random variable of the random variable in the process from which the K distribution was derived. The process for K distributed intensity is given by

$$I = n \cdot w, \tag{C-93}$$

where n is the slowly varying process that is governed by gamma statistics, and w is the fast varying process defined by negative exponential statistics. Taking the expected value of eq. C-93 to the mth power and using the fact that n and w are independent processes, yields

$$E\left[I^m\right] = E\left[n^m\right]E\left[w^m\right] \quad , \tag{C-94}$$

from which the moments for n and w can be computed separately. Eq. C-94 is the product of the moments of the gamma distribution with the moments for the negative exponential distribution. Given that the PDFs for n and w as defined in the beginning of this appendix are

$$p(n) = \frac{n^{\alpha-1}}{\Gamma(\alpha)} \left[\frac{\alpha}{n_o}\right]^{\alpha} e^{-\alpha n/n_o} \tag{C-95}$$

and

$$p(w) = \frac{1}{w_o} e^{-w/w_o} \quad , \tag{C-96}$$

the moments for n and w are directly derivable, yielding

$$E\left[n^m\right] = (n_o/\alpha)^m \ (\alpha+m-1)(\alpha+m-2)\ldots\alpha \tag{C-97}$$

$$E\left[w^m\right] = (w_o)^m \ m! \quad . \tag{C-98}$$

Combining eqs. C-97 and C-98 along with eq. C-94, the moments for the intensity process, I, are

$$E\left[I^m\right] = (n_o w_o/\alpha)^m \ m! \ (\alpha+m-1)(\alpha+m-2)..\alpha \ . \tag{C-99}$$

Eq. C-99 is the exact equation for the moments of the K distribution that would be obtained if eq. C-92 was used

to compute the moments. Hence, the derivation of the moments by the method above tend to substantiate that a modulation process can be modeled with the use of conditional statistics.

HK Moments

Since the HK moments are derivable from a process that contains both a deterministic and a random part, taking the expected value of the process directly becomes more tedious. An easier method is to use the PDF for the HK distribution in eq. C-92. Evaluating the integral in eq. C-92 is almost impossible if the final form for the HK distribution as defined in eq. C-66 is used for p(I). Using a definition for p(I) in a somewhat unusual form leads to a very nice solution for the HK moments.

Starting with eq. C-44

$$p(I) = \frac{1}{\Gamma(\alpha) w_o} \left[\frac{\alpha}{n_o}\right]^{\alpha} \int_0^{\infty} n^{\alpha-2} e^{-\alpha n/n_o - (I+A^2)/nw_o} \cdot I_o(2\alpha\sqrt{I}/nw_o)\, dn \qquad \text{(C-100)}$$

and eq. C-92, the moments for the HK distribution are

$$E\left[I^m\right] = \frac{1}{\Gamma(\alpha) w_o} \left[\frac{\alpha}{n_o}\right]^{\alpha} \int_0^{\infty} n^{\alpha-2} e^{-\alpha n/n_o} \int_0^{\infty} I^m \cdot e^{-(I+A^2)/nw_o} I_o(2A\sqrt{I}/nw_o)\, dI\, dn \,. \qquad \text{(C-101)}$$

The integral over I is simply the mth moment for the

Rician distribution. Using the results of Appendix B for the Rician distribution along with the substitution $b = nw_o$, the integral over I can be evaluated, yielding

$$E\left[I^m\right] = \frac{m!(\alpha/n_o)^\alpha}{\Gamma(\alpha)w_o} \sum_{k=0}^{m} \binom{m}{m-k} \frac{w_o^{m+1-k} A^{2k}}{k!} \cdot \int_0^\infty n^{\alpha-1+m-k} e^{-\alpha n/n_o} dn \ . \quad \text{(C-102)}$$

Using the identity from page 255 of reference [23]

$$\Gamma(z)/d^z = \int_0^\infty t^{z-1} e^{-dt} dt \ . \quad \text{(C-103)}$$

With $z = \alpha+m-k$, $d = \alpha/n_o$, and $\rho = A^2/n_o w_o$, and after some algebra, the moments for the HK distribution are given by

$$E\left[I^m\right] = \frac{m!(w_o n_o)^m}{\alpha^m} \sum_{k=0}^{m} \binom{m}{m-k} \frac{\Gamma(\alpha+m-k)}{\Gamma(\alpha)} \frac{(\alpha\rho)^k}{k!} \ . \quad \text{(C-104)}$$

Substituting m = 1 to find the mean and then dividing eq. C-104 by the mean to the mth power yields the normalized moments for the HK distribution as

$$\frac{E\left[I^m\right]}{E\left[I\right]^m} = \frac{m!}{\alpha^m(1+\rho)^m} \sum_{k=0}^{m} \binom{m}{m-k} \frac{\Gamma(\alpha+m-k)}{\Gamma(\alpha)} \frac{(\alpha\rho)^k}{k!} \ . \quad \text{(C-105)}$$

It is interesting to note that in the evaluation of the integral over I in eq. C-101, the moments for the Rician distribution were computed. The next integral over

n simply averages the Rician moments with the gamma distribution. Again, the conditionalization process has shown up in the computation of the moments for the nonstationary processes.

I-K Moments

The moments for the I-K distribution can be found in the same manner as the HK moments. Using eq. C-89 as the form of the PDF for the I-K distribution

$$p(I) = \frac{(\sqrt{I}/A)^{\alpha-1}}{n_o w_o} \int_0^\infty \frac{\alpha}{x} e^{-x/n_o w_o - \alpha(A^2+I)/x} \cdot I_{\alpha-1}(2A\alpha\sqrt{I}/x)\, dx, \qquad \text{(C-106)}$$

along with eq. C-92, the moments for the I-K distribution are given by

$$E\left[I^m\right] = \frac{(1/A)^{\alpha-1}}{n_o w_o} \int_0^\infty \frac{\alpha}{x} e^{-x/n_o w_o - \alpha A^2/x} \cdot \int_0^\infty I^{m+\frac{\alpha-1}{2}} e^{-\alpha I/x} I_{\alpha-1}(2\alpha A\sqrt{I}/x)\, dI\, dx\,. \qquad \text{(C-107)}$$

Using the identity from page 720 of reference [22]

$$\frac{\Gamma(u+v+1/2)}{\Gamma(2v+1)} g^{-1} e^{g^2/2s} s^{-u} M_{-u,v}(g^2/s) = \int_0^\infty x^{u-1/2} e^{-sx} I_{2v}(2g\sqrt{x})\, dx\,, \qquad \text{(C-108)}$$

where $M_{u,v}(x)$ is defined as the Whittaker's function.

Making the substitutions $g = \alpha A/x$, $s = \alpha/x$, $u = m+\alpha/2$, and $v=\alpha/2-1/2$, yields

$$E\left[I^m\right] = \frac{\Gamma(m+\alpha)}{A^{\alpha} n_o w_o \Gamma(\alpha)} \int_0^{\infty} e^{-x/n_o w_o - \alpha A^2/2x} \, (x/\alpha)^{m+\alpha/2}$$

$$\cdot \, M_{-m-\alpha/2,\alpha/2-1/2}(\alpha A^2/x) \, dx \, . \qquad \text{(C-109)}$$

Using the identities from pages 1058 and 1059 of reference [22], respectively,

$$M_{\lambda,u}(z) = z^{u+1/2} \, e^{-z/2} \, {}_1F_1(u-\lambda+1/2;2u+1;z) \qquad \text{(C-110)}$$

and

$${}_1F_1(h;y;z) = e^z \, {}_1F_1(y-h;y;-z) \, . \qquad \text{(C-111)}$$

Eq. C-109 can be rewritten in the form

$$E\left[I^m\right] = \frac{\Gamma(m+\alpha)}{n_o w_o \Gamma(\alpha)} \int_0^{\infty} e^{-x/n_o w_o} \, (x/\alpha)^m$$

$$\cdot \, {}_1F_1(-m,\alpha;-\alpha A^2/x) \, dx \, . \qquad \text{(C-112)}$$

Relating the degenerate hypergeometric function to the Laguerre polynomials with the use of the identity from page 1037 of reference [22]

$$L_n^s(z) = {}_1F_1(-n;s+1;z) \cdot \binom{n+s}{n} \, , \qquad \text{(C-113)}$$

yields

$$E\left[I^m\right] = \frac{\Gamma(m+1)}{n_o w_o}\int_0^\infty e^{-x/n_o w_o}\,(x/\alpha)^m\, L_m^{\alpha-1}(-\alpha A^2/x)\,dx \quad . \quad \text{(C-114)}$$

Making the substitution for the Laguerre polynomials, and with the help of the identity from page 1037 of reference [22]

$$\frac{(n+s)!}{(n-k)!(s+k)!} = \frac{\Gamma(n+s+1)}{\Gamma(n-k+1)\,\Gamma(s+k+1)}$$

$$L_n^s(x) = \sum_{k=0}^{n}(-1)^k \binom{n+s}{n-k}\frac{x^k}{k!} \quad , \quad \text{(C-115)}$$

the moments for the I-K distribution become

$$E\left[I^m\right] = \frac{m!\,\alpha^{-m}}{n_o w_o}\sum_{k=0}^{m}\binom{m+\alpha-1}{m-k}\frac{(\alpha A^2)^k}{k!}\int_0^\infty x^{m-k}e^{-x/n_o w_o}\,dx \quad . \quad \text{(C-116)}$$

Using eq. C-103 to evaluate the integral in eq. C-116 and making the substitution $\rho = A^2/n_o w_o$, the moments for the I-K distribution reduce to

$$E\left[I^m\right] = \frac{(n_o w_o)^m\, m!}{\alpha^m}\sum_{k=0}^{m}\frac{\Gamma(m+\alpha)}{\Gamma(\alpha+k)}\frac{(\alpha\rho)^k}{k!} \quad . \quad \text{(C-117)}$$

Setting m = 1 to find the mean and then dividing eq. C-117 by the mean to the mth power, yields the normalized moments for the I-K distribution

$$\frac{E\left[I^m\right]}{E\left[I\right]^m} = \frac{m!}{\alpha^m(1+\rho)^m}\sum_{k=0}^{m}\frac{\Gamma(m+\alpha)}{\Gamma(\alpha+k)}\frac{(\alpha\rho)^k}{k!} \quad . \quad \text{(C-118)}$$

APPENDIX D

HIGH SPEED MOVIE EXPERIMENT

This appendix is intended to be a summary and a quick reference guide should more high speed 16 mm movies need to be processed. Several high speed 16 mm movies were taken at different locations behind the phase screens to gain further insight into the laser propagation problem. The movies were intended primarily for qualitative use rather than for quantitative measurements.

From the spectrum of the intensity fluctuations, it was determimed that most of the intensity fluctuations occurred at frequencies below 2,000 Hz. From the Nyquist theorem, the frame rate of the movie film was set to 4,000 frames per second. At this frame rate, the high frequency detail that would not normally be viewed with the naked eye could be seen. Typically the eye can only see frequencies up to about 10 to 15 Hz.

Standard 16 mm movie camera frame rates varied from 16 to 30 frames per second, which were much too slow to see the high frequency detail desired. The Nova camera, manufactured by James Ippolito and Company, was used to make the 16 mm movies, since it could take movies up to

9,999 frames per second. For a nominal frame rate of 4,000 frames per second, a motor control voltage of 60 volts was chosen. The actual frame rate of the camera varied between 2,300 and 4,800 frames per second. After 5 feet of film use, the camera speed was 2,300 frames per second and increased in speed until a maximum speed of 4,800 frames per second was obtained.

KODAK 7240 film on 100 foot reels was chosen as the 16 mm movie film. A feature of KODAK 7240 film is that changes in speed rates of a factor of 2 produce only slight variations in the exposed density level of the film. Using a reel size of 100 feet limited the total experiment time to about 1 second and a viewing time of about 2 minutes.

Since the laser beam needed to be incident directly on the film, all imaging optics in front of the film plane on the Nova camera had to be removed. For example, the aperture setting that would normally control the f-stop of the camera would only reduce the size of the laser beam on the film. Since the laser beam was collimated to 2 inches, a telescope with a magnification of 2.5, focused at infinity, was used to reduce the beam's diameter to 0.75 inches. With a 0.75 inch collimated beam, approximately 80% of the beam was incident on the film.

After the telescope and camera were aligned, it was necessary to determine the proper exposure setting of the film. The Hurter-Driffield curve was used to determine the exposure level required for a given density of the film [25]. In Figure 39, the H & D curve for KODAK 7240 film is shown. The X axis is in units of logarithm (log) of foot-candles•seconds and the y axis is the log of the inverse of transmission.

Both the frame rate and the intensity of the laser beam determine the exposure level

$$\tau = I \cdot t_e \ , \qquad \text{(D-1)}$$

where τ is the exposure level, I is the incident intensity and t_e is the exposure time. Since the frame rate was nominally 4,000 frames per second, this corresponded to a frame time of 250 microseconds. The camera limits the exposure time to 1/3 of the frame time. For a nominal frame rate of 4,000 frames per second, the exposure time was 83.3 microseconds.

Once the exposure time was known, a photometer was used to measure the intensity of the laser beam entering the camera. Two settings were chosen on the H & D curves for two different exposure levels. The first setting was for a laser beam intensity of 13 foot-candles and the second was for an intensity of 28 foot-candles. The film

exposed for 13 foot-candles of intensity was slightly over exposed, while the film exposed for 28 foot-candles of intensity was completely washed out. For all later films that were made, the laser beam's intensity was adjusted to 9.6 foot-candles. For the most part this gave very good results. In Figure 39, the two data points are for 9.6 and 28 foot-candles of laser beam intensity level. The intensity levels of 9.6 and 28 foot-candles corresponds to exposure levels of 8.16E-4 and 2.38E-3 foot-candles• seconds, respectively.

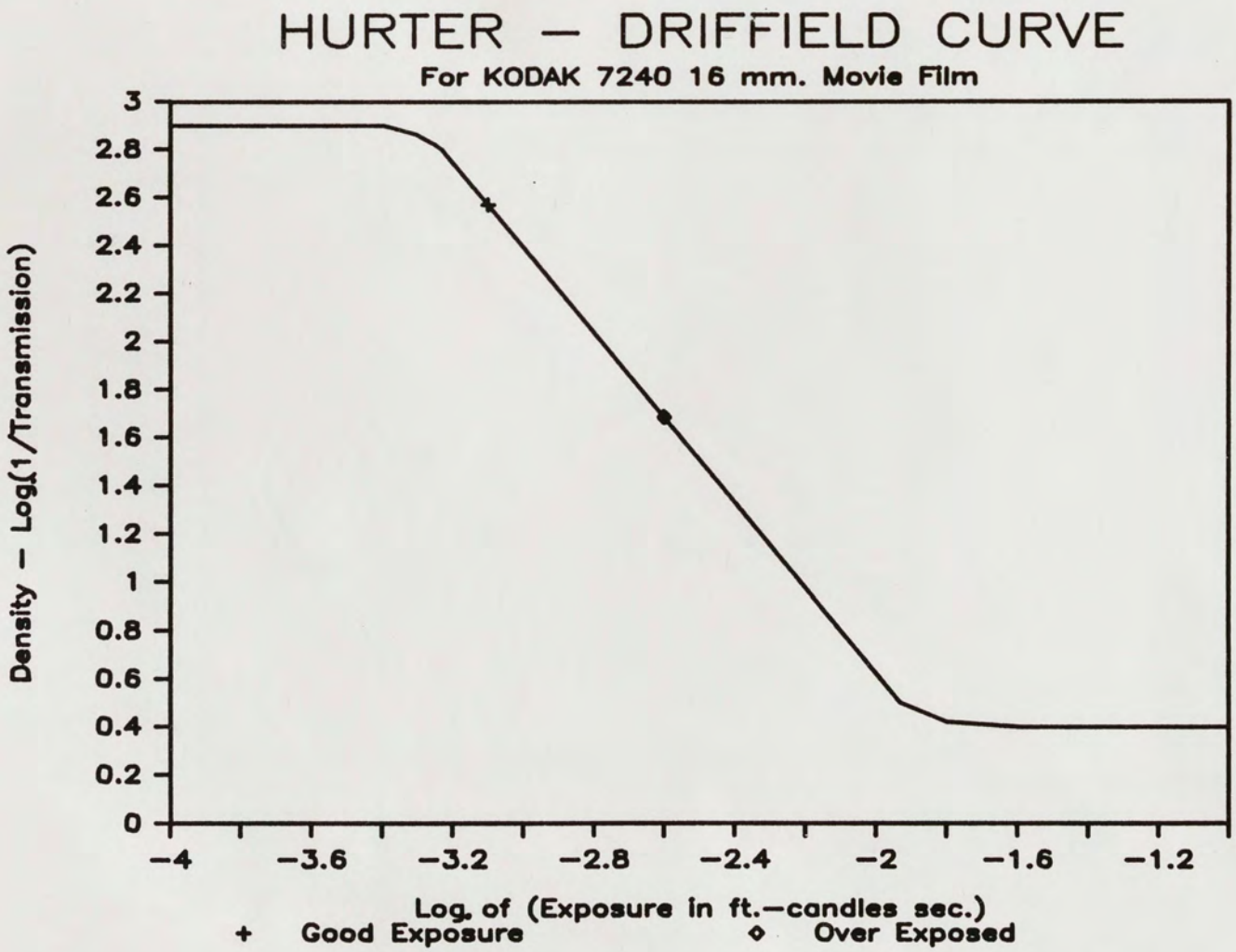

Figure 39. Hurter-Driffield Curve for KODAK 7240 16 Millimeter Movie Film.

APPENDIX E

IBM PC DATA ACQUISITION SYSTEM

An IBM PC computer system was used to sample and plot all of the data shown in this dissertation. Since an IBM PC normally does not include data acquisition software or hardware, a data acquisition board was purchased from Metrabyte Corporation. The board included 16 channels of analog inputs that are capable of being sampled at a maximum rate of 100,000 Hz by an analog to digital converter. In addition, the board included four digital input/output lines, a digital interval timer, and two digital to analog outputs. A limited software package was included with the board so that Basic language programs could be used to interface with the board.

For sample rates above 1,000 Hz, the maximum number of data points that could be sampled at any one time was 32,767. This limitation was not a function of the board, but a limitation in the way the IBM PC performs its direct memory access (DMA). Even though the computer is capable of addressing up to one million bytes, the DMA integrated circuit (IC) can only access 65,535 bytes at a time. To get around this problem, the IBM PC uses a 4 bit random

access memory (RAM) IC. This formats the memory into 16 pages of 65,535 bytes for a total of 1 million bytes. On a DMA transfer, only 65,535 bytes of data can be moved at one time.

Since each data sample generated by the data acquisition board uses 2 bytes of memory, only 32,767 samples can be taken at a time. A technique was developed to convert 32,767 bytes of one DMA page into a temporary storage buffer. This storage buffer was then divided into 2 sections, a low and a high buffer area. When the DMA was writing data to the low buffer area, a short Assembly language program took the data stored in the high buffer area and moved it into a different location of memory. Then, when the DMA was writing data to the high buffer area, the Assembly language program moved data from the low buffer area to another location in memory; this is the same principle as ping-pong memory manipulations.

From the memory map of the IBM PC, it was concluded that the total of 655,360 bytes of memory available could not all be used for data. The last 65,544 and the first 196,608 bytes of memory were used by the disk operating system (DOS) and the data acquisition programs [26; 27]. In addition, the total memory available for use by the data acquisition system depended on the version of DOS that the IBM PC was using. Because there was a need for

the data acquisition system to work with all present versions of DOS, DOS version 3.2 (the current version) was used to determine the maximum memory available. Since all the available memory in the computer was used, all resident programs, any ANSI.SYS file, or any CONFIG.SYS file had to be removed before running any of the data acquisition software.

To implement this ping-pong buffer scheme, both an Assembly language and a Basic language program were written. In addition to the two programs that were written, the Assembly language driver program (DASH16.BIN) was used. A total of three programs, two Assembly language and one Basic language, were used in the development of the software for the data acquisition system.

The Assembly language program supplied by Metrabyte contained many different modes of operation that were readily interfaced with a user written Basic language program [28]. The mode of most interest was mode 6, since this was the DMA mode of operation. In mode 6, the data acquisition board continuously wrote to the 32,767 bytes storage buffer. Modes 0, 1, 7, 9, and 17 were also used. Mode 0 was used to initialize the data acquisition board; mode 1 was used to set beginning and ending analog inputs; mode 7 was used to stop DMA transfer started by mode 6;

mode 9 was used to convert the raw data into a usable form; and mode 17 was used to set the sampling rate of the board.

The two programs that were written were named MOVE.ASM and DATAAQ.BAS. MOVE.ASM is an Assembly language program that interfaces with the Basic language DATAAQ.BAS program. MOVE.ASM was used to move data from the high and low buffer areas to other locations in memory at a very high speed. DATAAQ.BAS monitors the progress of the sampling and controls when and where the data was moved. For a detailed understanding on how to interface an Assembly language program to a Basic language program, refer to The Peter Norton Programmer's Guide To The IBM PC [29].

Not only does DATAAQ.BAS control the logic for the data acquisition board, it is also a general purpose menu driven data acquisition software package. In general, DATAAQ.BAS can acquire data, save and retrieve data, plot data, compute the statistical moments for the data, and finally store and retrieve information about how the data was taken.

The data aquisition program (DATAAQ.BAS) is completely menu driven. The program was compiled using a Basic Compiler and then linked together with DASH16.BIN and MOVE.BIN using the linker. To use the program, just run the link version of DATAAQ (DATAAQ.EXE). A menu will

appear giving the user a choice of options. If the error "STRING CORRUPT ERROR" appears, the user forgot to remove either CONFIG.SYS, ANSI.SYS, or all resident programs in the system. Remove one of the above and reboot the system to clear all available memory and the error should disappear.

LIST OF REFERENCES

[1] Tatarski, V. I. Wave Propagation in a Turbulent Medium. Translated by R.S. Silverman. New York: McGraw Hill Book Co., 1961.

[2] Schatzel, K. "K-distributed Phase Differences in Turbulent Random Phase Screens." Journal of the Optical Society of America 73 (March 1983):269-76.

[3] Link, Donald J.; Phillips, Ronald L.; and Andrews, Larry C. "Theoretical Model for Optical-Wave Phase Fluctuations." Journal of the Optical Society of America A 4 (February 1987):374-77.

[4] Ziemer, R. E., and Tranter, W. H. Principles of Communications System, Modulation, and Noise. Boston: Houghton Mifflin Co., 1976, pp. 164-252.

[5] Nakagami, M. "The M-Distribution -- A General Formula of Intensity Distribution of Rapid Fading." reprint from Statistical Methods of Radio Wave Propagation. Oxford, England: Pergamom 1960.

[6] Middleton, David. An Introduction to Statistical Communication Theory. New York: McGraw Hill Book Co., 1960.

[7] Rice, S. O. "Mathematical Analysis of Random Noise." in Nelson Wax (ed.), Selected Papers on Noise and Stochastic Processes. New York: Dover Publications Inc., 1954, pp. 133-294.

[8] Jakeman, E.; Kleive, R. C.; Richards, P. H.; and Walker, J. G. "Application of Non-Gaussian Scattering of Laser Light to Measurements in a Propane Flame." Journal of Physics D: Applied Physics 17 (October 1984):1941-52.

[9] Jakeman, E., and Pusey, P. N. "Non-Gaussian Fluctuations in Electromagnetic Radiation Scattered by a Random Phase Screen. Intensity Theory." Journal of Physics A: Mathematical and General 8 (March 1975):369-91.

[10] Parry, G.; Pusey, P. N.; Jakeman, E.; and McWhirter, J. G. "Focusing by a Random Phase Screen." Optical Communications 22 (August 1977):195-201.

[11] Jakeman, E. "On the Statistics of K-Distributed Noise." Journal of Physics A: Mathematical and General 13 (January 1980):31-48.

[12] Andrews, L. C., and Phillips, R. L. "I-K Distribution as a Universal Propagation Model of Laser Beams in Atmospheric Turbulence." Journal of the Optical Society of America A 2 (February 1985):160-63.

[13] Andrews, L. C., and Phillips, R. L. "Mathematical Genesis of the I-K Distribution for Random Optical Fields." Journal of the Optical Society of America A 3 (November 1986):1912-1919.

[14] Phillips, R. L.; Andrews, L. C.; Jakeman, E.; and Walker, J. G. "The Statistical Properties of Laser-Light Scatter by Two Phase Screens." Proceedings of SPIE: Modeling and Simulation of Optoelectronic Systems 642 (March 1986):282-85.

[15] Bendat, Julius S., and Piersol, Allan G. Random Data: Analysis and Measurement. New York: Wiley-Interscience, 1971, pp. 344-79.

[16] Helstrom, Carl W. Probability and Stochastic Processes for Engineers. New York: MacMillan Publishing Co., 1984, pp. 139-47.

[17] Ward, K. D. "Compound Representation of High Resolution Sea Clutter." Electronic Letter 17 (August 1981):561-63.

[18] Cooper, George R., and McGillem, Clare D. Probabilistic Methods of Signal and System Analysis. New York: Holt, Rinehart, and Winston, Inc., 1971.

[19] Link, Donald J. "Phase Statistics for a Lightwave Traveling Through Turbulent Media." Ph.D. dissertation, University of Central Florida, 1985.

[20] Andrews, L. C.; Phillips, R. L.; and Shivamoggi, Bhimsen K. "Plane Wave Relations of the Parameters of the I-K Distribution to Strength of Turbulence and Inner Scale." Not yet published.

[21] Tough, R. J. A. "A Fokker-Planck Description of K-Distributed Noise." Not yet published.

[22] Gradshteyn, I. S., and Ryzhik, R. L. Tables of Integrals, Series, and Products. New York: Academic Press, 1980.

[23] Abramowitz, M., and Stegun, T. A. Handbook of Mathematical Functions. New York: Dover Publications Inc., 1972.

[24] Lebedev, N. N. Special Functions and Their Applications. New York: Dover Publications Inc., 1972.

[25] Goodman, Joseph W. Introduction to Fourier Optics. San Francisco: McGraw Hill Book Co., 1968, pp. 149-57.

[26] IBM Corp. Disk Operating System Technical Reference. Boca Raton, Fl.: IBM Corp., 1985.

[27] IBM Corp., and Microsoft Corp. Disk Operating System Version 3.20. Boca Raton, Fl.: IBM Corp., 1986.

[28] Metrabyte Corp. Dash-16/16F Operation Manual. Taunton, Ma.: Metrabyte Corp., 1986.

[29] Norton, Peter. The Peter Norton Programmer's Guide to the IBM PC. Bellevue, Wa.: Microsoft Press, 1985.